4-3-2017

Molecular-Size Selective Zeolite Membrane Encapsulated Novel Catalysts for Enhanced Biomass to Liquid (BTL) Processes

Ummuhan Cimenler
University of South Florida, ucimenler@mail.usf.edu

Molecular-Size Selective Zeolite Membrane Encapsulated Novel Catalysts for Enhanced Biomass to Liquid (BTL) Processes

by

Ummuhan Cimenler

A dissertation submitted in partial fulfillment
of the requirements for the degree of
Doctor of Philosophy in Chemical Engineering
Department of Chemical and Biomedical Engineering
College of Engineering
University of South Florida

Co-Major Professor: John N. Kuhn, Ph.D.
Co-Major Professor: Babu Joseph, Ph.D.
Aydin Sunol, Ph.D.
Qiong Zhang, Ph.D.
Shengqian Ma, Ph.D.

Date of Approval:
February 1, 2017

Keywords: Reforming, Reactant Selectivity, Tar, Diffusion Limitation, FTS, CRAFT

DEDICATION

I dedicate this dissertation to my beloved husband, Dr. Oguz Cimenler, who was always supportive to me during my study, my sweetheart daughter, Reyhan Cimenler, to my dear parents, brothers and sister.

ACKNOWLEDGMENTS

I would like to express my deepest appreciation to my adviser, Dr. John N. Kuhn, for his advice, patience and guidance throughout my study and giving opportunity to work with him.

I would like to acknowledge to Dr. Babu Joseph and Dr. Aydin Sunol who were always helpful and guided me with their key comments about my study. I feel so lucky to have such an important scholars in my committee.

I would like to also acknowledge my committee members Dr. Shengqian Ma and Dr. Qiong Zhang for the guidance, feedbacks and comments.

I would like to gratefully acknowledge the funding received from the Ministry of National Education of Turkish Republic for my PhD study.

I would like thank to the all Heterogeneous Catalysis & Materials Chemistry Group members: Dr. Yolanda Daza, Dr. Sandy Pettit, Dr. Selasi Blavo, Dr. Selma Hokenek, Debtanu Maiti, Ryan Kent, Nada Elsayed and others for all their invaluable help and support. I would like to thank to Ms. Catherine Burton for her patience and corrections on my dissertation draft.

TABLE OF CONTENTS

LIST OF TABLES

LIST OF FIGURES

ABSTRACT

80% of energy usage in the word comes from fossil fuels (coal, oil, natural gas) and among the fossil fuels, oil is the most consumed energy source especially in transportation. However, due to concerns about energy demand and energy sustainability, global warming and dependency on foreign oil, generation of renewable fuels is crucial for transportation. Biomass to Liquid (BTL) is a promising process available to produce renewable liquid fuels. BTL fuels have great potential to meet the growing demand for liquid fuels, mitigating climate change, and providing value to rural areas. However, there are two major challenges with biofuels produced from BTL. One of the major challenge is the H_2:CO ratio of biomass gasification product is insufficient for production of hydrocarbon fuels due to formation of methane and tars. The steam reforming of hydrocarbons, to improve the H_2:CO ratio, is generally conducted as part of the gas conditioning. However, tars cause the catalysts to deactivate rapidly. Secondly, for fuels produced from the gasification route regardless of feedstock source, there is an economy-of-scale issue. Therefore, it is desirable to seek ways of process intensification to allow small scale plants to be more economical. Zeolites can be used to solve these challenges since they have reactant selectivity property.

To achieve a catalyst capable of reforming methane without potential for deactivation by tars, the encapsulation of a core reforming catalyst with porous zeolite shell is examined in this dissertation. After detailed introduction in the first chapter, a composite H-β zeolite membrane encapsulated 1.6wt%Ni/1.2wt%Mg/$Ce_{0.6}Zr_{0.4}O_2$ steam reforming catalyst was prepared by a

physical coating method in the second chapter of the study. Scanning Electron Microscopy (SEM) and Energy Dispersive Spectroscopy (EDS) analyses indicated that H-β zeolite was coated successfully on the core reforming catalyst. The pore size of H-β zeolite shell was between 0.43 and 0.57 nm, as measured by the HK method. Steam reforming of CH_4 and C_7H_8 (as a tar model) were conducted with the composite H-β zeolite coated reforming catalyst, the two components individually, and physical mixtures of the two components as a function of temperature (780–840°C). CH_4 conversion was enhanced by a factor of 2–3 (depending on temperature) for the composite catalyst as compared to the core reforming catalyst individually even though the zeolite did not have any activity alone. Possible reasons for the enhanced CH_4 conversion include confined reaction effects (increase residence time within pores) of the catalyst containing the zeolite coating and/or Al^{3+} promotion of the active sites. Alternatively, due to molecular-size selectivity, the composite H-β zeolite coated reforming catalyst demonstrated a decrease in C_7H_8 conversion when compared to the uncoated reforming catalyst. The results validate the use of size selective catalysts to control molecular traffic and enhance the reforming reactant selectivity.

A composite catalyst consisting of an outer layer of zeolite membrane encapsulating an inner reforming catalyst core was synthesized by a double physical coating method to investigate reactant selectivity (ratio of methane/toluene conversion rate) in steam reforming of methane (CH_4) and toluene (C_7H_8). A double encapsulation (51 wt % H-β zeolite) of a 1.6 wt % Ni−1.2 wt % Mg/$Ce_{0.6}Zr_{0.4}O_2$ steam reforming catalyst was compared to a singly coated composite catalyst (34.3 wt % H-β zeolite) to investigate zeolite thickness effects on the conversion of different sized hydrocarbons. The increase in the zeolite content from 34.3 to 51 wt % decreased both CH_4 and C_7H_8 conversions (by up to 14% depending upon the temperature) as a result of the increase in diffusional limitations. Weisz−Prater criteria and Thiele moduli calculations confirmed that the

reactions were performed under internal diffusion limitations. The C_7H_8 conversion of the 51 wt % composite (SR@β51%) catalyst was similar to the zeolite alone, indicating negligible contribution from the protected catalyst core. The reactant selectivity increased by up to 1.5 times on SR@β51% in comparison to the SR@β34.3% composite. Combined reforming at 800 °C on the SR@β51% catalyst indicated that the catalyst was stable during the 10 h time on stream.

Continuing this work, a non-acidic Silicalite-1 zeolite membrane encapsulated 1.6wt%Ni-1.2wt%Mg/$Ce_{0.6}Zr_{0.4}O_2$ steam reforming composite catalyst, synthesized by a physical coating method, was used to investigate effect of encapsulation on size selective steam reforming, using methane (CH_4) and toluene (C_7H_8) as representative species. Weisz-Prater Criteria and Thiele moduli calculations indicated internal diffusion limitations. Combined reforming of CH_4 and C_7H_8 at 800°C on the composite catalyst demonstrated stability during the 10 h time on stream while uncoated SR catalyst deactivated. The non-acidic Silicalite-1 encapsulated catalyst showed decreases (~2-7%) in both CH_4 and C_7H_8 conversions compared to acidic H-β zeolite confirming that shell acidity did contribute to conversion and suggesting that shell defects/grain boundaries were responsible for the C_7H_8 conversion.

Finally, low temperature 0.16wt%Pt–1.34wt%Ni–1.00wt%Mg/$(Ce_{0.6}Zr_{0.4})O_2$ reforming catalyst was triple coated with H-β zeolite (60 wt% of zeolite) to be utilized synthesis of combination steam reforming catalyst (SR) and Fischer-Tropsch Synthesis (FTS) catalyst (CRAFT) for a single-step conversion of methane to liquid fuels. Scanning electron microscopy (SEM) image and energy-dispersive spectroscopy (EDS) analysis result demonstrated that H-β zeolite was successfully encapsulated onto the low temperature reforming catalyst. The catalyst was tested in steam reforming of methane (CH_4) and toluene (C_7H_8) and the results was compared with 51 wt%. While CH_4 conversions are very similar on the 60wt% composite catalyst

with 51wt% composite catalyst, no C_7H_8 conversion was seen on the 60 wt% composite catalyst. Thus, it is concluded that the 60 wt% composite catalyst can be utilized to synthesis CRAFT catalyst.

CHAPTER 1: INTRODUCTION[1]

In recent years, encapsulation of particles and molecules has received attention and many studies have been performed in the synthesis encapsulated structure to increase stability and control accessibility of the confined species and to control size and shape of materials for applications in catalysis, nanoelectronics, nano-optics, biomedicine and material science[1] [2] [3]. (Figure 1.1).

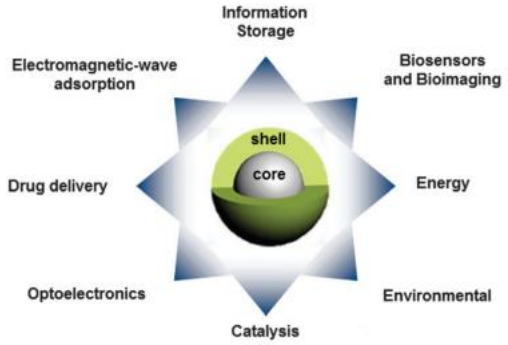

Figure 1.1 Applications of the encapsulated nanoparticles.
Adapted with permission from Royal Society of Chemistry (from ref. 4)[4].

Encapsulated structures can be classified as core-shell (or egg-shell) which is a single noble metal core encapsulated by a shell, yolk-shell or rattle-type structures which is a single movable noble metal core inside a hollow shell, multicore-shell (or pomegranate-like) which is multiple supported or unsupported noble metal cores coated with a metal oxide shell (Figure 1.2).

[1] This chapter has been accepted as a book chapter of "Encapsulated Catalysts" Book by "Elsevier".

Figure 1.2 Schematic illustration of core–shell, hollow, and yolk–shell catalysts. Adapted with permission from Royal Society of Chemistry (from ref. 5)[5].

Heterogeneous catalysts encapsulated in inorganic materials (such as zeolites and SiO_2) are also focus of interest for inexpensive, selective, and stable catalysts for XTL process steps (e.g., Hydrocarbon Reforming, Water-Gas Shift (WGS) and Fischer-Tropsch Synthesis (FTS)) since interactions between components can lead to improved properties over the single-components. Moreover, encapsulated catalytic structures opens the possibility of preserving the catalysts from deactivation and increase selectivity of the catalysts due to the effect of encapsulation. Eggshell, multicore-shell and yolk-shell structures are the most studied encapsulated structures in the literature as XTL catalysts.

Although the encapsulated structures demonstrate many advantages, there is also a disadvantage for catalytic reactions[6]. The shell layer could lower the diffusion rates of the reactants toward the active cores. Diffusion of molecules through the pores of a zeolite occurs in a regime that is called "configurational diffusion"[7, 8]. Configurational diffusion occurs when the pore size is on the order of the molecular size and continuously molecule-wall interaction occurs (Figure 1.3). Very small changes in between pore diameter and molecular dimensions can cause large differences in the diffusion coefficients of the reactants and this brings shape selectivity (reactant or product selectivity) property of the zeolites[7, 8].

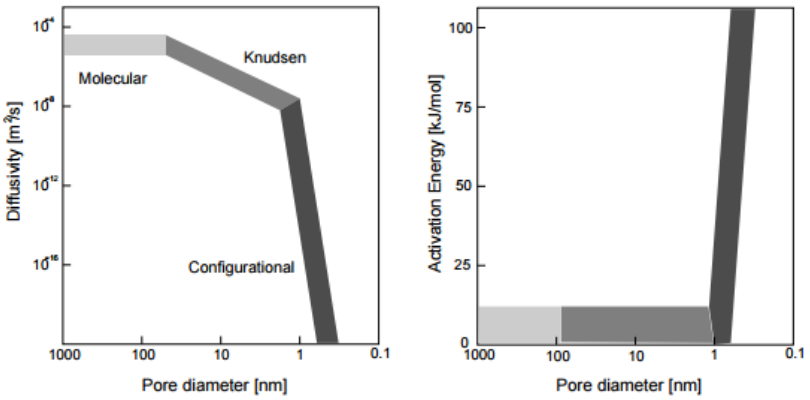

Figure 1.3 Effect of pore size on the diffusivity and activation energy of diffusion. Reproduced with permission from American Chemical Society (from ref. 9)[9].

Thus, encapsulated catalysts with a specific size and pore channels can turn this disadvantage to advantage. For example, using suitable zeolites as a shell layer can protect the core catalyst from deactivation causing by coking because zeolites have reactant selectivity property which means the microporous character of the zeolites with uniform pore dimensions allows certain molecules to enter the crystals while rejecting others with large molecular size[10] (Figure 1.4a). Thus, the core catalyst can be protected from deactivation by hindering unwanted molecules from accessing the core and causing deactivation.

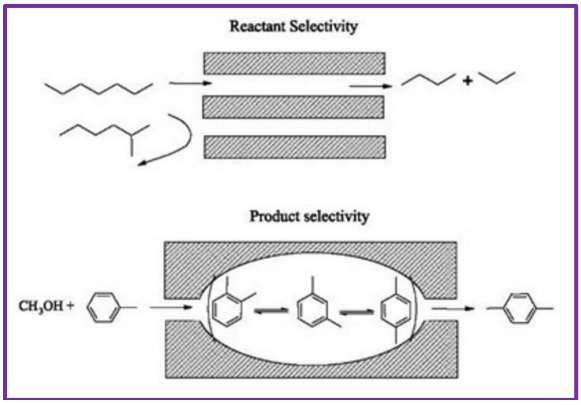

Figure 1.4 Reactant and product selectivity. Reproduced with permission from Elsevier (from ref. 11)[11].

The encapsulated catalysts can also use as a bifunctional catalyst to combine two different active sites in one particle. If the core catalyst which is used for a reaction is encapsulated with a shell membrane which is used as a catalyst for another reaction, the reactants could be converted by the shell to intermediate which can then access the inner core catalyst. To leave the core catalyst, all the intermediates must enter the membrane channels, where they converted into the final products at the active sites in the membrane [12]. For instance, many studies [11-19] have used core-shell bifunctional catalysts for Fischer-Tropsch Synthesis core catalyst with a zeolite membrane shell which is used for isomerization and cracking reaction since zeolites have acidic property, varied molecular diffusion rate in their pores and product selectivity property (Figure 1.4) which occurs when some of the product formed within the pores are too bulky to diffuse out as observed products. Thus, the products are converted to smaller molecules on the active sites of the shell while diffusing away from the core. In FTS encapsulated catalysts, reactants pass through the zeolite membrane pores and reach the core FT catalyst where hydrocarbons form. When the formed hydrocarbons diffuse through the zeolite porous, they are cracked and isomerized by acidic sites of the zeolite to achieve a synthetic gasoline [15] (Figure 1.5).

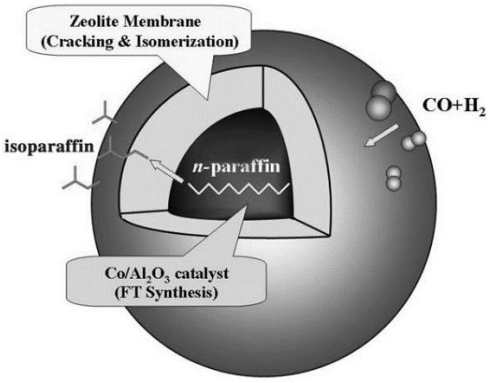

Figure 1.5 A schematic image of the capsule catalyst role in the FTS reaction. Reproduced with permission from John Wiley and Sons (from ref. 12)[12].

In addition, encapsulated structure can help to protect the core catalyst from deactivation caused by sintering due to migration and high temperature since the outer shells isolate the catalytically active nanoparticle cores and prevent the possibility of sintering of core particles during catalytic reactions even under harsh reaction conditions [4, 6, 20] (Figure 1.6).

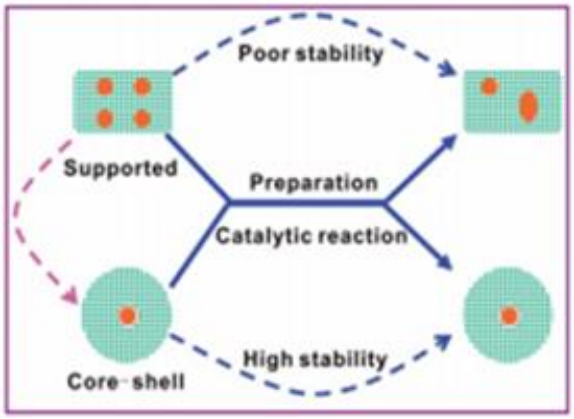

Figure 1.6 Difference of supported and encapsulated catalysts in terms of inhibiting migration and aggregation. Reproduced with permission from Royal Society of Chemistry (from ref. 6)[6].

The mobility of reactants in the encapsulated catalyst also plays important role to obtain high activity. Galanti et al. have recently proposed that the change in polarity of the shell network, (especially thermosensitive hydrogel shell) alters the mass transport from bulk to the catalyst through shell medium [21]. Another study demonstrated that the catalytic activity of the encapsulated nanoparticles is decreased when shrinking the network by increasing the temperature and this occurred due to an increased diffusional resistance mass transport within the shrunk network[22] (Figure 1.7).

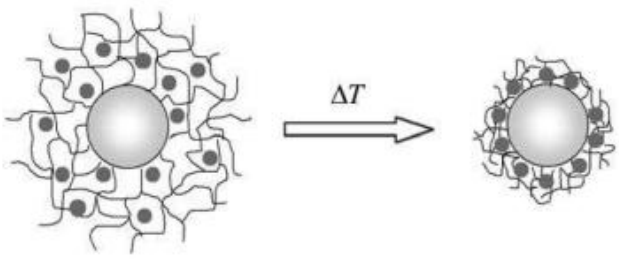

Figure 1.7 PS-NIPA-Ag composite particles consisting of thermosensitive core–shell particles in which Ag nanoparticles are embedded. The composite particles are suspended in water which swells the thermosensitive network attached to the surface of the core particles. In this state the reagents can diffuse freely to the nanoparticles that act as catalysts. At higher temperatures (T>308C) the network shrinks and the catalytic activity of the nanoparticles is strongly diminished. Reproduced with permission from John Wiley and Sons (from ref. 22)[22].

According to Galanti et al. [21], the reactants diffuse through a free-energy environment of the shell. This environment impacts the reactants' solvation free energies when entering the shells from bulk, which is regarded as adsorption free energy or transfer free energy. As an example, the free energy of a reactant may be lowered upon entering the network and thus the number of reactant molecules in the network will be increased, so that their increased concentration in the vicinity of the catalyst will lead to a higher reaction rate. In their study, based on this explanation, a theory was developed to calculate the total reaction rate of core–shell catalysts with multiple catalysts embedded in the shell[21].

As explained, there are many advantages of the encapsulated catalysts. In this chapter, studies made in the literature for inorganic encapsulated catalysts for XTL processes will be reviewed and discussed. Catalytic application of the encapsulated catalysts in which the core is a metal and shell is the mesoporous or microporous inorganic materials (such as zeolites, SiO_2, CeO_2 etc.) in the reforming, water-gas shift (WGS) and Fischer-Tropsch Synthesis (FTS) steps of the XTL processes will be explained.

CHAPTER 2: BACKGROUND AND LITERATURE SURVEY[2]

2.1 Hydrocarbon Reforming

Reforming is a key step of the XTL process to produce syngas (CO and H_2). Syngas can be synthesized using three processes: steam reforming, CO_2 reforming (dry reforming) and oxy methane reforming (partial oxidation). The combination of steam and oxy reforming can also be used as a fourth process which is known as auto thermal reforming (ATR). In the auto thermal reforming, steam and oxygen are combined in proportions to give a net $\Delta H \sim 0$ [23]. Steam reforming (1), CO_2 reforming (dry reforming (2)), oxy methane reforming (3), and auto thermal reforming (4) reactions are given below:

$$CH_4\,(g) + H_2O\,(g) \longrightarrow CO\,(g) + 3H_2\,(g) \qquad (1)$$

$$CH_4\,(g) + CO_2\,(g) \longrightarrow 2CO\,(g) + 2H_2\,(g) \qquad (2)$$

$$CH_4\,(g) + 1/2\ O_2\,(g) \longrightarrow CO\,(g) + 2H_2\,(g) \qquad (3)$$

$$4CH_4\,(g) + 2H_2O\,(g) + O_2\,(g) \longrightarrow 10H_2\,(g) + 4CO\,(g) \qquad (4)$$

Catalysts for steam reforming are transition metals from group VIII such as Ni, Pd, Co, Rh, Ru, Pt and Ir [24-26]. Similarly, most of the catalysts studied for dry reforming are Ni, Pd, Pt, Ru, Co, Rh, and Ir[27-29]. SiO_2, Al_2O_3, TiO_2, La_2O_3, CaO, MgO, CeO_2 and ZrO_2have been used as oxide supports and K, Mg, Ca and La have been used as promoters to improve the performance of catalysts [23, 29-31].

[2] This chapter has been accepted as a book chapter of "Encapsulated Catalysts" Book by "Elsevier".

Catalyst deactivation one of the biggest challenge in catalytic steam reforming and dry reforming processes. Nickel is inexpensive relative to the other metals and thus it is most studied catalyst for reforming processes. However, supported Ni catalysts deactivate by carbon formation, sulfur poisoning, and loss of active sites due to the sintering of nickel particles[32, 33]. Ni particle size is an important factor for the activity of steam reforming catalysts since smaller particles will provide a larger surface for reaction and improved catalyst activity [34]. Smaller particles have also been reported to be more resistant to carbon formation [34]. Thus, encapsulation of the Ni particles may prevent the possibility of sintering during catalytic reactions causing by migration and high temperature since encapsulation of the Ni catalyst with a stable shell will keep particle size smaller by inhibiting the migration and aggregation and help to protect catalyst from coking.

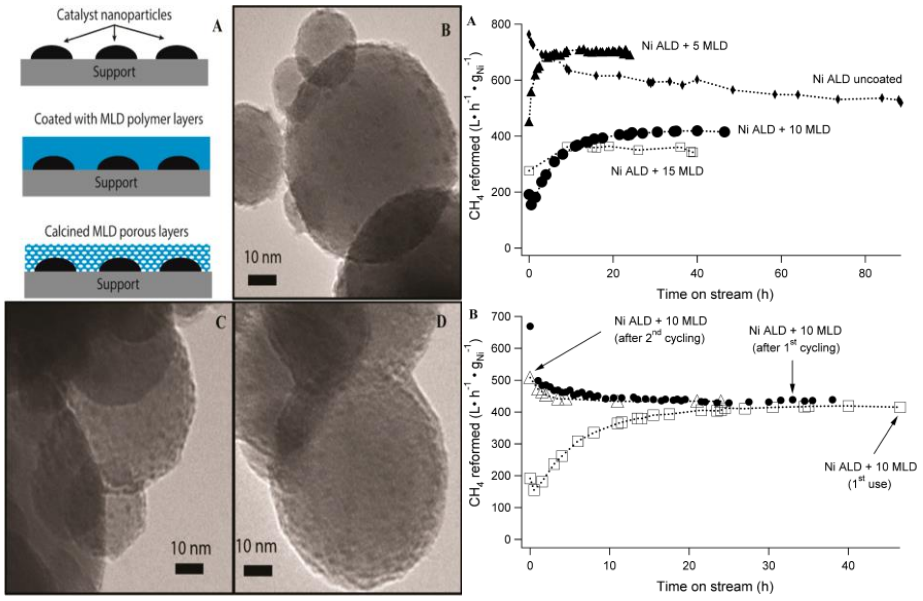

Figure 2.1 Left figure: (A) MLD coating process. (B) Ni nanoparticles; (C) 5-MLD cycles and (D) 10-MLD cycles. Right figure: (A) Dry reforming at 973 K (B) Effect of cycling on the DRM rates. Reproduced with permission from American Chemical Society (from ref. 36)[36].

Encapsulation of supported Ni catalysts in an inorganic systems for reforming process have been studied recently to protect the catalysts from deactivation and improve their performance.

High reaction temperatures can be employed to thermodynamically inhibit coke formation [35]. However, high temperatures increase catalyst sintering, thereby reducing conversion and coke resistance. Thus, to hinder sintering and coking of Ni particles during the dry reforming (DRM), Gould et al.[36] prepared a porous alumina coated Ni/Al_2O_3 particles using molecular layer deposition (MLD). The study found that the dry reforming rates for the MLD-coated catalysts stayed stable for 108 h. while uncoated catalyst continuously deactivated during DRM at 973 K (Figure 2.1).

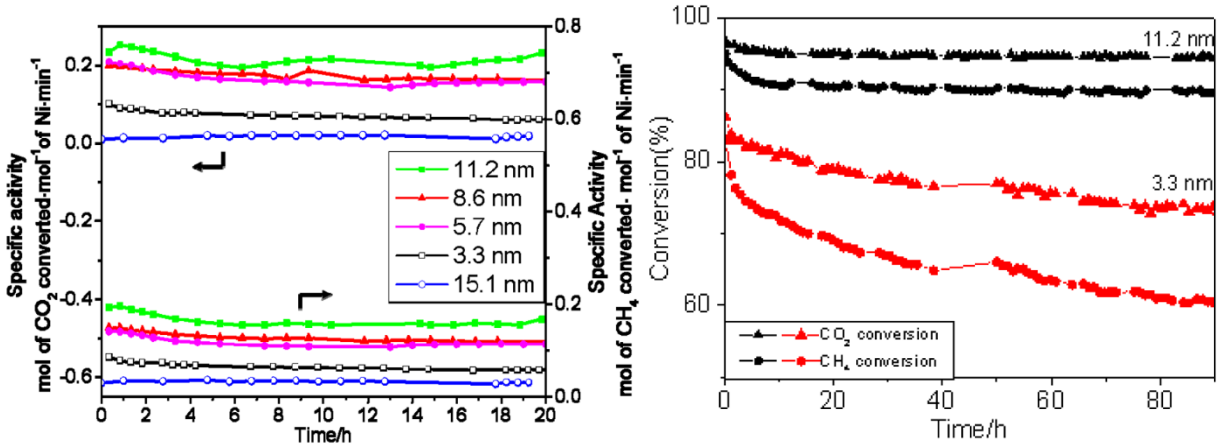

Figure 2.2 Specific activity for $Ni@SiO_2$ and $Ni{-}yolk@Ni@SiO_2$ with different shell thicknesses (a). Conditions: 800 °C, GHSV = 1440 $L{\cdot}g{-}1\ cat{\cdot}h{-}1$, Wcat = 0.01 g, CO_2:CH_4:N_2 = 1:1:1. Stability test for $Ni@SiO_2$ with 3.3 nm shell thickness and $Ni{-}yolk@Ni@SiO_2$ with 11.2 nm shell thickness (b). Conditions: 800 °C, GHSV =36 000 $mL{\cdot}g{-}1\ cat{\cdot}h{-}1$, CO_2:CH_4:N_2 = 1:1:1. Reproduced with permission from American Chemical Society (from ref. 37)[37].

In addition to improved stability, encapsulation of the reforming catalysts have been also studied to achieve high activity. Encapsulation can yield large interfaces between materials, which contributes to active metal-support interactions. For instance, Li et al. synthesized a yolk−satellite−shell structured $Ni{-}yolk@Ni@SiO_2$ with a different shell thicknesses (3.3 nm, 5.7 nm, 11.2 nm and 15.1 nm) for dry reforming to obtain high catalytic activity and stability[37]. The authors found that a small increase in shell thickness from 3.3 to 5.7 nm resulted in a nearly

doubled increase in CH_4 specific activity and a tripled increase in CO_2 specific activity (Figure 2.2a). The 11.2 nm shell thickness Ni−yolk@Ni@SiO_2 demonstrated the most stable and active result for the with CH_4 and CO_2 specific activities (Figure 2.2b).

In another study, Li et al. synthesized Ni@Ni-Mg phyllosilicate core−shell catalysts by the hydrothermal treatment of Ni@SiO_2 nanoparticles to increase the exposed Ni area for reactants [38]. The authors improved of catalytic performance of DRM reaction due to the high Ni accessibility, strong basicity, and high structural stability of the Ni@Ni- phyllosilicate core−shell catalyst. Besides the stability and activity, encapsulation of the reforming catalysts is used to improve reactant selectivity. Reactant selectivity is a property of the porous materials which occurs when only part of the reactant molecules are small enough to diffuse through the pores [11] (Figure 1.4). For this aim, catalysts are encapsulated with a microporous material such as zeolites since they have uniform pore dimensions and microporous character permits small molecules to enter the crystals while rejecting others with large molecular size [10].

2.2 Water-Gas Shift Reaction

The water gas shift (WGS) is a catalytic process to convert CO and H_2O to produce H_2 as shown in reaction (5). This process was first reported by Mond and Langer in 1888 [39]. WGS catalysis has an important role in the industry for the production of ammonia, methanol, and hydrogen [40]. This reaction is also used in XTL process to produce synthetic fuel with the steam reforming of hydrocarbons, to adjust the H_2/CO ratio of the produced gas stream.

$$CO\,(g) + H_2O\,(g) \longleftrightarrow CO_2\,(g) + H_2\,(g) \qquad \Delta H°_{298} = -41.2 kj/mol \qquad (5)$$

To balance between kinetics and thermodynamic limitations, the WGS reaction is usually conducted in two or three-stage catalytic converters instead of one to make the process more economical [41]. The first stage is a high temperature step that is operating at 320-450°C, favoring

fast CO consumption and minimizing catalyst bed volume and the second stage is low temperature step that is operating at 200-240°C to get higher conversions [42, 43].

The catalyst selection for WGS reaction depend on which stage that the catalyst will be used. There are two main types of WGS catalysts. The first type is promoted iron oxide catalysts which are high temperature shift (HTS) catalysts[42, 44]. They are active at high temperatures (320–450°C). The second type is copper oxide catalysts which are low temperature shift (LTS) catalysts and used at relatively low temperatures (180–260°C) [42, 45, 46]. Besides these catalysts, precious metal- based catalysts (mainly platinum and gold) have been studying recently for use in fuel cell applications [47-49].

Despite developments on Fe and Cu catalysts, rapid deactivation is major issue over such catalysts[50, 51]. Addition noble metals, use different promoters, improving strong metal– support interaction with porous structures or confined metal into a well-defined channel are some of the methods that are used in the literature to solve deactivation problems[52]. Encapsulating metals with inorganic shells such as SiO_2, Al_2O_3, CeO_2, ZrO_2, Fe_2O_3, and TiO_2 are currently receiving great attention due to their high thermal stability and high level of metal–support interaction [52-54]. For instance, Yeung et al**.** reported that the microemulsion prepared ceria encapsulated noble metal catalysts which show a comparable or even higher catalytic activity towards the WGS reaction than those catalysts prepared by traditional methods due to the intimate contact with noble metal particle and cerium oxide [53, 55, 56]. In another study, Yeung et al**.** compared the WGS and methanation activities of commercial $Cu/ZnO/Al_2O_3$, Co-precipitated 2% Pt/ceria, Wet impregnated 5% Pt/ceria, Ceria encapsulated 5% Pt and ceria encapsulated 5%Pt -5%Au core-shell catalysts and they found that bimetallic core of Pt and Au in a 1:1 ratio at 5wt% with respect to the ceria shell showed the highest WGS activity with no methanation activity.[45] Saw et al**.**

synthesized bimetallic Ni-Cu core encapsulated by a CeO_2 shell catalyst using combined method of positive emulsion and self-assembly [52]. They varied the core loadings and compared with conventional impregnation method in the WGS reaction and they found that the core-shell catalyst exhibited higher catalytic activity at 500°C than the supported catalyst with the same metal loadings due to high level of metal-support interaction and small bimetallic Ni-Cu particle size. Wieder et al. synthesized an alumina-supported, Pd@CeO_2, core-shell catalyst having 1 wt % Pd and 9 wt % ceria for the water-gas-shift (WGS) reaction and found that the Pd@CeO2 catalyst initially exhibited similar WGS rates to that of a conventional Pd/ceria catalyst, but the catalyst deactivated severely over the period of 1 h. This deactivation was explained that the reduced Pd@CeO_2/ Al_2O_3 catalysts do not adsorb CO thus these catalysts lose activity for the WGS reaction as they undergo reduction [57].

Cargnello et al. developed a new synthesis method for Pd@CeO_2 core shell nanoparticles that are easily dispersible in common organic solvents since the dispersibility core-shell structures with oxide shells is a key property for avoiding formation of aggregates[58]. They demonstrated that the Pd@CeO_2 core–shell impregnated Al_2O_3 support showed significant CO uptake and the Pd is accessible to CO and water, implying that the ceria shell must be porous [58]. In later study, Cargnello et al**.** synthesized and compared 1-wt% Pd-CeO_2 catalysts prepared by co-precipitation of Pd nanoparticles with ceria (Pd@CeO_2-CP), by a microemulsion procedure (Pd@CeO_2-ME), and by normal impregnation of Pd salts (Pd/CeO_2-IMP) to test the concept that Pd-CeO_2 catalysts could be more stable for the water-gas-shift (WGS) reaction when the Pd is embedded in CeO_2 [59]. The authors found that Pd@CeO_2-ME sample demonstrated good stability for WGS, suggesting that more effective encapsulation of Pd can limit the sintering of the metal phase and resulting in stable catalysts under high temperature reaction (400°C) as shown in Figure 2.3.

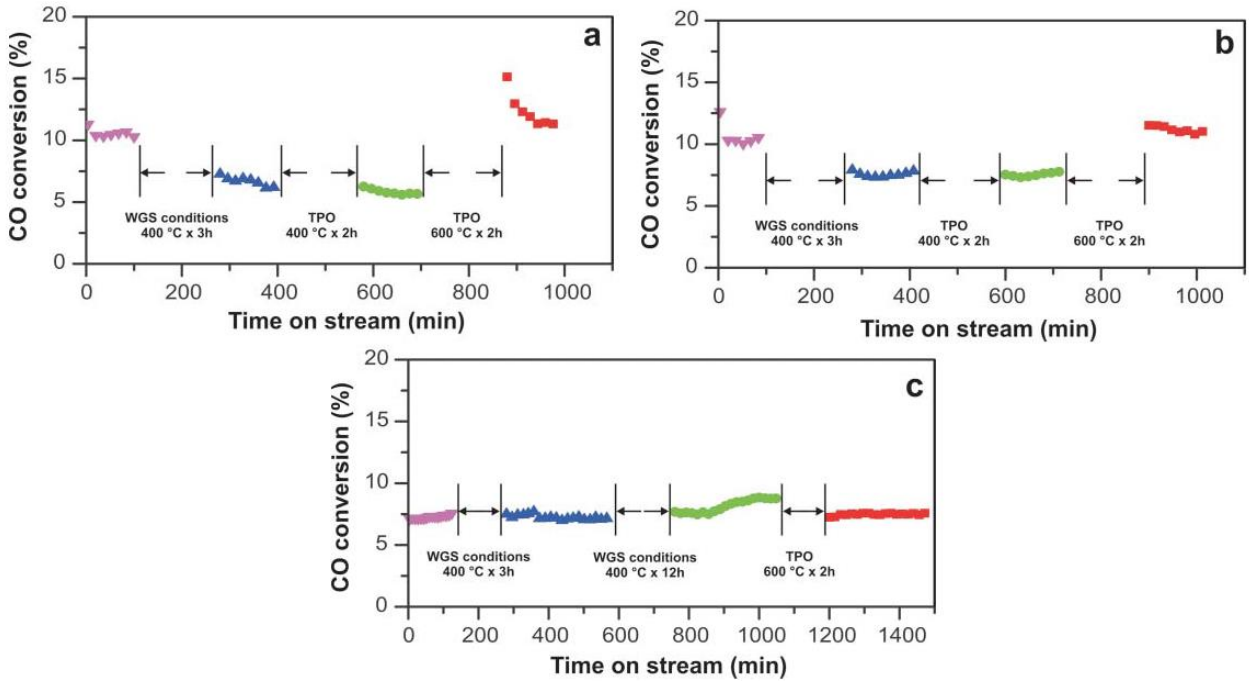

Figure 2.3 CO conversions at 250 ℃ (a,b) and 300 ℃ (c) under WGSR conditions of Pd/CeO_2-IMP (a), Pd@CeO_2-CP (b) and Pd@CeO_2-ME (c) catalyst after different subsequent treatments. Reproduced with permission from Royal Society of Chemistry (from ref. 59)[59].

2.3 Fischer-Tropsch Synthesis

Fischer-Tropsch Synthesis (FTS) is the last step of the various XTL technologies and employed to synthesize liquid fuel from syngas. Franz Fischer and Hans Tropsch discovered Fischer-Tropsch Synthesis in 1922 converting a mixture of carbon monoxide and hydrogen to hydrocarbons using an iron catalyst [60]. The FTS reaction is a strongly exothermic polymerization reaction (ΔH=-165-204 kJ/mol CO) [61-67].

The most common Fischer–Tropsch catalysts are Fe, Co, Ni, Rh, and Ru[67-70]. Co and Fe have been mostly used in industry due to their advantages such as low price (compared to Rh and Ru) and lower methane selectivity (compared to Ni based catalysts) [67, 70, 71]. However, promoters are required for Fe and Co catalysts to achieve good activity and selectivity. Although hydrocarbons produced by FTS reaction are sulfur, nitrogen, and aromatics-free, which makes the

FTS products capable of being desirable fuels, desired product selectivity of FTS reaction is low[72]. In order to obtain high selectivity in FTS reaction, 'egg-shell' Co catalysts have been developed by Exxon[73, 74] and core-shell type catalysts have been studied widely since then. Especially using zeolites to encapsulate core FTS catalysts is the most chosen method to increase the desirable product selectivity since zeolites have product selectivity property (Figure 1.4), varied molecular diffusion rate in their pores and acidic property. They are also used as hydrocracking and isomerization catalysts in industry due to their acidic property.

The details of the Fischer-Tropsch Synthesis reactions (main and side reactions) are demonstrated in Table 2.1.

Table 2.1 Reactions in the Fischer-Tropsch Synthesis (FTS)
Reproduced with permission from Elsevier (from ref. 68) [68]

Main Reactions:		
1. Parrafins	$(2n+1)H_2 + nCO \rightarrow C_nH_{2n+2} + nH_2O$	**(6)**
2. Olefins	$2nH_2 + nCO \rightarrow C_nH_{2n} + nH_2O$	**(7)**
3. WGS Reaction	$CO + H_2O \leftrightarrow CO_2 + H_2$	**(8)**
Side Reactions:		
4. Alcohols	$2nH_2 + nCO \rightarrow C_nH_{2n+2}O + (n-1)H_2O$	**(9)**
5. Catalyst oxidation/reduction	(a) $M_xO_y + yH_2 \leftrightarrow yH_2O + X\text{m}$	**(10)**
	(b) $M_xO_y + yCO \leftrightarrow yCO_2 + xM$	**(11)**
6. Bulk carbide formation	$yC + xM \leftrightarrow M_xC_y$	**(12)**
7. Boudouard reaction	$2CO \rightarrow C + CO_2$	**(13)**

In zeolite encapsulated bifunctional catalysts, the reactants first diffuse the zeolite membrane porous and arrive to FTS sites, which convert the syngas into long-chained linear hydrocarbons. These intermediate products desorb and diffuse through to the acidic sites of the zeolite shell where they undergo further hydrocracking and isomerization to form desired branched hydrocarbons (i.e., gasoline cut) to exit the catalyst (Figure 2.4) [12, 15]. The role of the encapsulated catalyst structure is to separate two active sites where the different reactions catalyzed

independently which is crucial for product selectivity. Moreover, the encapsulated bifunctional catalyst is expected to show high selectivity in a consecutive reaction as it improves the collision possibility between intermediates and active sites significantly[12]. The main difference of the encapsulated catalyst and the conventional bifunctional catalysts that are prepared by mixing is the active sites are distributed randomly in the conventional bifunctional catalysts. Thus, the cascade reactions happen randomly, which cause the intermediate products can leave without reacting at the other active sites which means low desired product selectivity[12]. Furthermore, shape selectivity for the products also is expected since molecules of different sizes have a different diffusion efficiency in the membrane channels [12, 14]. Thus, low diffusion rate of the long-chain hydrocarbons forces them stay in the zeolite membrane layer longer which means having a higher chance of isomerization and cracking reaction inside the membrane[15].

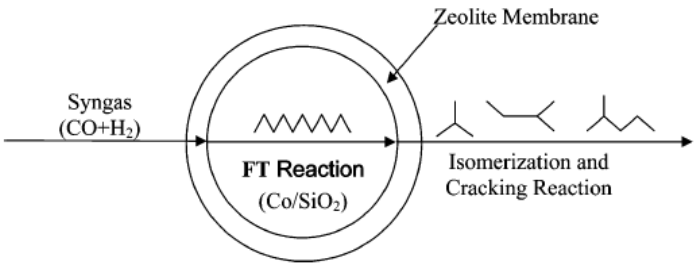

Figure 2.4 A schematic image of the capsule catalyst role in the FTS reaction. Reproduced with permission from American Chemical Society (from ref. 15)[15].

There are many studies on the literature about the zeolite encapsulated FTS catalyst. For instance, Bao et al**.** studied core/shell catalyst which H-beta zeolite membrane was coated directly onto the surface of a Co/Al_2O_3 pellet to increase the selectivity of isoparaffins in the FTS reaction [12]. The authors observed that the formation of C_{12+} hydrocarbons suppressed completely and the middle isoparaffins became the main products. Yoneyama et al. synthesized Co/SiO_2 core and

HZSM-5 zeolite shell FTS catalyst to produce isoparaffins from synthesis gas[19]. The authors obtained low methane selectivity and high isoparaffin selectivity in FTS reaction using Co/SiO_2/HZSM-5 hybrid catalyst for one-step isoparaffin production from syngas. Li et al**.** investigated H-β zeolite-enwrapped Co/Al_2O_3 FTS catalyst and they also got extremely high isoparaffin selectivity and the catalyst stayed stable for 10 h without deactivation[16]. He et al**.** encapsulated H-ZSM-5 membrane onto the surface of the Co/SiO_2 pellet to increase selectivity of light hydrocarbon in FTS reaction [15]. They found that long-chain paraffin selectivity reduced when use encapsulated catalyst due to secondary isomerization and hydrocracking on the zeolite shell [15]. In another study, He et al**.** examined the thickness effect of the H-ZSM-5 zeolite shell on selectivity of the FTS reaction and they found that methane selectivity increased with the zeolite membrane thickness since H_2 diffuses more quickly than CO through the shell[14]. Bao et al. synthesized H-ZSM-5/fused-iron core-shell catalyst for the synthesis reaction of isoparaffin from syngas [13]. The result of their study showed that the formation of C_{10+} hydrocarbons suppressed completely and the middle isoparaffins became the main products and they achieved low methane selectivity. Yang et al. synthesized H-ZSM-5 zeolite shell on the Co/SiO_2 FTS catalyst using physically adhesive method and hydrothermal synthesized method and compared their catalytic performance with physically mixed catalyst on the direct synthesis of light isoparaffin from syngas [18]. The authors observed that the selectivity of light isoparaffin obtained by zeolite capsule catalysts increase sharply and the formation of heavy hydrocarbons suppressed comparing to physically mixed H-ZSM-5 and Co/SiO_2 catalyst. Yang et al. synthesized H-ZSM-5 and Silicalite-1 zeolite encapsulated $Cu/ZnO/Al_2O_3$ core-shell catalysts for Dimethyl ether (DME) production from syngas and compare the activity and selectivity with uncoated catalyst. The authors found

that the higher DME selectivity but lower activity (CO% conversion) on the core-shell catalysts due to the coverage of the active sites by zeolite crystals[17] (Figure 2.5).

catalyst	Si/Al[b]	zeolite (%)	CO conversion (%)	selectivity (%)		
				MeOH	DME	others
CZA			44.02	98.38	0.50	1.12
CZA-Z[c]	32	7.60	5.59	3.41	96.59	0.00
CZA-S[d]	221	9.63	30.40	21.43	78.57	0.00
CZA-M[e]	163	10.0	58.07	57.29	40.51	2.20

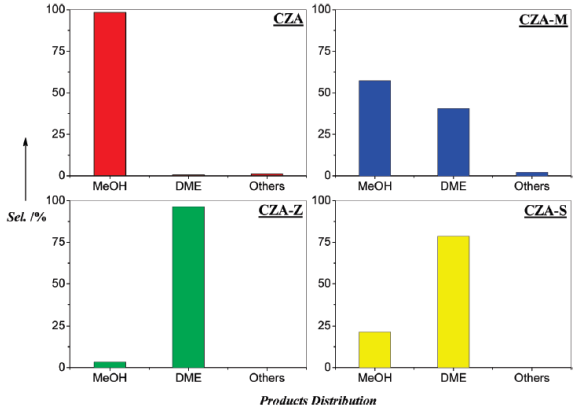

Figure 2.5 Catalyst catalytic performance in syngas to DME reaction and products distribution of $Cu/ZnO/Al_2O_3$ catalyst (CZA), H-ZSM-5 and Silicalite-1 zeolite capsule catalysts (CZA-Z and CZA-S, respectively) and the physically mixed catalyst (CZA-M). Reproduced with permission from American Chemical Society (from ref. 17)[17].

To sum up, XTL processes have received an immense deal of interest in recent years. Although these processes are very attractive, active, selective, and stable catalysts for XTL process steps (e.g., Reforming, Water-Gas Shift (WGS) and Fischer-Tropsch Synthesis (FTS)) are crucial to achieve affordable synthetic fuel. Encapsulated catalysts (core-shell, yolk-shell etc.) have been studied widely in the literature over the last several years to increase stability and activity and product and reactant selectivity for applications in catalysis, especially in Reforming, Water-Gas Shift (WGS) and Fischer-Tropsch Synthesis (FTS). Encapsulating metals with inorganic shells such as SiO_2, Al_2O_3, CeO_2, ZrO_2, Fe_2O_3, and TiO_2 are currently receiving great attention due to

their high thermal stability and high level of metal–support interaction for the water-gas shift. Coating the Fe or Co catalysts is studied to obtain high product selectivity (especially isoparaffin selectivity) for FTS step in the XTL processes. The studies have been done in the literature about encapsulated catalysts give promising results that is showed encapsulation can be used to increase stability, activity, control the reactant selectivity and obtain high desirable product in the XTL processes.

2.4 Objectives

As mentioned in the previous section, XTL processes are promising processes to produce synthetic liquid fuels from biomass natural gas, and coal. Among the XTL processes, biomass to liquid process (BTL) particularly attractive since it is a sustainable, environmentally friendly source of carbon for liquid fuel production. Although BTL is a promising process, production synthetic fuel from the gasification route, regardless of feedstock source, there is an economy-of-scale issue which means it requires very large and expensive production facilities. Moreover, the first gasification and steam reforming step in these processes is highly endothermic and lose enormous amounts of energy to the surroundings. The Fischer-Tropsch Synthesis (FTS) step is exothermic, so the energy released here cannot be recycled back to the first step.

In one routes of BTL process, biomass is gasified to produce a gas mixture of CO, CO_2, H_2 and hydrocarbons including methane and heavier hydrocarbons such as tars. Steam reforming (SR) is used to convert the methane and other hydrocarbons to carbon monoxide and hydrogen. The Fischer-Tropsch process (FTS) is a technique to convert a mixture of carbon monoxide and hydrogen, called synthesis gas or syngas, into hydrocarbon chains of varying lengths.

Methane and Toluene steam reforming, Water-gas shift (WGS), and Fischer-Tropsch Synthesis (FTS), reactions are as follows:

$$CH_4 + H_2O \longrightarrow CO + 3H_2 \qquad \Delta H° = 206.1\ kj/mol$$

$$C_7H_8 + 7H_2O \longrightarrow 7CO + 11H_2 \qquad \Delta H° = 869.1\ kj/mol$$

$$CO + H_2O \longrightarrow CO + 3H_2 \qquad \Delta H° = -41.1\ kj/mol$$

$$CO + (2n+1)H_2 \longrightarrow C_nH_{2n+2} + nH_2O$$

Another main challenge in this route is H2:CO ratio in the product. The preferred ratio of H_2:CO ratio is 2 for Fischer-Tropsch Synthesis but biomass is hydrogen deficient and the ratio is further decreased by a significant portion of the hydrogen atoms remaining locked in hydrocarbons, especially methane. The steam reforming of hydrocarbons, to improve the H2:CO ratio, is generally conducted as part of the gas conditioning. However, tars (single and polycyclic aromatic hydrocarbons with a molecular weight equal or higher than benzene) cause the steam reforming catalysts to deactivate rapidly, which decreases the methane conversion to syngas. To achieve a catalyst capable of reforming methane without potential for deactivation by aromatic hydrocarbons, the method of encapsulation using a multi-core reforming catalyst with porous zeolite shell was studied. Zeolite encapsulated core-shell reforming catalyst can allow CH_4 and H_2O to enter the core reforming catalyst and reduce or prevent larger molecules (i.e., C_7H_8).

The *overall objective* of this dissertation is to evaluate the ability of a zeolite coating to control the reactant selectivity to develop a composite catalyst for production of synthetic fuel from biomass derived syngas. For this main objective, in the 2nd Chapter of this study, 34.3 wt% H-β zeolite encapsulated 1.6wt%Ni/1.2wt%Mg/$Ce_{0.6}Zr_{0.4}O_2$ composite SR catalyst was studied to investigate reactant selectivity effect of the H-β zeolite shell on methane and toluene (as a tar model) steam reforming. In the 3rd chapter, the effect of zeolite shell thickness, which is proportional to zeolite amount added, on the reactant selectivity was studied on 51 wt% H-β zeolite encapsulated 1.6wt%Ni-1.2wt%Mg/$Ce_{0.6}Zr_{0.4}O_2$ steam reforming composite catalyst. In the 4th

Chapter, zeolite acidity effect was studied on the reactant selectivity using a 51 wt% non-acidic silicalite-1 zeolite encapsulated 1.6wt%Ni-1.2wt%Mg/$Ce_{0.6}Zr_{0.4}O_2$ steam reforming composite catalyst. Lastly, in the 5th chapter, 60 wt% H-β zeolite encapsulated low temperature 0.16wt%Pt–1.34wt%Ni–1.00wt%Mg/$(Ce_{0.6}Zr_{0.4})O_2$ steam reforming composite catalyst was synthesized for use in the combination of steam reforming and Fischer-Tropsch synthesis catalyst.

CHAPTER 3: MOLECULAR-SIZE SELECTIVE H–β ZEOLITE-ENCAPSULATED CE-ZR/NI-MG CATALYSTS FOR STEAM REFORMING[3]

3.1 Introduction

Biomass gasification and subsequent fuel synthesis (BTL) is one route for the conversion of biomass to fuels. In this process, biomass is gasified to produce syngas, a mixture of CO, CO_2, H_2, H_2O, contaminants, and hydrocarbons including methane and heavier hydrocarbons such as tars [75]. Steam reforming (SR) is used to further convert the methane and other hydrocarbons to syngas [76]. The main reactions in SR of tar (using toluene as a surrogate) contaminated methane are as follows [77-79]:

$$CH_4 + H_2O \longrightarrow CO + 3H_2 \qquad \Delta H° = 206.1\ kj/mol \qquad (1)$$

$$CO + H_2O \longrightarrow CO_2 + H_2 \qquad \Delta H° = -41.1\ kj/mol \qquad (2)$$

$$C_7H_8 + 7H_2O \longrightarrow 7CO + 11H_2 \qquad \Delta H° = 869\ kj/mol \qquad (3)$$

Reaction (1) is methane steam reforming, Reaction (2) is water-gas shift and Reaction (3) is toluene steam reforming reactions. A main challenge in this route is the low H_2:CO ratio in the product. The H_2:CO ratio is required as 2 for Fischer-Tropsch Synthesis and methanol synthesis, but biomass is hydrogen deficient and the ratio is further decreased by a significant portion of the hydrogen atoms remaining locked in hydrocarbons, especially methane. Syngas produced from

[3] Reprinted with permission from U. Cimenler, Babu Joseph, and J. N. Kuhn Molecular-size selective H-β zeolite-encapsulated Ce-Zr/Ni-Mg catalysts for steam reforming. *Applied Catalysis A: General* 505 (2015): 494-500.

biomass gasification typically has a H_2:CO ratio of approximately 1 and substantial CH_4 amounts (i.e., H_2:CO:CH_4 = 1:1:0.5) [75]. The steam reforming of hydrocarbons, to improve the H_2:CO ratio, is generally conducted as part of the gas conditioning. However, tars (single and polycyclic aromatic hydrocarbons with a molecular weight equal or higher than benzene [80]) cause the catalysts to deactivate rapidly, which decreases the methane conversion to syngas [81].

The development of a catalyst that can reform methane in the presence of tars could allow the tars to be removed via scrubbing methods following the high temperature processing steps, which would improve the thermal integration of the overall process and permit the use of catalysts over longer lifetimes as catalyst regeneration steps (repeated high temperature processing of nickel catalysts causes sintering and loses of activity [82]) would be needed less frequently. These benefits would contribute positively to the economics.

To achieve a catalyst capable of reforming methane without potential for deactivation by tars, the encapsulation of a core reforming catalyst with porous shell is examined here. Zeolites have been used for their specific properties such as microporosity, molecular sieve and good hydrothermal stability [10, 83, 84]. The micropores permit some small molecules to enter the core and reject large molecules [10]. Thus, a zeolite encapsulated catalyst could allow CH_4, H_2O to the core reforming catalyst and reduce or prevent larger molecules (i.e., C_7H_8).

Although Ni catalysts are widely studied SR catalysts, coke formation and rapid deactivation are some challenges in these catalysts [85-90]. CeO_2 is a largely used promoter with Ni to decrease sintering, improve oxygen storage capacity (OSC), and increase sulfur tolerance [88, 91, 92]. The use of zirconia in conjunction with ceria increases OSC, which is extremely important to the stability, redox property, activity and selectivity of the catalyst [85, 93-95]. Addition of MgO with high basicity can reduce coke formation and sintering by decreasing Lewis acid sites [96, 97]. A

catalyst of Mg promoted Ni supported on Ceria-Zirconia (1.6wt%Ni-1.2wt%Mg/$Ce_{0.6}Zr_{0.4}O_2$) was selected for this study. Mg and Ni weight percentage and Ce:Zr molar ratio were selected as 8 % and 0.6:0.4, respectively, since higher methane conversion was found [85] when this formulation is compared to different ones involving the same components. The main purpose of this study is to investigate the ability of a zeolite coating to control the conversion via reforming of hydrocarbon reactants based on their size. An H-β zeolite shell was used to coat the core SR catalyst since its pores are between the sizes of CH_4 and C_7H_8 (tar model) and it has good thermal stability properties [98-100]. With further refinement, this approach is anticipated to be of use selective conversion of hydrocarbons via reforming and benefit BTL processes.

3.2 Experimental

3.2.1 Synthesis

3.2.1.1 Synthesis of H-β Zeolite

The H–β zeolite was synthesized by a hydrothermal synthesis method as reported by Li et al.[101]. To prepare the H–β zeolite precursor solution, 14.4 g of 25 wt% Tetraethylammonium Hydroxide (TEAOH) in water (Acros Organics, Inc.), 4.1 g of SiO_2 (99.98% pure; CAB-O-SIL M-5, scintillation grade, Acros Organics, Inc.), 0.3 g of $((CH_3)_2CHO)_3Al$ (Aluminum iso-propoxide, ≥ 98% pure; Sigma– Aldrich, Inc.), and 3.6 g of deionized water were mixed under continuous stirring at room temperature for 2 h. Then, the H–β zeolite precursor solution was added into the hydrothermal synthesis equipment and it was kept at 155°C for 3 days for crystallization. The resulting material was centrifuged to separate liquid and solid phases. The solid part was washed with distilled water until its pH value was less than 8. Then, it was dried at 120°C for 12 h and was calcined at 550 °C for 8 h. The composition of the

H–β zeolite precursor solution was prepared with a Si/Al=47.24 ratio. (Please see Appendix F for flowchart)

3.2.1.2 Synthesis of 1.6wt%Ni-1.2wt%Mg/$Ce_{0.6}Zr_{0.4}O_2$ Steam Reforming Core Catalyst

The core SR catalyst 1.6wt%Ni-1.2wt%Mg/$Ce_{0.6}Zr_{0.4}O_2$ was synthesized in two steps. First, molar ratio 0.6:0.4 Cerium-Zirconium oxide catalayst was synthesized by a co-precipitation method as reported by Rossignol et al.[102]. For this, $Ce(NO_3)_3x6H_2O$ (99.5% pure; Alfa Aesar, 6.5 g) and $ZrO(NO_3)_2xH_2O$ (99.9% pure; Alfa Aesar); 2.49 g were dissolved in deionized (DI) water and precipitated by the addition of NH_4OH (27% w/w NH_3; Mallinckrodt Chemicals) to form a hydrous Ce/Zr solution. This mixture was filtered and re-dissolved into a 0.25M NH_4OH solution. The dilute solution was re-filtered and dried in an oven at 60°C for 1 h followed by 120°C overnight. Then, the dried catalyst was calcined at 800°C for 4 h. Second, Ni (8% by weight) and Mg (8% by weight) were loaded to the oxide support by wet impregnation (WI) as reported by Walker et al. [85]. For the WI method, appropriate amounts of salts were dissolved in deionized water. This homogeneous solution was added drop wise to the support until incipient wetness and dried at 120°C for 2 h. This step was repeated until all of the metal nitrate solution had been added to the support. Following the final drying step, the catalyst was calcined at 500°C for 4 h.

3.2.1.3 Synthesis of H-β Zeolite Coated Composite Steam Reforming Catalyst

H-β zeolite coated composite SR catalyst was prepared by physical coating (PhyC) method as given by Pinkaew et al. [103] Silica sol (Ludox: 40 wt.%, Sigma Aldrich, Inc.) was used as binder for H-β zeolite to SR catalyst. 3.07 g of silica sol was diluted with 1.5 times DI water (~4.6 g) by weight. Then, diluted silica sol was added to 1.03 g SR catalyst dropwise and 0.54 g of H-β zeolite powder was mixed with the moistened SR catalyst in a round bottomed flask, followed by vigorously shaking until the formation of one uniform zeolite shell coating on the surface of core

catalyst. The obtained catalyst was calcined at 500°C for 2 h to increase the mechanical strength of zeolite shell, which resulted in a 34.3 wt% of H-β zeolite encapsulated composite SR catalyst. Pellet size of encapsulated composite catalyst was between 0.64-1 mm. 14 wt% H-β zeolite encapsulated composite catalyst was also synthesized in the same method to compare with the 34.3 wt% sample. (Please see Appendix F for flowchart).

3.2.1.4 Preparation of Physical Mixture Catalyst

The physical mixture of SR and H-β zeolite catalyst was prepared by mechanically mixing the SR catalyst and H–β zeolite. The mass of H–β zeolite was 34.3wt%, a loading that was the same as for the encapsulated catalyst. To prepare the physical mixture catalyst for CH_4 SR reaction 7.4 mg catalyst and 3.87 mg H-β zeolite and for C_7H_8 SR reaction 10.3 mg catalyst and 5.4 mg H-β zeolite were used. To assess the H-β zeolite's role, a physical mixture catalyst with SR catalyst and Al_2O_3 was also prepared instead of using H-β zeolite based on 34.3 wt%.

3.2.2 Characterization Methods

X-ray diffraction (XRD), N_2 Physisorption, Scanning Electron Microscopy (SEM) and Energy Dispersion Spectroscopy (EDS) were used to characterize the catalysts. The X-ray diffraction (XRD) patterns were obtained on a Bruker AXS XRD in a step mode employing CuKα radiation (0.154 nm). The machine was operated in a Bragg angle (2θ) range of 5°-90° for H-β zeolite and H-β zeolite coated composite SR catalyst and 15°-90° for SR catalyst. The step size was 0.02 for H-β zeolite, 0.004 for SR catalyst. The X-ray tube was operated at 40 kV and at 40 mA. N_2 Physisorption experiments were performed using a Quantachrome Autosorb-iQ to obtain BET surface area and Horvath-Kawazoe (HK) method pore size distributions of the catalysts. The morphology of the samples was investigated with a Hitachi S-800 SEM coupled to an Ametek EDAX which can simultaneously provide the surface elemental composition information.

3.2.3 Steam Reforming

The reactions were carried out in a fixed bed quartz U-tube microreactor with an internal diameter of 4 mm. The catalyst was loaded between two layers of high temperature quartz wool. The U- tube reactor was placed into a Thermoscientific Thermolyne tube furnace. The furnace temperature was controlled using a Eurotherm 3110 PID controller. The U-tube reactor was fed from a manifold that was connected to Alicat Scientific mass flow controllers and two quartz bubblers. Helium was used as carrier gas in the system and in both the toluene and steam bubblers. Total flow rate was 75 sccm (0.64 % CH_4, 0.64 % H_2O, % 98.7 He) for CH_4 SR and 32.6 sccm (1 % C_7H_8, 7% H_2O, % 92 He) C_7H_8 SR. The reactor outlet was connected to a Perkin Elmer Gas Chromatography (GC) to analyze the effluent gas from reactor using Hayesep-D packed column and thermal conductivity detector (TCD). All of the feed and outlet lines were wrapped with heating tape to prevent condensation prior to entering the GC.

The sample with high H-β zeolite (34.3 wt%) loading that was encapsulated by the composite catalyst was the only composite catalyst used in the reactions The reason of not using the 14 wt% H-β zeolite encapsulated samples in the reactions was explained in the characterization results section. The mass of catalysts for CH_4 SR were 11.3 mg for SR catalyst alone, H-β zeolite coated SR catalyst, and physically mixed catalysts with H-β zeolite-SR catalyst and Al_2O_3-SR catalyst. Another mass (17.2 mg) of the H-β zeolite coated composite SR catalyst was also tested to compare same amount of SR catalyst (11.3 mg SR catalyst and 5.9 mg H-β zeolite of 17.2 mg H-β zeolite coated composite SR catalyst based on 34.3%). The mass of catalysts for C_7H_8 SR were 10.3 mg for the SR catalyst alone, 15.7 mg H-β zeolite coated SR catalyst and 15.7 mg physically mixed catalyst (10.3 mg SR catalyst and 5.4 mg H-β zeolite of 15.7 mg based on 34.3%) and 5.4 mg H-β zeolite. Reaction conditions were 780-800-820-840° C, atmospheric pressure, and

stoichiometric feeds (i.e., molar ratio of CH_4/H_2O = 1 and C_7H_8/H_2O=7 for the respective reactions). The reactions were also conducted on $Ce_{0.6}Zr_{0.4}O_2$ support by itself, H-β zeolite alone, and blank reactor at the same reaction conditions. There was not any conversion during CH_4 SR and only conversion for the H-β zeolite alone during C_7H_8 SR.

The reaction procedure was similar for both the CH_4 and C_7H_8 SR reactions. The catalysts were heated (ramp rate of 10°C/min) under helium gas (5 sccm) to 120°C and held there for 30 min. The samples were then heated (10 °C/min) to 800°C in helium gas (50 sccm) and the gas flow was switched to 5% H_2/He (50 sccm) for a 2 h reduction. After the reduction, the temperature was increased (rate of 10°C/min) to the highest reaction temperature and reactions were started. After conversions reached steady state at each temperature the subsequent temperatures were conducted sequentially in decreasing order.

The Mears criteria were calculated for the various catalysts ranged from ~10^{-3} to ~10^{-5} and thus indicated that external transport limitations (since each << 0.15) were not present in this study. The Weisz-Prater Criteria were also calculated and, for CH_4 SR, the values were ~10^{-7} for the uncoated catalyst and ~4 for H-β zeolite coated SR catalyst. According to Weisz-Prater Criterion, there was no internal mass diffusion limitations for uncoated SR catalyst since ~ 10^{-7} <<1. However; there was internal mass diffusion limitations for H-β zeolite coated SR catalyst since 4 >1. An analysis of the C_7H_8 reforming was also conducted and resulted in similar values and conclusions.

Methane and toluene conversion and product selectivity were calculated using the following equations:

$$\text{CH}_4 \text{ conversion} = X_{CH4} = \left(1 - \frac{Moles\ of\ of\ CH4\ out}{Moles\ of\ of\ CH4\ in}\right) * 100$$

$$C_7H_8 \text{ conversion} = X_{C7H8} = \left(1 - \frac{Moles\ of\ of\ C7H8\ out}{Moles\ of\ of\ C7H8\ in}\right) * 100$$

$$\text{Selectivity of a product} = S_P = \left(\frac{Moles\ of\ a\ certain\ carbon\ product}{\sum moles\ of\ carbon\ products}\right) * 100$$

3.3 Results and Discussion

3.3.1 Catalyst Characterization

The XRD patterns of pure H-β zeolite powder (a), H-β zeolite coated composite catalyst (b), bare SR catalyst (e), C_7H_8 SR post-reaction H-β zeolite coated composite catalyst (c) and C_7H_8 SR post-reaction physical mixture catalyst (d) are presented in Figure 3.1. Miller indices are also shown for each diffraction line with the red and black text indicating the contributions from the SR and H-β zeolite phases, respectively. The diffraction pattern of the prepared H-β zeolite and SR catalyst are consistent with the standard H-β zeolite framework structure in the zeolite database and literature indicating the successful synthesis of H-β zeolite and SR catalyst [85, 99, 104].

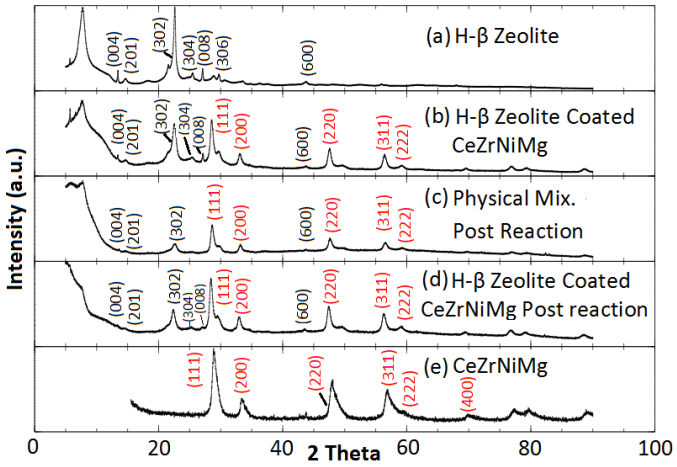

Figure 3.1 XRD patterns of H-β zeolite (a), H-β zeolite coated SR catalyst (b), C_7H_8 SR post-reaction sample of physical mixture (c), C_7H_8 SR post-reaction sample of H-β zeolite coated SR catalyst (d) SR catalyst (e). Red and black miller indices indicate SR catalyst and H-β zeolite peaks, respectively. CeZrNiMg represents SR catalyst.

In addition, the synthesized H-β zeolite coated composite catalyst XRD peaks perfectly matched with the synthesized H-β zeolite and SR catalyst, as given in Figure 3.1. Therefore, it can be concluded that there were no obvious changes in the SR catalyst during the preparation process of zeolite capsule catalyst. When post-reaction patterns are compared with the pre-reaction patterns, all H-β zeolite and SR catalyst diffraction lines are still present, which indicated that the materials were not altered under reforming conditions.

BET analysis was performed and the results are listed in Table 3.1. The respective BET surfaces areas of H-β zeolite and $Ce_{0.6}Zr_{0.4}O_2$ were determined as 784 m^2/g and 39 m^2/g, which are consistent with standard H-β zeolite (with the similar Si/Al ratio) and $Ce_{0.6}Zr_{0.4}O_2$ surface areas found [85, 101, 105]. The surface area of $Ce_{0.6}Zr_{0.4}O_2$ slightly decreased from 39 m^2/g to 35 m^2/g when 8wt% Ni and 8wt% Mg were loaded to the oxide support. A similar decrease upon metal loading was also seen in literature [85, 106]. The reason for surface area diminishment is explained as pore blockage by the loaded metals [85]. The H-β zeolite coated composite catalysts of 34.3 wt % and 14 wt % possessed BET surface areas of 196 and 78 m^2/g, which are between the H-β zeolite and SR catalyst surface areas and it is expected that the composite catalyst with more of the zeolite would have a higher surface area.

Table 3.1 BET surface area results

Catalyst	BET Surface Area (m^2/g)
H-β zeolite	784[a]
Ce0.6 Zr0.4O2	39
1.6wt%Ni-1.2wt%Mg/$Ce_{0.6}Zr_{0.4}O_2$	35[b]

Table 3.1 (Continued)

H-β zeolite coated composite 1.6wt%Ni-1.2wt%Mg/$Ce_{0.6}Zr_{0.4}O_2$ (34.3 wt% zeolite)	196[b]
H-β zeolite coated composite 1.6wt%Ni-1.2wt%Mg/$Ce_{0.6}Zr_{0.4}O_2$ (14 wt% zeolite)	78

[a] The average of two batches of samples is reported.
[b] The average of repeated experiment of the same sample is reported.

The pore size distribution of H-β zeolite and C_7H_8 SR post-reaction H-β zeolite coated catalysts (34.3%) were analyzed with Horvath-Kawazoe (HK) method. The isotherms are shown in Figure 3.2, with the pore size distribution results as inserts. The pore sizes relative to the selected hydrocarbon reactants of interest are also noted. In Figure 3.2 (A; insert), the pore size of H-β zeolite is between 0.43-0.57 nm, which is smaller than C_7H_8 (0.67 nm) and larger than CH_4 (0.4 nm). This result confirmed that H-β zeolite should be able to be used for enhance CH_4 conversion relative to C_7H_8 conversion based on size arguments.

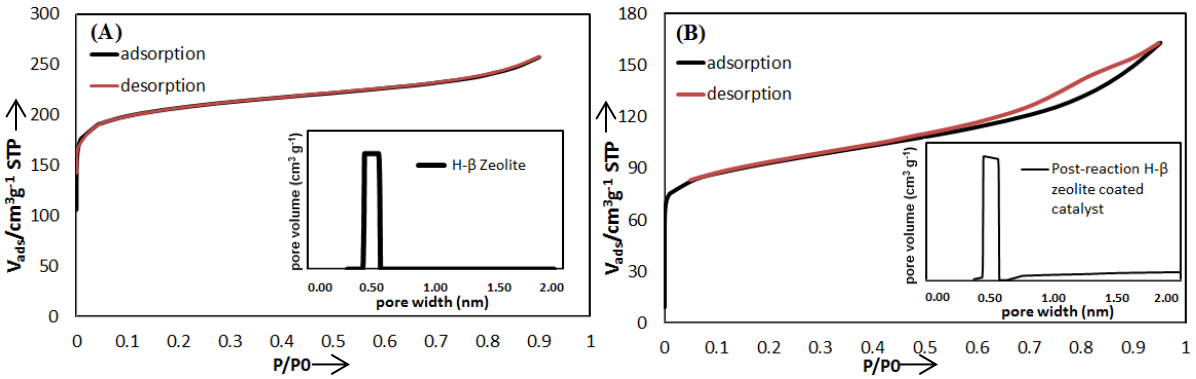

Figure 3.2 Isotherms and pore size distributions of pre-reaction H-β zeolite (A) and C_7H_8 SR post-reaction H-β zeolite coated composite catalyst (34.3wt% H-β zeolite) (B).

In Figure 3.2 (B), the isotherm and pore size distribution (insert) is shown for the C_7H_8 SR post-reaction H-β zeolite coated composite catalyst. After reaction, pore size was found between 0.43-0.57 nm and this result showed pore size did not change during the reactions. The primary

difference, other than the lower specific surface area, in the composite catalyst compared to the zeolite alone is the presence of mesopores (indicated by the hysteresis) contributed by the $(Ce,Zr)O_2$ support. The mesopores in the composite catalyst, but not the zeolite alone, was confirmed by the BJH pore size analyses. However, these results are not indicative that the core SR catalyst was completely coated by the zeolite shell.

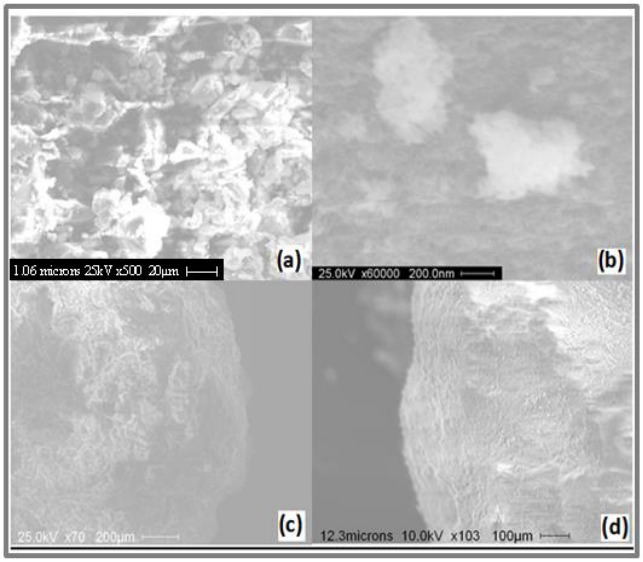

Figure 3.3 SEM images, (a) and (b) SR catalyst, (c) 14 wt % H-β zeolite coated composite catalyst and (d) 34.3 wt% H-β zeolite coated composite catalyst surfaces

SEM images of the SR catalyst, 14 wt% and 34.3 wt% H-β zeolite coated composite catalyst surface SEM images are compared and presented in Figure 3.3. Images (a) and (b) present the SR core catalyst and images (c) and (d) show the 14 wt% and 34.3 wt% H-β zeolite coated composite catalyst surfaces, respectively. As it is seen from the Figure 3.3 (c), the 14 wt% H-β zeolite coated composite catalyst surface is not even, which indicates that this sample is not coated very well. However, 34.3 wt% H-β zeolite coated composite catalyst shell is very uniform and homogeneous. This distinction can be seen as color difference in the 14 wt% and 34.3 wt% H-β

zeolite coated composite catalysts since 34.3 wt% sample's surface has pure white like H-β zeolite's color, 14 wt% sample's surface has very similar color with SR catalyst.

EDS result (Table 3.2) shows that Mg and Ce core catalyst elements are on the surface of 14 wt% H-β zeolite coated composite catalyst. However, Ce, Mg, Zr and Ni on 34.3 wt% H-β zeolite coated composite catalyst were not detected. Hence, from SEM images and EDS analyses, it can be concluded that 34.3 wt% H-β zeolite coated composite catalyst is coated with H-β zeolite, but 14 wt% sample is either not completely coated or the coating contains some thin areas. Thus, 34.3 wt% H-β zeolite coated composite catalyst was used for the reaction studies.

Table 3.2 EDS results of 14wt% and 34.3wt% H-β zeolite coated composite SR catalysts

Elements (wt%)	**Si**	**Al**	**Mg**	**Ce**	**Zr**	**Ni**	**Total**
14 wt% H-β zeolite coated catalyst	92	2	2	4	-	-	100
34.3 wt% H-β zeolite coated catalyst	97	3	-	-	-	-	100

3.3.2 Reaction Results

CH_4 SR conversions with the SR catalyst (curve (a)), H-β zeolite coated composite catalyst (curves (b) and (d) of different total catalyst loading), and physically mixed SR and H-β zeolite catalysts (curves (c) and (e); identical replicate experiments) are presented in Figure 3.4 as a function of temperature (Example GC peaks and CH_4 SR conversion calculation for the sample 34.3 wt% H-β zeolite encapsulated composite catalyst 17.2 mg total catalyst and reaction temperature is for 800 °C is given in Appendix G). Carbon balances are compiled in Table 3.3 and indicated that significant coke formation was not occurring due to the high accounting of the

carbon species. Results showed that the CH_4 conversion increased with increasing temperature for all catalysts. This case was more notable for the uncoated SR catalyst (Figure 3.4 curve (a)) which is consistent with Weisz-Prater Criterion calculation result as discussed in section 2.3 that showed that this catalyst was not mass transfer limited and thus Arrhenius-type behavior would be expected.

Surprisingly, the H-β zeolite shell on the SR catalyst significantly increased the CH_4 conversion when comparing the SR catalyst alone (curve (a)) with the composite catalysts (curves (b) and (d)). Compared to the SR catalyst alone (curve (a)), the composite catalysts are compared both at the same total catalyst mass (curve (d)) and the same SR catalyst mass (curve (b)). Whereas it is not surprising that increasing the total catalyst mass of the composite catalyst increased the conversion (comparison of curves (b) and (d)), both composite catalyst loadings, even the one with less SR catalyst than the SR catalyst alone, yielded higher CH_4 conversion compared to the SR catalyst alone even though there was no CH_4 conversion for the zeolite by itself. Physically mixed SR and H-β zeolite catalysts were also investigated (curves (c) and (e)). These are replicate experiments to show the typical reproducibility of the catalyst experiments. The physically mixed catalysts demonstrated similar (only at highest temperature tested) or higher CH_4 conversions compared to the SR catalyst alone. Also, compared to the composite catalysts, the physically mixed catalysts possessed lower CH_4 conversions. The temperature dependency of every sample containing (physically mixed and coated) the zeolite demonstrated behavior consistent with diffusional limitations, which was in agreement with the values of the Weisz-Prater Criterion.

The higher catalytic activity of the catalyst containing zeolite compared to the uncoated SR catalyst could be explained by three different ways. The first reason could be acidity of H-β zeolite shell. It is well-known that zeolites present good performance for catalytic cracking due to their

acidic properties. The higher catalytic activity of H-β zeolite shell is compatible with literature. Wang et al. studied CH_4 SR reaction on HZSM-5 supported Ni catalyst and they observed that very high CH_4 conversion with zeolite supported catalyst [107]. A second reason could be that the Al^{3+} interact with active sites of SR catalyst and promote the reaction. Third, the higher activity of the composite catalysts could be explained by confined reaction effects [12]. A confined reaction environment would increase reaction intermediates contact time with active metal sites and result in increased CH_4 conversion. The fact that the composite catalyst yielded higher conversions than the physical mixtures is consistent with a confined reaction effect, as there is less spatial restriction between the reactants and active sites for the physical mixtures than the composite catalysts. The Al^{3+} promotion and zeolite acidity effect would not be the reason by themselves, unless there are undetectable interactions between the components (beyond just the physical interface; e.g., migration of Al) because the physically mixed catalysts have an equivalent area of interaction between the zeolite and SR catalyst components as the composite catalysts. To further probe these potential explanations, a physical mixture of SR catalyst and Al_2O_3 was prepared (instead of H-β zeolite, compared on same total and component masses as curve (d)) and result is showed in curve (f). The physical mixture of the SR catalyst with Al_2O_3 also has higher CH_4 conversion than steam reforming catalyst by itself and similar CH_4 conversion with physical mixtures containing the zeolite. Since this alumina is not microporous and alumina is generally considered to have weaker acidity than zeolites, this result confirmed that the promotion of the Al^{+3} ion is one of the factors contributing the increased activity when comparing the physically mixed catalysts and SR catalyst by itself. To conclude, the confined reaction effect is proposed to play a large role in the higher conversion of the composite catalyst compared to both the SR catalyst alone and the physical mixture of the SR catalyst with various components. The Al^{+3} promotion plays a key role of the

physically mixed catalyst, both as compared to the SR catalyst alone. The set of experiments, including the controls, suggests that both factors play a role in the high conversion of the composite, layered catalyst.

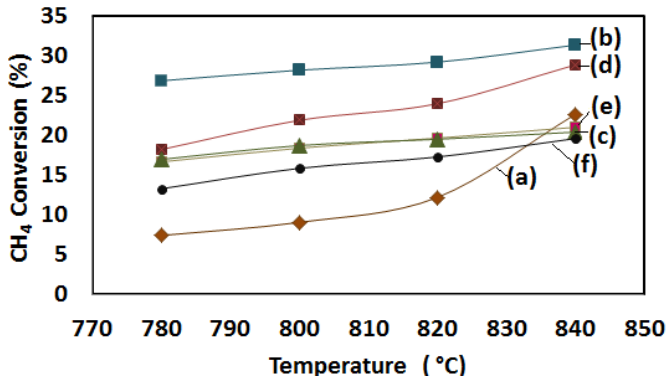

Figure 3.4 CH_4 steam reforming results. (a) Uncoated SR catalyst, (b) 17.2 mg and (d) 11.3 mg H-β zeolite coated (34.3 wt%) composite catalyst, (c) and (e) Physical mixture catalyst of H-β zeolite and SR catalyst, (f) Physical mix. catalyst with Al_2O_3 and SR catalyst.

C_7H_8 SR was performed as a function of temperature (Figure 3.5) on SR catalyst alone (curve (a)), H-β zeolite coated composite catalyst (curve (b)), physically mixed SR and H-β zeolite catalysts (curve (c)) and just H-β zeolite (curve (d)). Again, carbon balances (Table 3.3) indicated that significant coke formation was not occurring due to the high accounting of the carbon species.

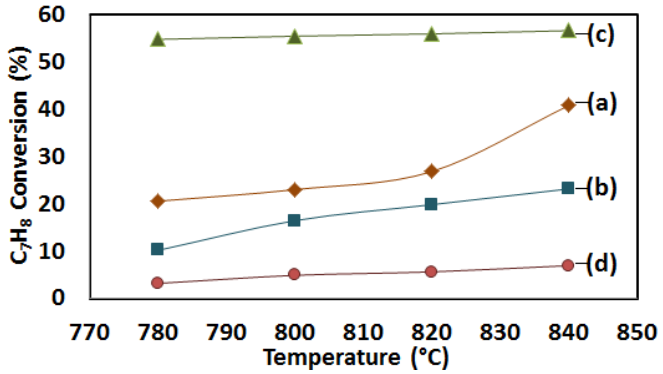

Figure 3.5 C_7H_8 steam reforming results. (a) Uncoated SR catalyst, (b) 34.3 wt% H-β zeolite coated composite catalyst, (c) Physical mixture of H-β zeolite and SR catalyst, (d) H-β zeolite.

As shown in Figure 3.5, the C_7H_8 SR results followed similar trends with CH_4 SR results except H-β zeolite coated composite catalyst result. The physically mixed catalyst with H-β zeolite and SR catalyst (curve(c)), which has same amount of SR catalyst with curve (a), has significantly higher C_7H_8 conversion due to the reasons that are mentioned above. Moreover, H-β zeolite has measurable C_7H_8 conversion, unlike CH_4 SR, as can be seen in curve (d). This also contributed to C_7H_8 conversion on the physically mixed catalyst reaction. The H-β zeolite coated composite catalyst (curve (b)) has lower C_7H_8 conversion than uncoated SR catalyst (curve (a)) unlike CH_4 SR due to shape selectivity effect of H-β zeolite. H-β zeolite pores has smaller dimensions than C_7H_8 molecular dimension (0.67 nm) and its porous hindered entering and reaching C_7H_8 molecules to the steam reforming catalyst and reacting on it, partially. However coating SR catalyst with H-β zeolite reduced the catalytic activity on C_7H_8 SR, it could not prevent the activity completely. Although not observed via the characterization, small cracks in the H-β zeolite shell could be responsible for the presence of this activity. The small cracks could be the result of imperfect growth, but the grain boundaries due to the inherent polycrystallinity of the zeolite H-β zeolite shell is also a likely contribution. Most synthetic zeolites are polycrystalline [108] and polycrystallinity could cause increased permeability due to defects in intercrystalline spaces [109]. Encapsulation with thicker H-β zeolite shell on the SR catalyst could help to reduce the amount of cracks and thereby could reduce the activity.

While H-β zeolite encapsulated SR catalyst curves are exponential shapes, uncoated and physically mix catalysts curves are more linear shape in Figure 3.4 and Figure 3.5. This result was expected due to the internal diffusion limitation in the H-β zeolite coated SR catalysts as indicates in section 2.3.

The selectivity of the carbon products of the reactions were calculated to investigate the H-β zeolite coating effect on carbon product selectivity and results are given in Figure 3.6. CO % selectivity increases and CO_2 % selectivity decreases with increasing temperature for uncoated SR catalyst in CH_4 SR as seen in Figure 3.6 (a). However, CO % selectivity is very high and does not change much with temperature when H-β zeolite coated on SR catalyst. The reason could be water gas shift reaction for high CO_2 % selectivity when using uncoated SR catalyst. Physical mixture catalyst indicated CO % selectivity between uncoated and coated SR catalyst's CO % selectivity in the CH_4 SR reaction. H-β zeolite coated, uncoated SR and physical mixture catalyst's CO % selectivity did not change much with temperature and demonstrate very high CO selectivity in C_7H_8 SR as seen Figure 3.6 (b).

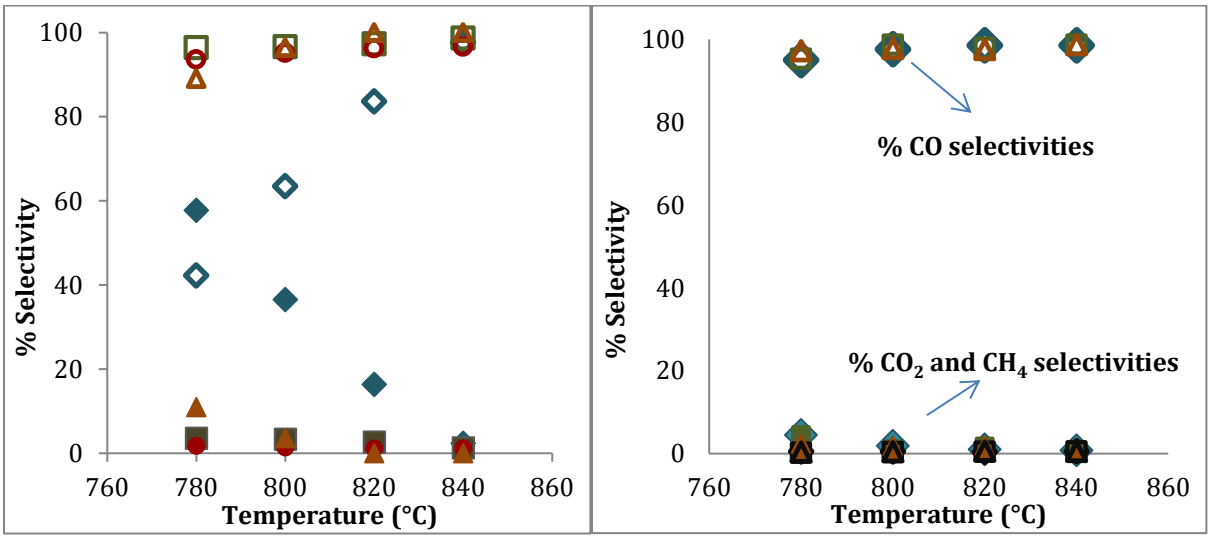

(a) **(b)**

Figure 3.6 % Selectivity of the carbon products of reactions (a) % selectivity for CH_4 SR reaction (b) % selectivity for C_7H_8 SR reaction. Blue diamond indicates uncoated SR catalysts, Green quare and red circle indicate 11.3 mg and 17.2 mg H-β zeolite coated catalysts respectively, orange triangle indicates physical mixture catalysts for both reactions. Unfilled, filled and filled-black lined markers demonstrate CO, CO_2 and CH_4 % selectivity, respectively.

Table 3.3 CH_4 and C_7H_8 SR reaction carbon balances

CH_4 SRR				**C_7H_8 SRR**			
Uncoated Steam Reforming catalyst		**H-β zeolite coated SR catalyst**		**Uncoated Steam Reforming catalyst**		**H-β zeolite coated SR catalyst**	
Temp. (°C)	$\|\%Error\|$	Temp.(° C)	$\|\%Error\|$	Temp.(° C)	$\|\%Error\|$	Temp.(° C)	$\|\%Error\|$
840	1.4	840	4.3	840	0.7	840	4.6
820	0.6	820	3.4	820	1.6	820	2.2
800	0.5	800	3.5	800	5.4	800	0.7
780	1.5	780	3.7	780	6.4	780	0.8

CHAPTER 4: EFFECT OF ZEOLITE MEMBRANE SHELL THICKNESS ON REACTANT SELECTIVITY FOR HYDROCARBON STEAM REFORMING USING LAYERED CATALYSTS[4]

4.1 Introduction

Microporous materials are of great industrial importance as catalysts, membranes for separation, sorbents and ion-exchange materials due to their large surface areas and well defined pores with molecular dimensions.[110-114] Zeolites, which are crystalline aluminosilicate microporous materials with well-ordered channels, are interesting as selective catalysts because of their ability to control diffusion among reactants and products (shape selectivity).[111, 112, 115-118] Although Barrer [119] first recognized zeolite's high surface area and molecular dimensions of the pores and applied them to the separation of linear and branched hydrocarbons in 1940's, the concept of "shape-selectivity" was described first by Weisz and Frilette in 1960.[120] Shape selectivity is divided into three groups based on whether pore size limits the entrance of the reacting molecule (reactant selectivity), the departure of the product molecule (product selectivity), or the formation of certain transition states (restricted transition state selectivity).[11, 121] Shapeselective catalysis can be used to increase yields of preferred products by product selectivity or tohinder undesirable reactions by reactant selectivity.[121, 122] In our prior study, the proficiency

[4] Reprinted with permission from U. Cimenler, B. Joseph, and J. N. Kuhn. Effect of Zeolite Membrane Shell Thickness on Reactant Selectivity for Hydrocarbon Steam Reforming Using Layered Catalysts. *Energy & Fuels* (2016). Copyright © 2016, American Chemical Society.

of a zeolite membrane encapsulation was studied to control the conversion using reactant selectivity property during steam reforming of various sized hydrocarbon reactants as a way to prevent potential deactivation by tars in biomass-to-liquid processes.[123] An H-β zeolite membrane (pore size 0.43-0.57 nm) was used to encapsulate the inner SR catalyst since its pores are between the sizes of CH_4 (0.4 nm) and C_7H_8 (tar model-0.67 nm).[124] Results showed that, due to mass transfer effects, the composite H-β zeolite coated reforming catalyst demonstrated a decrease in C_7H_8 conversion and increase in CH_4 conversion when compared to the uncoated reforming catalyst. Although C_7H_8 conversion decreased when coated with the zeolite membrane, C_7H_8 was still converted by 34.3 wt% zeolite coated composite catalyst due to the cracks in the H-β zeolite membrane formed during the C_7H_8 SR reaction. The objective of the current study is to examine if the selectivity can be improved by increasing the shell thickness, which was controlled by increasing the zeolite amount added. Tsapatsis et al. studied zeolite membrane thickness effect on separation n-butane (0.43nm) and isobutane (0.55nm) using MFI type zeolite (pore size is 0.55 nm).[125] The authors found that increasing zeolite membrane thickness reduces the isobutane flux through the membrane due to the elimination of defects in the thicker zeolite membranes.

In the current effort, a double coating technique was applied to increase the zeolite loading (since limitations exist to add 51 wt % zeolite in a single step) and to achieve a thicker zeolite shell. The 51 wt % H-β zeolite was coated onto an SR a catalyst in two steps and steam reforming reactions were performed to investigate the zeolite shell thickness on the both CH_4 and C_7H_8 conversions for the composite catalyst. The conversion of hydrocarbons on this catalyst was compared with the performance of a 34.3 wt % zeolite coated composite catalyst and several control samples (components individually and their physical mixtures).

4.2 Experimental

4.2.1 Synthesis

4.2.1.1 Synthesis of H-β Zeolite

The H-β zeolite was synthesized with the method (hydrothermal synthesis) described in our previous study.[124] 14.4 g of 25 wt% Tetraethylammonium Hydroxide (TEAOH) in water (Acros Organics, Inc.), 4.1 g of SiO_2 (99.98% pure; CAB-O-SIL M-5, scintillation grade, Acros Organics, Inc.), 0.3 g of $((CH_3)_2CHO)_3Al$ (Aluminum iso-propoxide, ≥98% pure; Sigma–Aldrich, Inc.), and 3.6 g of deionized (DI) water was used to prepare H-β zeolite precursor solution. All chemicals were mixed under continuous stirring at room temperature for 2 h. The H-β zeolite precursor solution was added into an autoclave and it was kept at 155°C for 3 days for crystallization. After that, the solution was centrifuged to separate liquid and solid phases. The solid part was washed with distilled water until its pH value was less than 8. Then, it was dried at 120°C for 12 h and was calcined at 550 °C for 8 h. (Please see Appendix F for flowchart).

4.2.1.2 Synthesis of 1.6wt% Ni-1.2wt% Mg /$Ce_{0.6}Zr_{0.4}O_2$ Steam Reforming Core Catalyst

To synthesize core SR catalyst 1.6wt%Ni-1.2wt%Mg/$Ce_{0.6}Zr_{0.4}O_2$, molar ratio 0.6:0.4, Cerium-Zirconium oxide support was synthesized first by a co-precipitation method as reported by Rossignol et al.[102] For this, $Ce(NO_3)_3 \times 6H_2O$ (99.5% pure metal basis; Alfa Aesar, 6.5 g) and $ZrO(NO_3)_2 \times H_2O$ (99.9% pure metal basis; Alfa Aesar; 2.49 g) were dissolved in DI water and precipitated by the addition of NH_4OH (27%, w/w NH3; Mallinckrodt Chemicals) to form a hydrous Ce/Zr solution. This mixture was filtered and re-dissolved into a 0.25 M NH_4OH solution. The dilute solution was re-filtered and dried in an oven at 60 °C for 1 h followed by 120 °C overnight and calcination was performed at 800 °C for 4 h. Ni (1.6% by weight) and Mg (1.2% by weight) were loaded to the oxide support by wet impregnation (WI) as reported by Walker et al.[126]

For the WI method, appropriate amounts of $Mg(NO_3)_2 \times H_2O$ (99.999% pure metal basis; Alfa Aesar) and $Ni(NO_3)_2 \times 6H_2O$ (99.9985% pure metal basis; Alfa Aesar) were dissolved in DI water. This homogeneous solution was added drop wise to the support until incipient wetness and dried at 120 °C for 2 h. This step was repeated until all of the metal nitrate solution had been added to the support. Following the final drying step, the catalyst was calcined at 500 °C for 4 h. (Please see Appendix F for flowchart).

4.2.1.3 Synthesis of H-β Zeolite Coated Composite Steam Reforming Catalyst

The 51 wt % H-β zeolite coated composite SR catalyst was prepared by double physical coating method by modifying the single physical coating (physically adhesive) method given in the literature.[18, 103] Silica sol (Ludox: 40 wt%, Sigma–Aldrich, Inc.) was used as binder for H-β zeolite to SR catalyst. Silica sol (3.08 g) was diluted with 1.5 times DI water (4.6 g) by weight. The encapsulation of the H-β zeolite was performed in two steps. First, 0.52 g SR catalyst was wet impregnated by spraying the prepared silica sol solution and 0.16 g of the H-β zeolite powder was mixed with the moistened SR catalyst in a round bottomed flask, and was shook vigorously until zeolite shell formed. The obtained catalyst was dried at 120°C for 12 h and calcined at 500°C for 3 h. Then, the resulting material was wet impregnated one more time with prepared silica sol solution and 0.38 g of H-β zeolite powder was mixed with the moistened SR catalyst in a combustion boat, vigorously and carefully shaken until the formation of second zeolite shell coating. The obtained catalyst was dried again at 120°C for 12 h and calcined at 500°C for 3 h to increase the mechanical strength of zeolite shell, which resulted in a 51 wt% of H-β zeolite encapsulated composite SR catalyst. (Please see Appendix F for flowchart).

4.2.1.4 Preparation of Physical Mixture Catalyst

The physical mixture of SR and H-β zeolite catalyst was prepared by mechanically mixing the SR catalyst and H-β zeolite. The mass of H-β zeolite was 51 wt%, a loading that was the same as for the encapsulated catalyst. To prepare the physical mixture catalyst for CH_4 SR reaction 11.3 mg SR catalyst and 12.3 mg H-β zeolite and for C_7H_8 SR reaction 10.3 mg catalyst and 10.7 mg H-β zeolite were used. As control experiments to assess the H-β zeolite's role and space velocity effects on C_7H_8 conversion, physical mixture catalysts with SR catalyst/silicon dioxide (SiO_2) and SR catalyst/Silicon Carbide were also prepared instead of using H-β zeolite based on 51 wt% .

4.2.2 Characterization Methods

XRD was conducted using a Bruker AXS XRD equipped with CuK radiation source (0.154 nm) at 40 kV and 40 mA. The machine was operated in a Bragg angle (2θ°) range of 20–90°. The step size was 0.02 for H- zeolite, 0.004 for SR catalyst. N_2 Physisorption experiments were performed using a Quantachrome Autosorb-iQ to obtain BET surface area, pore volumes, and Saito and Foley (SF) method for pore size distributions. The samples were outgassed at 200°C overnight for H-β zeolite and coated composite catalysts and 2 h for SR catalyst prior to N_2 physisorption. The morphology of the samples was determined with a Hitachi S-800 SEM equipped with an Ametek EDAX which provide the information of surface elements (using tilt angle of 30°). In order to obtain the sample cross-section of the composite catalyst, SPI-Chem Cold Mount Epoxy Kit was used. To get cross section of the sample first, the resin and hardener was mixed and epoxy release agent was spread as a thin layer on the edge and the surface of a mold. Then, samples were placed the bottom of the mold and the mixture was slowly poured over the samples and allowed to dry about 24 h. After solidification, the resin was removed from the mold and polished carefully to view the particles cross-section. Finally, samples were coated gold-

palladium with a layer of using a Denton vacuum desk II sputter coater, to make sample conductive prior to imaging.

4.2.3 Reaction Studies

The reactions were performed using Thermoscientific Thermolyne furnace and a fixed bed quartz U-tube microreactor (internal diameter of 4 mm). The catalyst was loaded between two layers of high temperature quartz wool in the U- tube and it was placed into the furnace. Temperature of the furnace was controlled using a Eurotherm 3110 PID controller. A manifold that was connected to Alicat Scientific mass flow controllers and two quartz bubblers (toluene and steam) was used to feed the U-tube reactor. Total flow rate was 75 sccm (0.64% CH_4, 0.64% H_2O, 98.7% He) for CH_4 SR and 32.6 sccm (1% C_7H_8, 7% H_2O, 92% He) C_7H_8 SR and 32.6 sccm(1% C_7H_8, 1.5% CH_4, 7% H_2O, 90.5% He) for CH_4-C_7H_8 SR reactions together and steady state experiment. A Perkin Elmer Gas Chromatography (GC) that has Hayesep-D packed column and thermal conductivity detector (TCD) was used to analyze the effluent gas from reactor. All of the feed and outlet lines were wrapped with heating tape to prevent condensation prior to entering the GC. The mass of catalysts for CH_4 SR were 23.6 mg H-β zeolite coated SR catalyst (11.3 mg SR catalyst and 12.3 mg H-β zeolite of 23.6 mg based on 51wt%), 17.2 mg 51 wt% H-β zeolite coated SR catalyst (to compare the total equal mass of catalyst with 34.3 wt%), 23.6 mg physically mixed catalysts with H-β zeolite-SR catalyst, SiO_2-SR catalyst (11.3 mg SR catalyst and 12.3 mg H-β zeolite or SiO_2 of 23.6 mg based on 51wt%) and 12.3 mg H-β zeolite by itself. The mass of catalysts for C_7H_8 SR were 21 mg H-β zeolite coated SR catalyst and physically mixed catalyst with H-β zeolite, SiO_2 or and SiC catalyst (10.3 mg SR catalyst and 10.7 mg H-β zeolite, SiO_2 or SiC of 21 mg based on 51wt %) and 10.7 mg H-β zeolite by itself. CH_4-C_7H_8 SR reaction was performed for 23.6 mg and 21 mg H-β zeolite coated SR catalyst to analyze CH_4 and C_7H_8

conversion, respectively in presence of both reactant. Reaction conditions were 780-800-820-840 °C, atmospheric pressure, and stoichiometric feeds (i.e., molar ratio of CH_4/H_2O= 1 and C_7H_8/H_2O= 1/7 for the respective reactions). A long term steady-state experiment (10h) was also conducted utilizing the 23.6 mg 51 wt% H-β zeolite coated composite catalyst and 11.3 mg uncoated SR catalyst at 800 °C with molar ratio of $CH_4/C_7H_8/H_2O$ = 1.44/1/7. Information for the reactions (reaction type, catalyst composition, catalyst amount) and the notation used for each catalyst from this point forward is included in Table 4.1.

Table 4.1 Reaction types, catalysts composition and amounts

CH_4 Steam Reforming Total Flow Rate: 75 sccm (0.64%CH_4-0.64%H_2O-98.7%He)		
Catalyst Composition	**Notation**	**Catalyst amount (mg)**
Uncoated steam reforming catalyst:1.6wt%Ni-1.2wt%Mg/$Ce_{0.6}Zr_{0.4}O_2$	Uncoated SR	11.3
51wt% zeolite coated composite steam reforming catalyst	SR@ β51%	23.6 and 17.2
34.3wt% zeolite coated composite steam reforming catalyst	SR@ β34.3%	17.2
Physical mixture of H-β zeolite/SR catalyst	PM-51%β/SR	23.6 (11.3 mg SR-12.3mg H-β zeolite)
Physical mixture of Silicon dioxide/SR catalyst	PM-51% SiO_2/SR	23.6 (11.3 mg SR-12.3mg SiO_2)
H-β zeolite by itself		12.3
C_7H_8 Steam Reforming Total Flow Rate: 32.6 sccm (1% C_7H_8, 7% H_2O, 92% He)		
Catalyst Composition	**Notation**	**Catalyst amount (mg)**
Uncoated steam reforming catalyst:1.6wt%Ni-1.2wt%Mg/$Ce_{0.6}Zr_{0.4}O_2$	Uncoated SR	10.3
51wt% zeolite coated composite steam reforming catalyst	SR@ β51%	21
34.3wt% zeolite coated composite steam reforming catalyst	SR@ β34.3%	15.7
Physical mixture of H-β zeolite/SR catalyst	PM-51%β/SR	21 (10.3 mg SR-10.7mg H-β zeolite)
Physical mixture of Silicon dioxide/SR catalyst	PM-51% SiO_2/SR	21 (10.3 mg SR-10.7mg SiO_2)

Table 4.1 (Continued)

Physical mixture of Silicon Carbide/SR catalyst	PM-51% SiC/SR	21 (10.3 mg SR-10.7mg SiO_2)
H-β zeolite by itself (powder)		10.7
H-β zeolite by itself (pellet)		10.7
CH_4-C_7H_8 Steam Reforming Total Flow Rate: 32.6 sccm (1% C_7H_8, 1.5% CH_4, 7% H_2O, 90.5% He)		
Catalyst Composition	**Notation**	**Catalyst amount (mg)**
51wt% zeolite coated composite steam reforming catalyst	SR@ β51%	23.6 and 21
CH_4-C_7H_8 Steam Reforming Long Term Steady-State Experiment (10h) Total Flow Rate: 32.6 sccm (1% C_7H_8, 1.5% CH_4, 7% H_2O, 90.5% He)		
Catalyst Composition	**Notation**	**Catalyst amount (mg)**
51wt% zeolite coated composite steam reforming catalyst	SR@ β51%	23.6
Uncoated steam reforming catalyst:1.6wt%Ni-1.2wt%Mg/$Ce_{0.6}Zr_{0.4}O_2$	Uncoated SR	11.3

Weight hour space velocity (WHSV) and Gas hourly space velocity (GHSV) were calculated using the following equations:

$$\text{WHSV} = \left(\frac{Total\ mass\ feed\ to\ the\ reactor}{Total\ catalyst\ weight}\right) = h^{-1}$$

$$\text{GHSV} = \left(\frac{Total\ volumetric\ feed\ to\ the\ reactor}{Total\ catalyst\ volume}\right) = h^{-1}$$

High space velocities were used to keep conversions relatively so that differential rates could be used in the transport limitation calculations. Reactant selectivity was defined using the following equation:

$$\text{Reactant Selectivity} = \left(\frac{Conversion\ Rate\ of CH_4}{Conversion\ Rate of\ C_7H_8}\right)$$

Product selectivity was calculated using the following equation:

$$\text{Selectivity of a product} = S_P = \left(\frac{Moles\ of\ a\ certain\ carbon\ product}{\sum moles\ of\ carbon\ products}\right) * 100$$

Weisz-Prater Criterion (for calculation internal diffusion limitations, C_{WP}), Thiele modulus (Φ_n) and effectiveness factor (η) were calculated using the following equations:

$$C_{WP}=\frac{(-r_{Aobs}{}')*q_c*R^2}{D_e*C_{As}}$$

$$\Phi_n=R\sqrt{\frac{-r'_{As}*q_c}{D_e*C_{As}}}$$

$$\eta=\frac{3}{\Phi n^2}(\Phi\coth(\Phi)-1)$$

where $-r_{Aobs}{}'$ is measured values of the rate of reaction, q_c is density of solid catalyst, R is radius of the catalyst particle, D_e is effective diffusivity, C_{As} is reactant concentration external to the pellet.

4.3 Results and Discussion

4.3.1 Catalyst Characterization

XRD was performed to determine whether the zeolite phase was successfully formed in composite catalysts. The results for uncoated SR catalyst (a), pure H-β zeolite powder (b), SR@ β51% catalyst (c), CH_4 and C_7H_8 SR post reaction SR@ β51% catalyst (d) and (e), respectively and CH_4-C_7H_8 SR steady-state experiment post reaction SR@ β51% catalyst (f) are shown in Figure 4.1 with Miller indices as red and black text indicating the SR and H-β zeolite phases, respectively. The XRD patterns of the SR catalyst (a) and H-β zeolite (b) indicated that H-β zeolite and SR catalyst were synthesized successfully since their diffraction patterns are consistent with the literature[16, 126,124]. The SR@ β51% catalyst profile perfectly matched with the H-β zeolite and SR catalyst showing that composite catalyst did not change during the preparation process.

XRD patterns of the CH_4 and C_7H_8 SR post-reaction samples corresponded to all H-β zeolite and SR catalyst diffraction lines indicating the structure of the composite catalysts were maintained during the reactions. In addition to the CH_4 and C_7H_8 SR post-reaction samples, the XRD pattern of steady-state post-reaction sample also matched with XRD patterns of the pre-

reaction composite catalyst which is evidence that the synthesized SR@ β51% catalyst was not altered under reforming conditions even after 10 h.

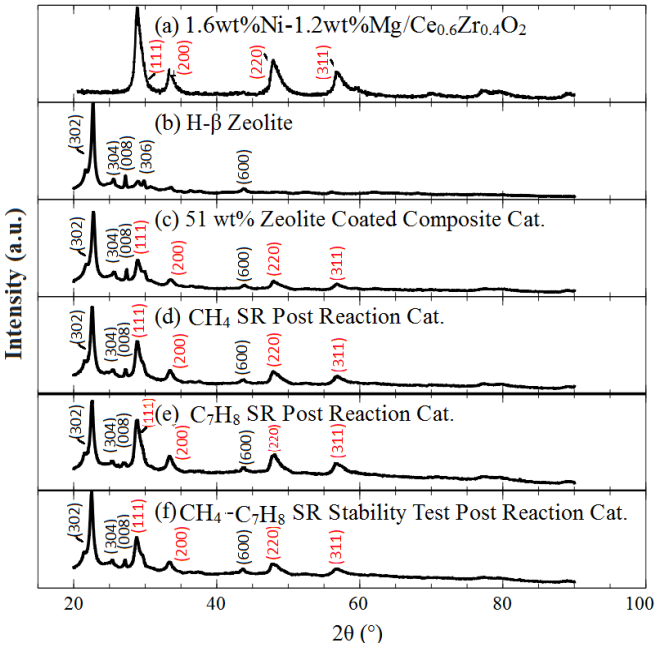

Figure 4.1 XRD patterns. (a) SR catalyst, (b) H-β zeolite, (c) SR@ β51%, (d) and (e) CH_4 and C_7H_8 SR post-reaction sample of SR@ β51%, (f) CH_4 and C_7H_8 SR post reaction steady-state experiment post-reaction sample of SR@ β51%. Red and black Miller indices indicate SR catalyst and H-β zeolite phases, respectively.

BET surface areas, total pore volumes, mesopore volumes (BJH method) and micropore volumes (SF method) of the pre and post-reaction samples and steady-state experiment post-reaction sample are listed in Table 4.2. The BET surfaces areas of H-β zeolite and $Ce_{0.6}Zr_{0.4}O_2$ were determined as 722.5 m^2/g and 31.8 m^2/g which agreed with previously reported values.[16, 124, 126] Decreasing surface area of $Ce_{0.6}Zr_{0.4}O_2$ as loading Ni and Mg is due to the pore blocking which is also good agreement with previous work and the literature[123, 126]. The specific surface area of the SR@ β51% catalyst was between the surface areas of the H-β zeolite and SR core catalyst as expected. BET surface areas and total pore volumes decreased slightly after CH_4 and C_7H_8 SR

reactions, especially in C_7H_8 SR reactions. The surface area and pore volume of post-reaction sample also decreased. The reason for decreasing surface areas and pore volume could be correlated to slight deactivation at the beginning of the reactions.

Table 4.2 BET surface area and pore volume results

Catalyst	BET Surface Area (m^2/g)	Total Pore Volume (cm^3/g)	Mesopore Volume (BJH Method) (cm^3/g)	Micropore Volume (SF Method) (cm^3/g)
H-Beta Zeolite [a]	722.5	0.455	0.105	0.356
$Ce_{0.6}Zr_{0.4}O_2$	31.8	0.065	0.061	N/A
1.6wt%Ni-1.2wt%Mg/$Ce_{0.6}Zr_{0.4}O_2$	26.3	0.062	0.060	N/A
Fresh SR@ β51% sample	230.1	0.195	0.098	0.111
SR@ β51%sampleCH_4 SR post- reaction	203	0.169	0.082	0.096
SR@ β51%sample C_7H_8 SR post- reaction	139.1	0.140	0.084	0.066
SR@ β51% CH_4- C_7H_8 SR steady-state experiment test post-reaction [b]	153.2	0.145	0.086	0.070

[a] The average of two batches of samples is reported.
[b] The average of three repeating physisorption experiment on the same sample is reported

As presented in Figure 4.2, the micropore diameter of the SR@ β51% catalyst are similar between the pre- and post-reaction samples and the micropore size did not change after 10 h TOS at 800°C. A slight decrease in pore volume after the reaction was consistent with physisorption analysis results. The micropore size of H-β zeolite alone was also analyzed and yield pore sizes ranging from 0.48-0.56 nm which is consistent with our previous study and it is smaller than C_7H_8 diameter (0.67 nm) and larger than CH_4 (0.4 nm) diameter.[124]

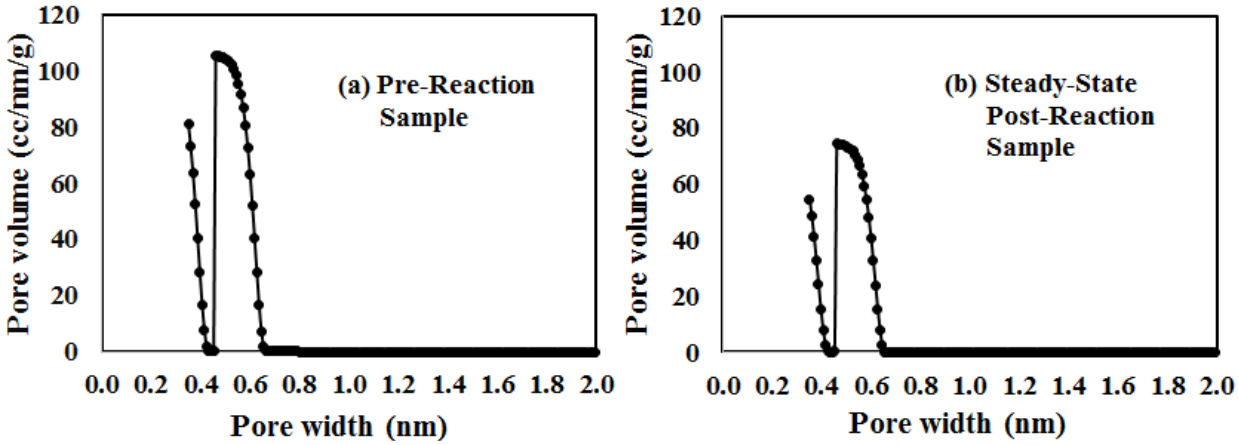

Figure 4.2 Pore size distributions. (a) Pre-reaction SR@ β51%, (b) CH_4-C_7H_8 SR steady-state experiment post-reaction SR@ β51%.

SEM images of SR@ β51% pre and post-reaction catalysts are shown in Figure 4.3. The SR@ β51% catalyst demonstrated very uniform and homogeneous shell in Figure 4.3(A), which help to judge further that the H-β zeolite shell coated successfully. The shell thickness was found about 139-142 μm from cross-section image of SR@ β51% catalysts in Figure 4.3 (B). SEM images of CH_4 SR post-reaction composite catalysts are given at low magnification and high magnification in the Figure 4 (C) and (D), respectively. No crack and coke formation were observed on the CH_4 SR post-reaction composite catalysts.

C_7H_8 SR post-reaction SR@ β51% and SR@ β34.3% catalyst are represented Figure 4.3 (E) and (F), respectively. Although coke formation was not seen on these samples, crack formation was noted. However, if SR@ β51% and SR@ β34.3% catalyst's SEM images are compared, crack formation was significantly reduced for the SR@ β51% catalyst sample due to the additional zeolite and decreasing the heating ramp rate from 10°C/min to 1°C/min.

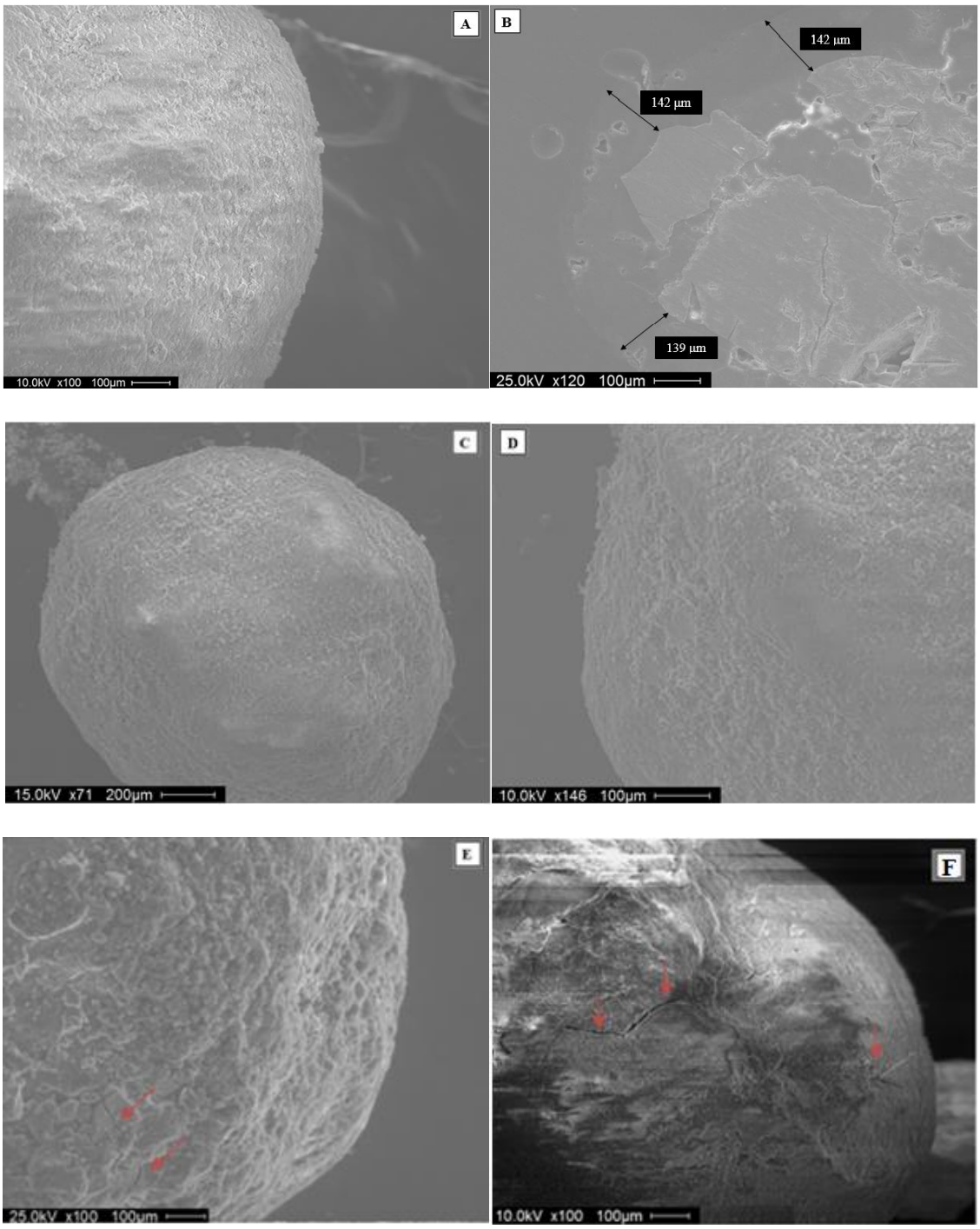

Figure 4.3 SEM images of SR@ β51% catalyst. (A) Pre-reaction sample (B) Cross-section of the composite catalyst, (C) and (D) CH_4 SR post-reaction samples, (E) and (F) C_7H_8 SR post-reaction SR@ β51% and SR@ β34.3% catalyst, respectively.

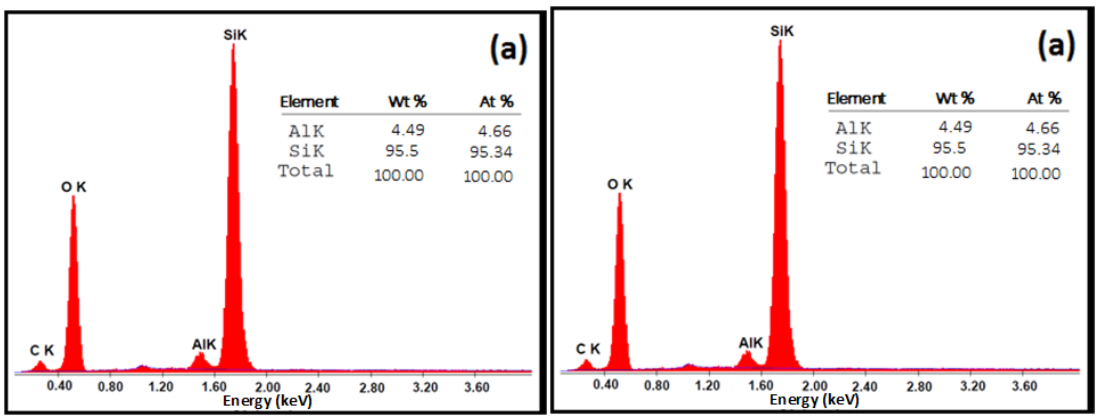

Figure 4.4 EDS results. (a) SR@ β51% catalyst, (b) Cross-section of SR@ β51% catalyst. Elemental composition analysis are averages 2 different spots at the same sample. The Si/Al ratio of H-β zeolite and SR@ β51% obtained by EDS compared in Table 4.3.

The Si/Al ratio of the composite catalyst surface is 20.5, slightly higher than that of the fresh H-β zeolite powder's Si/Al that is 19.7. Here, the increase of Si on the SR@ β51% catalyst can be explained by the use of silica sol as a binder. From EDS analysis, SEM images, and XRD patterns, the encapsulation of the core SR catalyst by H-β zeolite was deemed successful.

Table 4.3 Elemental compositions and Si/Al comparison

Sample	**Elemental Analysis (molar percentages)**		**Si/Al**
	Si	**Al**	
H-β zeolite	95.2	4.84	19.7
SR@ β51%	95.3	4.66	20.5

4.3.2 Reaction Results

CH_4 steam reforming was performed on uncoated SR catalyst, SR@ β51% catalyst (with 23.6 mg and 17.2 mg total amount of catalyst), PM-51%β/SR, PM-51%SiO_2/SR and the H-β zeolite alone to compare zeolite amount effect on CH_4 conversion and the results are presented in Figure 4.5 as a function of temperature. In addition, CH_4 and C_7H_8 (together as reactants) steam reforming was carried out with same temperature (840-780°C) and atmospheric pressure with

molar ratio of $CH_4/C_7H_8/H_2O$ = 1.44/1/7. Our previous work concluded that encapsulating the SR catalyst with H-β zeolite, CH_4 conversion increased due to confinement effect, zeolite acidity effect and/or Al^{3+} ion promotion effect.[124] When the uncoated SR catalyst (Figure 4.5 (a)) is compared with SR@ β51% catalyst (Figure 4.5 (c)), the SR@ β51% catalyst has higher CH_4 conversion than uncoated SR catalyst due to the reasons that mentioned above. Increasing the zeolite loading from 34.3wt% to 51 wt%, decreased the CH_4 conversion as observed by comparing (Figure 4.5 (b)) and (Figure 4.5 (c)). However, the conversion on the SR@ β51% catalyst was still higher or similar (at 840ºC) with uncoated SR catalyst (Figure 4.5 (a)). If Figure 4.5 curves (c) and (d) are compared, the decrease of the total catalyst mass of the composite catalyst decreased the conversion as expected. If the same total amount of catalysts (17.2 mg) are compared of the SR@ β51% and SR@ β34.3% in Figure 4.5 curves (b) and (d), the conversion on the SR@ β51% much less than SR@ β34.3% due to both less SR catalyst in SR@ β51% and higher diffusion limitation on the SR@ β51% than SR@ 34.3% catalyst. (Propagation of Uncertainty calculation example is given in Appendix D for CH_4 Conversion on 51wt% composite catalyst at 780°C)

PM-51%β/SR (Figure 4.5 (e)) showed less conversion than SR@ β51% catalyst conversion. The reason for lower conversion on physical mixture sample than composite catalyst even though both have same amount SR catalyst and H-β zeolite may be the lack of the confinement effect on physical mixture sample unlike SR@ β51% catalyst. A PM-51%SiO_2/SR was also studied to investigate H-β zeolite effect on CH_4 conversion. As in Figure 4.5 (e) and (f), the PM-51%β/SR sample has higher conversion than PM-51%SiO_2/SR sample due to the zeolite acidity and/or Al^{3+} promotion to the active sites. CH_4 steam reforming was performed on the H-β zeolite alone with same amount of H-β zeolite on the SR@ β51% catalyst and there was no methane conversion.

Simultaneous CH_4 and C_7H_8 steam reforming was also performed on SR@ β51% catalyst with molar ratio of $CH_4/C_7H_8/H_2O$ = 1.44/1/7 to investigate the C_7H_8 reactant effect on the CH_4 conversion and the result is presented on Figure 4.5 (g). CH_4 conversion decreased in presence of C_7H_8 due to pore blockage by C_7H_8 (comparison of curves (c) and (g)). This result was compatible with literature since Baertsch et al. [127] conducted a study to investigate permeation of the various sized hydrocarbons in MFI-type zeolites membrane and they observed that slowest species determines the permeation rates in the studies of species permeation. Although a decrease was seen in CH_4 conversion when C_7H_8 added as reactant, SR@ β51% catalyst demonstrated similar (at 840°C) or higher CH_4 conversions compared to the SR catalyst alone Figure 4.5 (a).

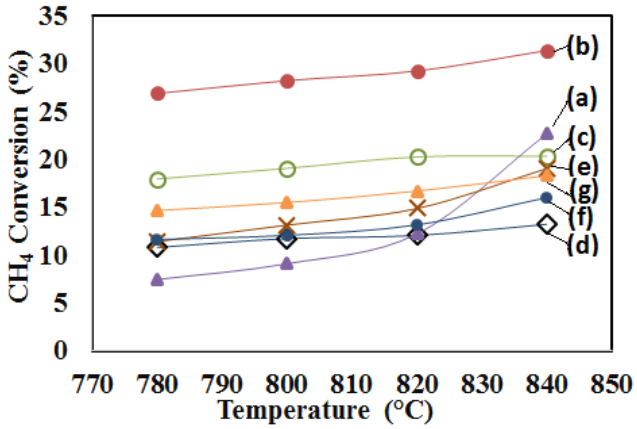

Figure 4.5 CH_4 steam reforming results. Conditions were 780-840°C, atmospheric pressure, molar ratio of CH_4/H_2O = 1. (a) Uncoated SR catalyst[123], (b) 17.2 mg SR@ β34.3% catalyst [124], (c) 23.6 mg and (d) 17.2 mg SR@ β51% catalyst, (e) PM-51%β/SR catalyst, (f) PM-51% SiO_2/SR catalyst and (g) CH_4-C_7H_8 steam reforming reaction with molar ratio of $CH_4/C_7H_8/H_2O$ = 1.44/1/7.

C_7H_8 steam reforming reaction was also performed on SR@ β51% catalyst, H-β zeolite as powder and pellet (with same amount H-β zeolite used in 51 wt% composite catalyst), PM-51%β/SR, PM-51%SiO_2/SR and PM-51%SiC/SR and the results are represented in Figure 4.6 as a function of temperature. The previous work showed that 34.3 wt% H-β zeolite coated composite

catalyst decreased the C_7H_8 conversion when compared to the uncoated reforming catalyst (Figure 4.6 (a) and (b)).[123] The SR@ β51% catalyst (Figure 4.6 (c)) demonstrated less conversion than SR@ β34.3% (Figure 4.6 (b)), since encapsulation with 51 wt% H-β zeolite on SR catalyst with two coatings helped to decrease the amount of cracks and increase the shell thickness. The SR@ β51% catalyst yielded similar conversion as to the H-β zeolite powder alone, as it seen in Figure 4.6 (c) and (d). This result indicated that the conversion of the SR@ β51% catalyst was caused by the H-β zeolite shell. Zeolites are widely used in catalytic cracking processes due to their acidic properties and H-β zeolite is one of the known acidic zeolites.[128, 129] Thus, encapsulation with non-acidic zeolite of similar pore size could help to further decrease the conversion for the composite catalyst. The PM-51%β/SR catalyst (Figure 4.6 (e)) which has same amount of SR catalyst with SR@ β51% catalysts has significantly higher C_7H_8 conversion because the shell was no longer there to prevent access to the SR catalyst core.

To investigate the surface area effect of the H-β zeolite, C_7H_8 SR reaction was also conducted on H-β zeolite pellet (same total amount with H-β zeolite powder). The results demonstrated that the C_7H_8 conversion decreased between 2.5-6% (depends on temperature) on the pellet form of H-β zeolite comparing to the powder form of H-β zeolite since pellet has less external surface area than the powder.

Combined CH_4 and C_7H_8 steam reforming was also performed on SR@ β51% composite catalyst with same amount of catalyst that is used to C_7H_8 steam reforming reaction with molar ratio of $CH_4/C_7H_8/H_2O$ = 1.44/1/7 to examine the CH_4 reactant effect on the conversion and the result is demonstrated on Figure 4.6 (h). C_7H_8-CH_4 SR reaction result in Figure 4.6 (h) presents very similar result with C_7H_8 SR reaction result in Figure 4.6 (c) since slowest species (C_7H_8) determines the permeation rates as explained above.

Table 4.4 WHSV and GHSV comparison for C_7H_8 SR

SAMPLE	**WHSV (h^{-1})**	**GHSV (h^{-1})**
SR catalyst	45.9	260000
PM-51%SiO_2/SR	22.5	156000
PM-51%β/SR	22.5	62400
PM-51%SiC/SR	22.5	208000

PM-51% SiO_2/SR and PM-51% SiC/SR with same amount and percentages with PM-51%β/SR were studied to investigate space velocity effect on C_7H_8 conversion and the results were demonstrated in Figure 4.6 (f) and (g), respectively. The weight hourly space velocity (WHSV) and gas hourly space velocity (GHSV) of the physical mixture samples and SR catalyst by itself for C_7H_8 SR reaction are compiled in Table 4.4. Since the WHSV were calculated on bed mass, the values represent the same mass of reforming catalyst (see Table 4.1). Of the 3 physical mixtures (Figure 4.6 (e), (f) and (g)), there is a trend that the conversion is inversely correlated to the GHSV. This result suggested that mass transfer limitations contribute to these differences. In addition, the findings confirmed that H-β zeolite improved the reforming conversion by its acidity and/or Al^{3+} promotion, which could include solid-state reactions between components at high temperatures. In addition, SiC is a common diluent for catalytic beds due to its inertness and high thermal conductivity. With its physical mixture yielding the lowest conversion and the endothermic reaction, it seems thermal gradients in the catalyst bed are not forming. C_7H_8 steam reforming reaction was also performed on SiO_2 and SiC by itself (using 10.7 mg) and with blank reactor (with a piece of quartz wool). Less than 1% conversion was seen on blank reactor and SiC and 1.08% conversion on SiO_2 at the 840 °C. Thus, contributions of these diluents to the conversion were minimal.

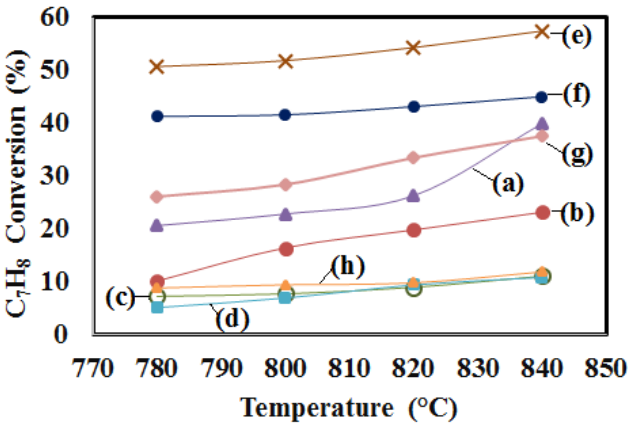

Figure 4.6 C_7H_8 steam reforming results. Reaction conditions were 780-840°C, atmospheric pressure, molar ratio of C_7H_8/H_2O=1/7. (a) Uncoated SR catalyst[124], (b) 34.3 wt% H-β zeolite coated composite catalyst[124], (c) SR@ β51% catalyst, (d) H-β zeolite, (e) PM-51%β/SR catalyst, (f) PM-51%SiO_2/SR catalyst (g) PM-51%SiC/SR catalyst and (h) CH_4-C_7H_8 steam reforming reaction on SR@ β51% with molar ratio of $CH_4/C_7H_8/H_2O$ = 1.44/1/7.

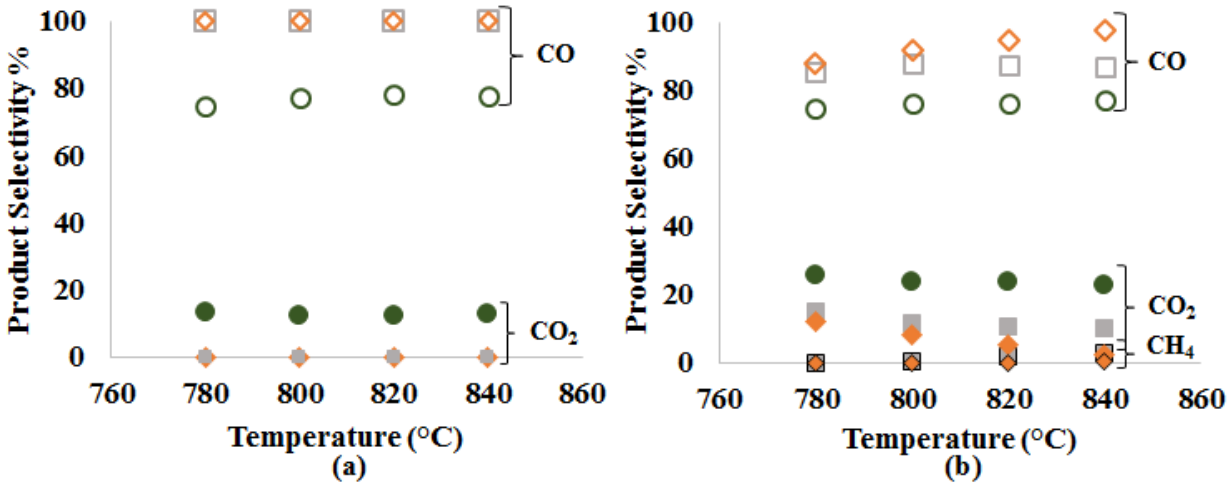

Figure 4.7 Product selectivity of the carbon product of CH_4 and C_7H_8 SR, (a) selectivity for CH_4 SR (b) selectivity for C_7H_8 SR. Grey square indicates SR@ β51%, orange diamond indicates PM-51%β/SR catalyst and green circle indicates CH_4-C_7H_8 steam reforming reaction on SR@ β51%. Unfilled, filled and filled-black-lined markers demonstrates CO, CO_2 and CH_4 % selectivity, respectively.

The product selectivity was calculated for carbon species as defined in section 3.2.3 for CH_4 and C_7H_8 steam reforming and the results were demonstrated in Figure 4.7 (a) and (b), respectively. The product selectivity results showed that the primarily product of the reaction was CO. This results is expected since the reaction was conducted with or near stoichiometric feeds.

Reactant selectivity was defined as the ratio of moles of methane converted to the moles of toluene converted. According to this definition, reactant selectivity was calculated for the uncoated SR catalyst, SR@ β34.3% and SR@ β51% catalysts to understand the zeolite membrane thickness effect on reactant selectivity and results were given in Figure 4.8. The reactant selectivity increased with increasing zeolite content because the zeolite shell hampered the C_7H_8 conversion rate more than the of CH_4 conversion rate. As discussed in section 3.3.3, this effect is caused by increased diffusion limitation with increasing zeolite shell thickness. The reactant selectivity decreased with increasing temperature due to the differences in activation energies limiting process (diffusion of reactants as discussed in section 3.3.3). The activation energy of toluene diffusion would be expected to be higher than that of methane, which makes the denominator of the reactant selectivity more sensitive to temperature than the numerator.

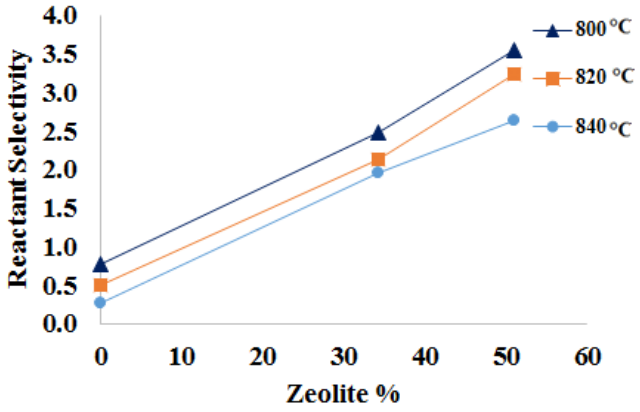

Figure 4.8 Reactant selectivity change with zeolite content and temperature

Long-term lab scale experiments (Figure 4.9) were conducted utilizing the uncoated SR and SR@ β51% catalysts at 800 °C and time on stream was 10 h with molar ratio of $CH_4/C_7H_8/H_2O$ = 1.44/1/7. The result indicated that while uncoated SR catalyst deactivated, SR@ β51% remained

stable for 10 h ((Figure 4.9 (a)) although a slight decrease of CH_4 conversion occurred at the beginning. The SR@ β51catalyst also showed constant C_7H_8 conversion (Figure 4.9 b) for 10 h.

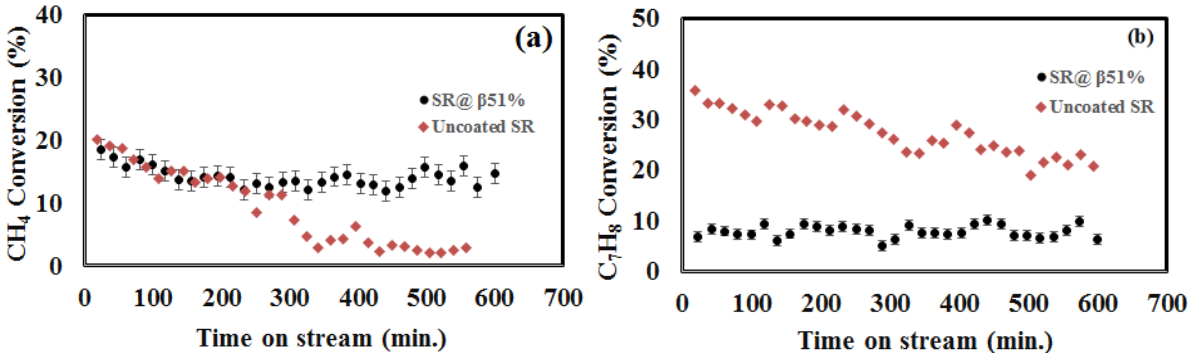

Figure 4.9 Simultaneous CH_4 and C_7H_8 steam reforming for SR@ β51% and uncoated SR catalysts. (a) CH_4 steam conversion with TOS and (b) C_7H_8 conversion with TOS.

4.3.3 Analyses of Internal Diffusion Limitations

Weisz-Prater Criteria, Thiele Moduli, and effectiveness factors were calculated for CH_4 and C_7H_8 SR on the SR@ β34.3% and SR@ β51% catalysts to examine the effect of internal diffusion limitations (Table 4.5). Effective diffusivities for CH_4 and C_7H_8 in the zeolite were taken from literature for respective temperatures of 250 K (for CH_4) and 320 K (for C_7H_8) [130, 131] and these values were corrected to the 1073 K (800°C) using a 3/2 power temperature dependency as suggested by Hirschfelder.[132] Reaction kinetics were assumed as first-order with respect to CH_4 and C_7H_8.[133, 134] Diffusional limitations were imposed by the H-β zeolite coating to all catalysts according to the Weisz-Prater Criteria since the all values found as bigger than 1. There were no diffusion limitations for uncoated SR since Weisz-Prater Criteria was found smaller than 1 in previous study .[123] Additionally, Thiele Modulus results showed that reactions were performed in the diffusion limited regimes since $\Phi_n^2 > 1$ for all reactions. If effectiveness factors of SR@ β34.3% and SR@ β51% catalysts are compared, the SR@ β51% catalyst has smaller values which

indicates that coating thicker zeolites increased diffusion limitation, which is compatible with reaction results. All of these analyses indicate that, while both CH_4 and C_7H_8 are under internal mass transfer limitations, the effect is much more severe for C_7H_8 due to the lower effective diffusion coefficient resulting from its larger size. Because of its small molecular size, the shell does not significant retard the transport of CH_4, which is consistent with the zeolite shell being approximately 10% of the pellet radius. For C_7H_8 SR, the reaction conversion by the core catalyst is under severe internal mass transfer limitations. However, the overall composite catalyst still has slight conversion because the zeolite shell was able to convert C_7H_8, as noted in the control experiment of the zeolite alone.

Table 4.5 Analysis of internal diffusion limitations

Sample	**Reaction**	**Internal diffusion limitation (C_{wp}, Weisz-Prater Criteria)**	**Thiele Modulus (Φ_n)**	**Effectiveness Factor (η)**	**Shell Thickness, (μm)**	**Radius of the composite catalyst, R (m)**
34wt%	CH_4 SR	179>1	13.4	0.21	95	$7.3*10^{-4}$
51 wt %		187>1	13.7	0.20	142	$1.29*10^{-3}$
34wt%	C_7H_8 SR	$9.8*10^{5}>>1$	2616	0.00115	95	$7.3*10^{-4}$
51 wt %		$1.4*10^{6}>>1$	3110	0.00096	142	$1.29*10^{-3}$

CHAPTER 5: HYDROCARBON STEAM REFORMING USING SILICALITE-1 ZEOLITE ENCAPSULATED NI-BASED CATALYST[5]

5.1 Introduction

Because of its attractive properties (molecular sieving behavior, high hydrothermal stability etc.), zeolite membranes have been prepared and studied recent years in several applications including gas separations, membrane reactors, and micro-reactors.[135-137] Core-shell architecture membrane micro-reactors, which consists of an inner particle encapsulated inside with a zeolite membrane, have attracted significant interest because of its promising applications in heterogeneous catalysis.[138] Two types of zeolite membrane have been reported based on the zeolite membrane function in the reaction unit: inert and active zeolite membranes.[139] The active zeolite membrane reactors shows catalytic activity with separation process in a catalytic zeolite membrane layer. However, in the inert zeolite membrane reactors, the zeolite membrane only demonstrates the separation function without catalytic activity. The applications of inert zeolite membrane reactors consist of delivering a reactant to increase reactant selectivity or removing a product to enhance conversion in equilibrium-limited reactions.[140] In prior work, we studied the ability of a zeolite membrane encapsulation to control the conversion using reactant selectivity property during steam reforming of various sized reactants as a way to prevent potential deactivation by tars in biomass-to-liquidprocesses.[123, 141] An H-β zeolite membrane (pore size 0.43-0.57 nm) was

[5] This chapter was accepted by "AlChE Journal".

used to encapsulate the inner SR catalyst since its pores are between the sizes of CH_4 (0.4 nm) and C_7H_8 (tar model;0.67 nm)[124, 141]. The mass transfer limitations imposed by the zeolite membrane led to the coated reforming catalyst to achieving higher reactant selectivity (ratio of CH_4 conversion to C_7H_8 conversion) when compared to the uncoated reforming catalyst. As expected, this selectivity effect was magnified as the thickness of the coating increased. However, the results showed that the H-β zeolite alone had some activity, possibly due to its acidity nature.[124, 141] It is well-known that most of zeolites present good performance as catalyst due to their acidic properties[142] and therefore are used in applications such as fluidized catalytic cracking (Y and USY)[143], hydrocracking (Y)[144, 145] and toluene disproportionation.[146] Therefore, encapsulation with a non-acidic zeolite on the SR catalyst with the same thickness that used previous study may help to reduce activity on the tar reforming. Thus, in this study, a 1.6wt% Ni-1.2wt% Mg /$Ce_{0.6}Zr_{0.4}O_2$ steam reforming catalyst was encapsulated with a Silicalite-1 zeolite to investigate the zeolite acidity effect on both CH_4 and C_7H_8 conversions for the composite catalyst. Silicalite-1 was chosen to encapsulate SR catalyst since it is a non-acidic zeolite, it does not contain Al^{3+} ions, and it is the prototype of shape-selective zeolite.[147,148]

5.2 Experimental

5.2.1 Synthesis

5.2.1.1 Synthesis of Silicalite-1 Zeolite

The Silicalite-1 zeolite was synthesized with the hydrothermal synthesis method as stated by Li et al.[149] 3.04 g of SiO_2 (99.98% pure; CAB-O-SIL M-5, scintillation grade, Acros Organics, Inc.), 3.07g Tetra-n-propylammonium Hydroxide (TPAOH, 40% w/w aq. Soln.; Alfa Aesar), 36.86g Ethyl Alcohol (>99.5% pure; Sigma–Aldrich, Inc.) and 216.18 g of deionized (DI) water was used to prepare Silicalite-1 precursor solution. All chemicals were mixed under continuous

stirring at room temperature for 90 min. The Silicalite-1 zeolite precursor solution was added into an autoclave and it was kept at 180°C for 2 days for crystallization. After that, the solution was centrifuged to separate liquid and solid phases. The solid part was washed with distilled water until its pH value was less than 8. Then, it was dried at 120°C for 12 h and was calcined at 550 °C for 10 h. (Please see Appendix F for flowchart).

5.2.1.2 Synthesis of 1.6wt% Ni-1.2wt% Mg /$Ce_{0.6}Zr_{0.4}O_2$ Steam Reforming Core Catalyst

To synthesize core SR catalyst 1.6wt%Ni-1.2wt%Mg/$Ce_{0.6}Zr_{0.4}O_2$, molar ratio 0.6:0.4 Cerium-Zirconium oxide support was synthesized first by a co-precipitation method as reported by Rossignol et al.[102] For this, Ce $(NO_3)_3 \times 6H_2O$ (99.5% pure metal basis; Alfa Aesar, 6.5 g) and $ZrO(NO_3)_2 \times H_2O$ (99.9% pure metal basis; Alfa Aesar; 2.49 g) were dissolved in DI water and precipitated by the addition of NH_4OH (27%, w/w NH3; Mallinckrodt Chemicals) to form a hydrous Ce/Zr solution. This mixture was filtered and re-dispersed into a 0.25 M NH_4OH solution. The dilute solution was re-filtered and dried in an oven at 60 °C for 1 h followed by 120 °C overnight and calcination was performed at 800 °C for 4 h. Ni (1.6% by weight) and Mg (1.2% by weight) were loaded to the oxide support by wet impregnation (WI) as reported by Walker et al.[126] For the WI method, appropriate amounts of $Mg(NO_3)_2 \times H_2O$ (99.999% pure metal basis; Alfa Aesar) and $Ni(NO_3)_2 \times 6H_2O$ (99.9985% pure metal basis; Alfa Aesar) were dissolved in DI water. This homogeneous solution was added drop wise to the support until incipient wetness and dried at 120 °C for 2 h. This step was repeated until all of the metal nitrate solution had been added to the support. Following the final drying step, the catalyst was calcined at 500 °C for 4 h. This catalyst is denoted as “uncoated SR” in the next sections. (Please see Appendix F for flowchart).

5.2.1.3 Synthesis of Silicalite-1 Zeolite Coated Composite Steam Reforming Catalyst

51 wt % Silicalite-1 zeolite coated composite SR catalyst was prepared by double physical coating method by modifying the method which is called physical coating (physically adhesive) method given in the literature.[18, 103] For this method, silica sol (Ludox: 40 wt%, Sigma–Aldrich, Inc.) was used as binder for Silicalite-1 to SR catalyst. 3.08 g of silica sol was diluted with 1.5 times DI water (4.6 g) by weight. The encapsulation with the Silicalite-1 zeolite was performed in two steps. First, SR catalyst (0.52 g) was wet impregnated by spraying the prepared silica sol solution and Silicalite-1 (0.27 g) powder was mixed with the moistened SR catalyst in a round bottomed flask, which was followed by vigorously shaking until the formation of zeolite shell coating on the surface of core catalyst. The obtained catalyst was dried at 120°C for 12 h and calcined at 500°C for 3 h. Then, the resulting material was wet impregnated one more time with prepared silica sol solution and Silicalite-1 zeolite (0.27 g) powder was mixed with the moistened SR catalyst in a combustion boat, vigorously and carefully shaken until the formation of second zeolite shell coating. The obtained catalyst was dried again at 120°C for 12 h and calcined at 500°C for 3 h to increase the mechanical strength of zeolite shell, which resulted in a 51 wt% of Silicalite-1 zeolite encapsulated composite SR catalyst. This catalyst is denoted as "SR@ Sil51%" and 51 wt % H-β zeolite coated composite SR that was synthesized previous study is denoted as "SR@ β51% "in the next sections when reaction results are compared. (Please see Appendix F for flowchart).

5.2.1.4 Preparation of Physical Mixture Catalyst

The physical mixture of SR and Silicalite-1 zeolite catalyst was prepared by mechanically mixing the SR catalyst and Silicalite-1 zeolite. The mass of Silicalite-1 zeolite was 51 wt%, a loading that was the same as for the encapsulated catalyst. To prepare the physical mixture catalyst

for CH_4 SR reaction 11.3 mg SR catalyst and 12.3 mg Silicalite-1 zeolite and for C_7H_8 SR reaction 10.3 mg catalyst and 10.7 mg Silicalite-1 zeolite were used. The physical mixture of SR and Silicalite-1 zeolite catalyst is denoted as "PM-51%Sil/SR" in the next sections.

5.2.2 Characterization Methods

XRD was conducted using a Bruker AXS XRD equipped with CuK radiation source (0.154 nm) at 40 kV and 40 mA. The machine was operated in a Bragg angle (2θ°) range of 20–90°. The step size was 0.02 for Silicalite-1 zeolite, 0.004 for SR catalyst. N_2 Physisorption experiments were performed using a Quantachrome Autosorb-iQ to obtain BET surface area, pore volumes, and Saito and Foley (SF) method for pore size distributions. The samples were outgassed at 200°C overnight for Silicalite-1 zeolite and coated composite catalysts and 2 h for SR catalyst prior to N_2 physisorption. The morphology of the samples was determined with a Hitachi S-800 SEM equipped with an Ametek EDAX which provide the information of surface elements (using tilt angle of 30°). To obtain cross section of the sample epoxy was used. After solidification of the epoxy, it was sanded and polished carefully to view the particles cross-section. Finally, samples were coated gold-palladium with a layer of using a Denton vacuum desk II sputter coater, to make sample conductive prior to imaging.

5.2.3 Reaction Studies

The reactions were carried out using Thermoscientific Thermolyne furnace and a fixed bed quartz U-tube microreactor (internal diameter of 4 mm). The catalyst was loaded between two layers of high temperature quartz wool in the U- tube and it was placed into the furnace. Temperature of the furnace was controlled using a Eurotherm 3110 PID controller. A manifold that was connected to Alicat Scientific mass flow controllers and two quartz bubblers (toluene and steam) was used to feed the U-tube reactor. Total flow rate was 75 sccm (0.64% CH_4, 0.64% H_2O,

98.7% He) for CH_4 SR and 32.6 sccm (1% C_7H_8, 7% H_2O, 92% He) C_7H_8 SR and 32.6 sccm (1% C_7H_8, 1.5% CH_4, 7% H_2O, 90.5% He) for CH_4-C_7H_8 SR and for a 10-hr time on stream experiment. A Perkin Elmer Gas Chromatography (GC) that has Hayesep-D packed column and thermal conductivity detector (TCD) was used to analyze the effluent gas from reactor. The mass of catalysts for CH_4 SR were 23.6 mg Silicalite-1 zeolite coated SR catalyst (11.3 mg SR catalyst and 12.3 mg Silicalite-1 zeolite of 23.6 mg based on 51wt%), 23.6 mg physically mixed catalysts with Silicalite-1 zeolite -SR catalyst, (11.3 mg SR catalyst and 12.3 mg Silicalite-1 zeolite of 23.6 mg based on 51wt%) and 12.3 mg Silicalite-1 zeolite by itself. The mass of catalysts for C_7H_8 SR were 21 mg Silicalite-1 zeolite coated SR catalyst and physically mixed catalyst with Silicalite-1 zeolite, (10.3 mg SR catalyst and 10.7 mg Silicalite-1 zeolite of 21 mg based on 51wt %) and 10.7 mg Silicalite-1 zeolite by itself. The reaction types, notations for the catalysts, and compositions-amount of the catalysts that used in the reactions is given in Appendix B Table B1. Reaction conditions were 780-800-820-840 °C, atmospheric pressure, and stoichiometric feeds (i.e., molar ratio of CH_4/H_2O= 1 and C_7H_8/H_2O= 1/7 for the respective reactions). A 10-hr time on stream experiment was also conducted utilizing the 23.6 mg 51 wt% Silicalite-1 zeolite coated composite catalyst at 800 °C with molar ratio of $CH_4/C_7H_8/H_2O$ = 1.44/1/7.

The reaction procedure was same for both the CH_4 and C_7H_8 SR reactions. The catalyst was heated (with a ramp rate 1°C/min) to 800 °C and then reduced with 5% H_2/He (50 sccm total flow) gas flow for 2 h. Then, the temperature was increased to the highest reaction temperature and reaction was started. Typical time-on-stream (TOS) was 1 h for each temperature for both reactions (CH_4 and C_7H_8 reforming experiments).

Product selectivity was calculated using the following equation:

$$\text{Selectivity of a product= } S_P = \left(\frac{Moles\ of\ a\ certain\ carbon\ product}{\sum moles\ of\ carbon\ products}\right) * 100$$

Weisz-Prater Criterion (for calculation internal diffusion limitations, C_{WP}), Thiele modulus (Φ_n) and effectiveness factor (η) were calculated using the following equations:

$$C_{WP}=\frac{(-r_{Aobs}{}')*q_c*R^2}{D_e*C_{As}}$$

$$\Phi_n=R\sqrt{\frac{-r'_{As}*q_c}{D_e*C_{As}}}$$

$$\eta=\frac{3}{\Phi n^2}(\Phi\coth(\Phi)-1)$$

where $-r_{Aobs}{}'$ is measured values of the rate of reaction, q_c is density of solid catalyst, R is radius of the catalyst particle, D_e is effective diffusivity, C_{As} is reactant concentration external to the pellet.

5.3 Results and Discussion

5.3.1 Catalyst Characterization

XRD was carried out to confirm whether the zeolite phase was successfully formed in the composite catalysts. The results for fresh SR@ Sil51% catalyst (a) and 10-hr time on stream experiment post-reaction composite SR@ Sil51% catalyst (b) shown in Figure 5.1 with Miller indices as red and black text demonstrating the SR and Silicalite-1 zeolite phases, respectively. The results for Ce-Zr catalyst (a) uncoated SR catalyst (b), pure Silicalite-1 zeolite powder (c), CH_4 SR post-reaction catalyst (d), and C_7H_8 SR post-reaction SR@ Sil51% catalyst (e) are given in the Appendix B Figure B2 (please see appendices). Diffraction lines were almost identical with the $Ce_{0.6}Zr_{0.4}O_2$ support (a) and SR catalyst (b) due to loaded Ni and Mg that prevented their detection. The XRD patterns of the Silicalite-1 zeolite (c) indicated that Silicalite-1 zeolite was synthesized successfully since its diffraction patterns are consistent with the literature.[150-152] The SR@ Sil51% catalyst profile perfectly matched with the Silicalite-1 zeolite and SR catalyst showing that composite catalyst did not change during the preparation process.

XRD patterns of the CH_4 and C_7H_8 SR post-reaction samples corresponded to all Silicalite-1 zeolite and SR catalyst diffraction lines indicating the structure of the composite catalysts were maintained during the reactions. Furthermore, the XRD pattern of 10-hr time on stream experiment post-reaction composite SR@ Sil51% catalyst also matched with XRD patterns of the pre-reaction composite catalyst which is evidence that the synthesized SR@ Sil51% catalyst was not changed under reforming conditions after 10 hr, as shown in Figure 5.1.

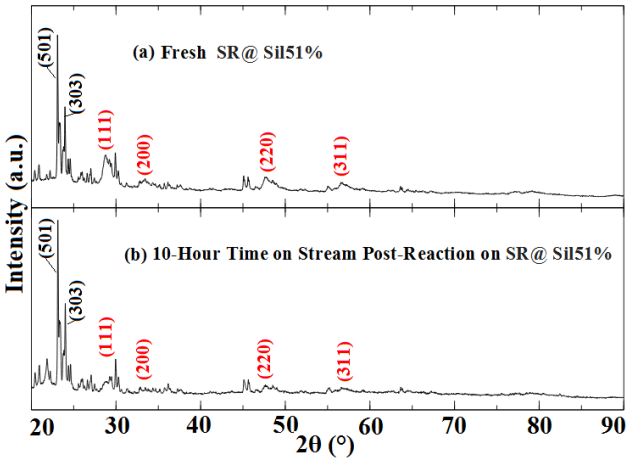

Figure 5.1 XRD patterns of the fresh and 10-hr time on stream post-reaction SR@ Sil51% catalysts. Red and black Miller indices indicate SR catalyst and Silicalite-1 zeolite phases, respectively.

BET surface areas, total pore volumes, mesopore volumes (BJH method) and micropore volumes (SF method) of the pre and post-reaction samples and 10-hr time on stream experiment post-reaction catalyst are demonstrated in Table 5.1. The BET surfaces areas of Silicalite-1 zeolite was determined as 361 m^2/g, which is comparable with literature[153]. The specific surface area of the SR@ Sil51% catalyst was found as 162 m^2/g that was between the surface areas of the Silicalite-1 zeolite and SR core catalyst, expectedly. BET surface areas did not change after CH_4 and C_7H_8 SR reactions.

Table 5.1 BET surface area and pore volume results

Catalyst	BET Surface Area (m^2/g)	Total Pore Volume (cm^3/g)	Mesopore Volume (BJH Method) (cm^3/g)	Micropore Volume (SF Method) (cm^3/g)
Silicalite-1 Zeolite	361	0.179	0.004	0.172
$Ce_{0.6}Zr_{0.4}O_2$	31.8	0.065	0.061	N/A
1.6wt%Ni-1.2wt%Mg/$Ce_{0.6}Zr_{0.4}O_2$	26.3	0.062	0.060	N/A
Fresh SR@ Sil51% sample	162	0.179	0.106	0.070
SR@ Sil51% sample CH_4 SR post-reaction	162	0.148	0.076	0.073
SR@ Sil51% sample CH_4 SR post-reaction	162	0.145	0.065	0.072

As presented in Figure 5.2, the micropore diameter of the SR@ Sil51% catalyst are similar between the pre- and post-reaction samples and the micropore size did not change during CH_4 SR reaction. A slight decrease in pore volume after the reaction was consistent with physisorption analysis results. The micropore size of Silicalite-1 zeolite alone was also analyzed and it gave a peak at 0.48 nm that is smaller than C_7H_8 diameter (0.67 nm) and larger than CH_4 (0.4 nm) diameter.

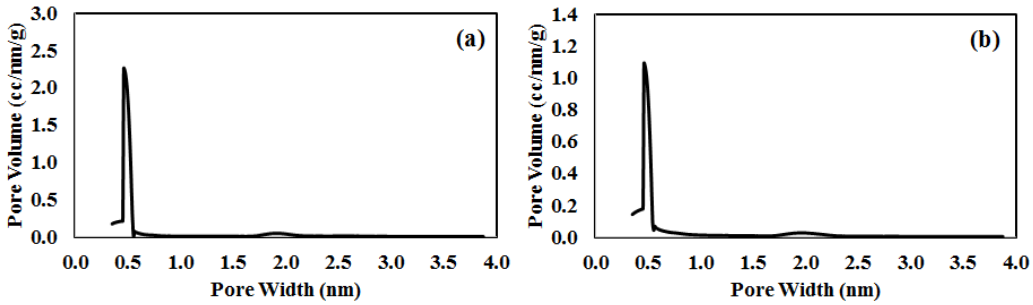

Figure 5.2 Pore size distribution. (a) Fresh SR@ Sil51% sample (b) CH_4 SR post-reaction SR@ Sil51%.

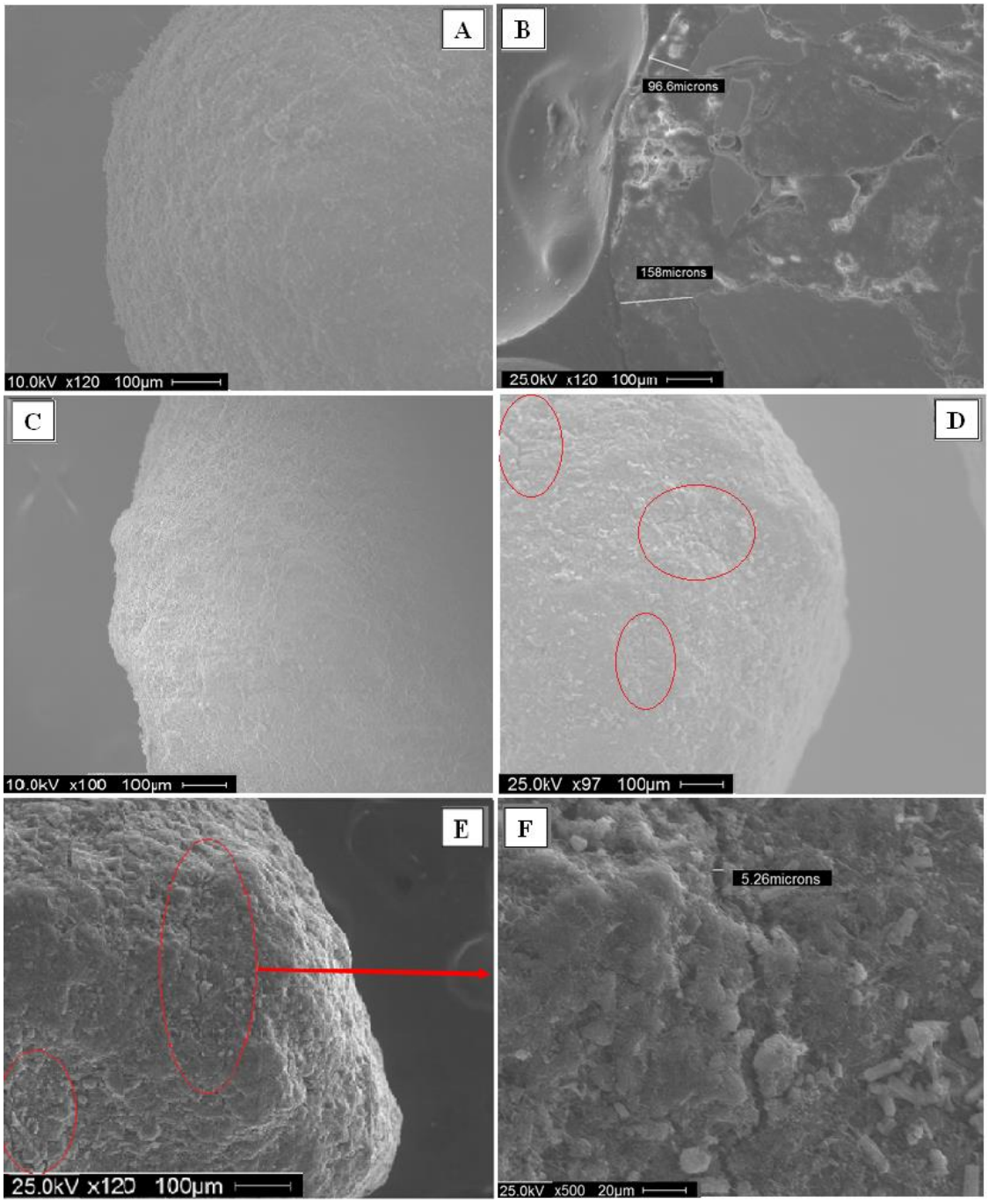

Figure 5.3 SEM images of SR@Sil51% catalyst. (A) Pre-reaction sample (B) Cross-section of the composite catalyst (C) CH_4 SR post-reaction sample, (D) C_7H_8 SR post-reaction sample and (E) and (F) CH_4-C_7H_8 SR 10-hr time on stream experiment post-reaction sample

SEM images of SR@ Sil51% pre and post-reaction catalysts are shown in Figure 5.3. The fresh SR@ Sil51% catalyst demonstrated very uniform and homogeneous shell in Figure 5.3 (A),

which showed the Silicalite-1 zeolite shell coated successfully. The shell thickness was found about 97-158 μm from cross-section image of SR@ Sil51% catalysts in Figure 5.3 (B). SEM images of CH_4 SR post-reaction composite catalyst (Figure 5.3 (C)) indicated no crack and coke formation on the CH_4 SR post-reaction composite catalysts. Some crack formation was noted on the C_7H_8 SR post-reaction SR@ Sil51% catalyst (Figure 5.3 (D)) and 10-hr time on stream experiment post-reaction sample (Figure 5.3 (E and F)) although coke formation was not seen on this sample.

EDS analysis was conducted to analyze the elemental composition of SR@ Sil51% pre-reaction catalyst and 10-hr time on stream experiment post-reaction sample and the results are shown in Figure 5.4, with weight and atomic percentages of elements as inserts. From the EDS spectrum of SR@ Sil51% catalyst (Figure 5.4 (a)), the SR core catalyst elements (Ni, Mg, Ce and Zr) were not detected on the surface of the composite catalyst which showed the encapsulation of the core SR catalyst by Silicalite-1 zeolite was presumed successful. The EDS spectrum of 10-hr time on stream experiment post-reaction sample (Figure 5.4 (b)) indicated that the zeolite membrane was not destroyed after the 10-hr time on stream experiment since SR core catalyst elements were not detected on the surface of the composite catalyst. From the cross-section EDS spectrum (Table 5.2), all the SR core catalyst elements and Silicalite-1 zeolite element (just Si) was detected.

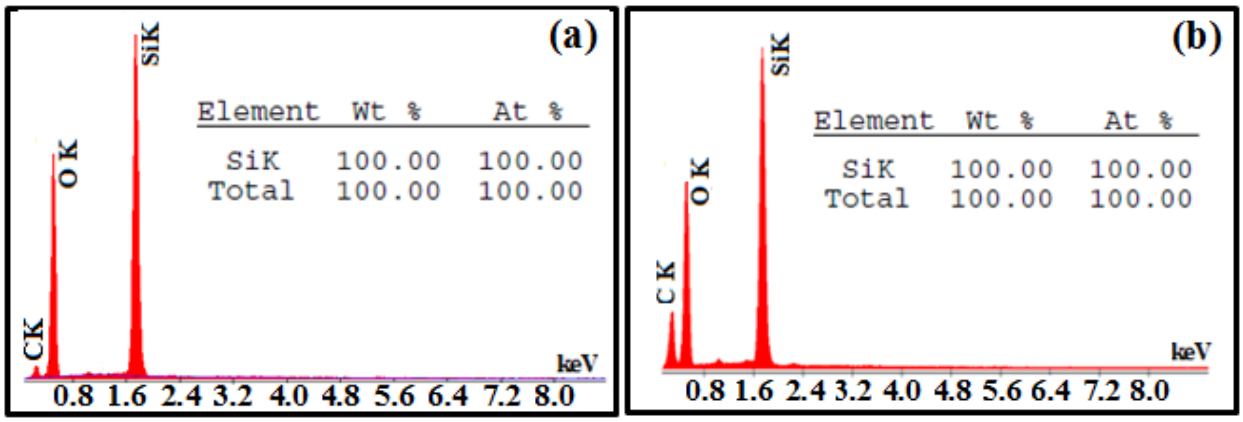

Figure 5.4 EDS results. (a) Fresh SR@ Sil51% catalyst, (b) 10-hr time on stream experiment on SR@ Sil51% catalyst

Table 5.2 The elemental composition via EDS of the cross section of SR@ Sil51% catalyst

	Wt% (*)	At% (*)
MgK	0.4	2.45
SiK	23.06	55.01
ZrL	18.65	13.74
CeL	55.45	26.55
NiK	2.01	2.25
Total	100	100

(*)Elemental composition analysis are averages 2 different spots at the same sample.

5.3.2 Reaction Results

The CH_4 steam reforming results on uncoated SR catalyst (a), SR@ β51% catalyst (b), SR@ Sil51% catalyst (c), and PM-51%Sil/SR (d) are shown in Figure 5.5 to compare the zeolite acidity effect. CH_4 steam reforming was also performed on the Silicalite-1 zeolite alone (with a same amount Silicalite-1 on the SR@ Sil51% catalyst) but no conversion was observed. Our previous work concluded that, when encapsulating the SR catalyst with H-β zeolite, CH_4 conversion increased due to confinement, zeolite acidity , and/or Al^{3+} ion promotion effects.[124] If the uncoated SR catalyst (Figure 5.5 (a)) is compared with SR@ β51% catalyst (Figure 5.5 (b)), the SR@ β51% catalyst has higher CH_4 conversion than uncoated SR catalyst. If the uncoated SR catalyst (Figure 5.5 (a)) is compared with SR@ Sil51% catalyst (Figure 5.5 (c)), the SR@ Sil51%

catalyst has also higher CH_4 conversion than uncoated SR catalyst. When SR@ Sil51% catalyst (Figure 5.5 (c)) is compared with SR@ β51% catalyst (Figure 5.5 (b)), SR@ Sil51% catalyst has less conversion than SR@ β51% catalyst since the SR@ Sil51% catalyst non-acidic zeolite and there is no Al^{3+}. These results all agreed with the confinement, zeolite acidity, and/or Al^{3+} ion promotion effects as reasons for the enhanced methane conversion. PM-51%Sil/SR (Figure 5.5 (d)) demonstrated less conversion than SR@ Sil51% catalyst. The factor for lower conversion on physical mixture sample than composite catalyst could be the lack of the confinement effect on PM-51%Sil/SR catalyst.

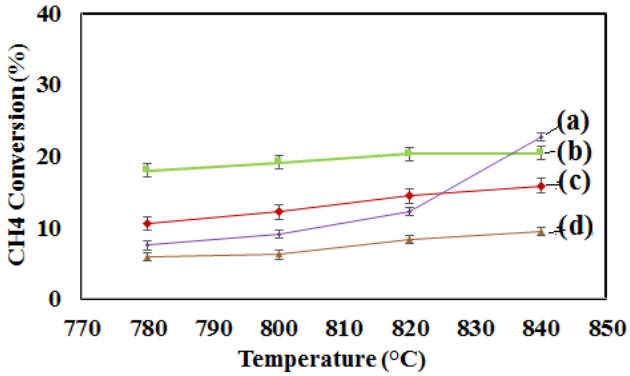

Figure 5.5 CH_4 steam reforming results. (a) Uncoated SR catalyst, (b) SR@ β51% catalyst,(c) SR@ Sil51% catalyst, (d) PM-51% Sil/SR catalyst. Conditions were 780-840°C, atmospheric pressure, molar ratio of CH_4/H_2O = 1.

The C_7H_8 steam reforming results on uncoated SR catalyst (a), SR@ β51% catalyst (b), SR@ Sil51% catalyst (c), PM-51%Sil/SR (d), and just Silicalite-1 zeolite (e) are shown in Figure 5.6 to compare the effect of zeolite acidity on C_7H_8 conversion. Our previous work showed that SR@ β51% catalyst demonstrated almost the same conversion with just H-β zeolite, resulting in the conclusion that zeolite acidity had effect on the C_7H_8 conversion.[124] If composite catalysts (Figure 5.6 (b) and (c)) are compared with SR core (Figure 5.6 (a)) and PM-51%Sil/SR catalysts (Figure 5.6 (d)), the SR core catalyst and PM-51%Sil/SR catalyst showed higher conversion and

more exponential behavior than the composite catalysts due to the diffusion limitation on the zeolite membrane shells. SR@ Sil51% catalyst (Figure 5.6 (c)) yielded less conversion than SR@ β51% catalyst (Figure 5.6 (b)) since silicalite-1 zeolite membrane shell non-acidic and unlike H-β zeolite membrane shell it is not playing role of the C_7H_8 conversion.

Since the Silicalite-1 zeolite by itself (Figure 5.6 (e)) yielded lower C_7H_8 conversion than SR@ Sil51% catalyst, C_7H_8 likely was able to diffuse, possibly through cracks or grain boundaries of the Silicalite-1 shell, to the SR core.

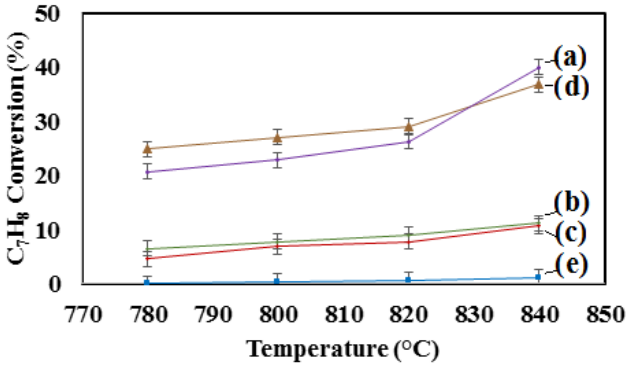

Figure 5.6 C_7H_8 steam reforming results. (a) Uncoated SR catalyst, (b) SR@ β51% catalyst, (c) SR@ Sil51% catalyst, (d) PM-51% Sil/SR catalyst (e) Silicalite-1 powder. Conditions were 780-840°C, atmospheric pressure, molar ratio of C_7H_8/H_2O=1/7.

The product selectivity was calculated for carbon species as defined in the "Reaction Studies" Section for CH_4 and C_7H_8 steam reforming and the results were demonstrated in Table 5.3 and Table 5.4 for PM-51%Sil/SR and SR@ Sil51%, respectively. The primary product of the reaction was found as CO which is expected result since the reaction was conducted with or near stoichiometric feeds.

Table 5.3 Product selectivity of the carbon product of CH_4 and C_7H_8 SR on PM-51%Sil/SR

	CH_4 SR				**C_7H_8 SR**			
	780 (°C)	**800 (°C)**	**820 (°C)**	**840 (°C)**	**780 (°C)**	**800 (°C)**	**820 (°C)**	**840 (°C)**
CO	100	100	100	100	97.1	99.2	97.1	97.5
CO_2	0	0	0	0	2.9	0.4	1.9	1.2
CH_4	-	-	-	-	0	0.4	1.0	1.2

Table 5.4 Product selectivity of the carbon product of CH_4 and C_7H_8 SR on SR@ Sil51%

	CH_4 SR				**C_7H_8 SR**			
	780 (°C)	**800 (°C)**	**820 (°C)**	**840 (°C)**	**780 (°C)**	**800 (°C)**	**820 (°C)**	**840 (°C)**
CO	100	100	100	100	100	100	99.7	97.1
CO_2	0	0	0	0	0	0	0	0
CH_4	-	-	-	-	0	0	0.3	2.9

A 10-hr time on stream experiment (Figure 5.7) were performed on SR@ Sil51% catalyst at 800 °C with molar ratio of $CH_4/C_7H_8/H_2O$ = 1.44/1/7 and the results compared with the identical experiment results on the uncoated SR. The results demonstrated that while uncoated SR catalyst deactivated, SR@ Sil51% remained stable for 10 h ((Figure 5.7 (a)).

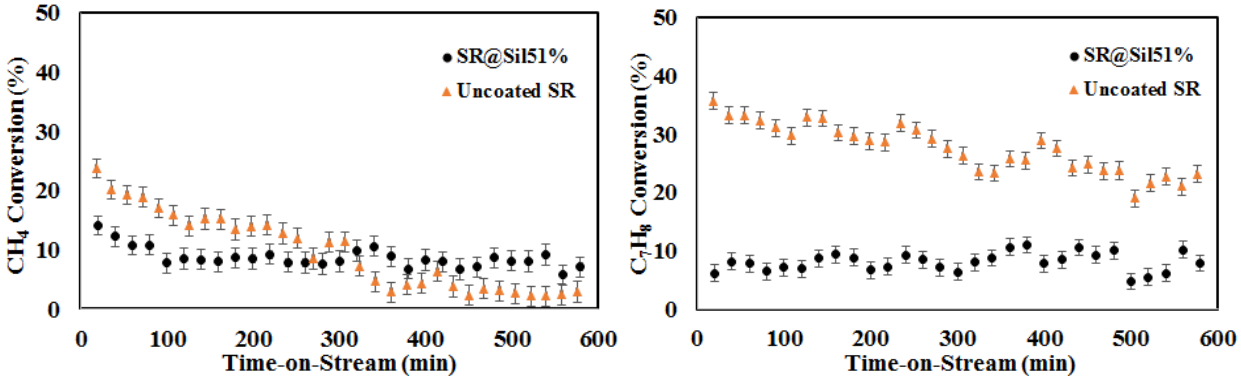

Figure 5.7 Simultaneous CH_4 and C_7H_8 steam reforming for SR@ Sil51% and uncoated SR catalysts. (a) CH_4 steam conversion with TOS and (b) C_7H_8 conversion with TOS.

The SR@ Sil51 catalyst also showed constant C_7H_8 conversion ((Figure 5.7 (b)) for 10 h. (The results for repeated experiment for simultaneous CH_4 and C_7H_8 steam reforming on SR@ Sil51% under the same condition with another batch of catalyst that synthesized same way is given in Appendix B Figure B2.)

5.3.3 Analyses of Internal Diffusion Limitations

Weisz−Prater criteria, Thiele moduli, and effectiveness factors were calculated for CH_4 and C_7H_8 SR on the SR@ Sil51% catalyst using the equations given in "Reaction Studies" Section to analyze the effect of internal diffusion limitations and the results demonstrated in Table 5.5 (Values that were used in the calculations of Weisz−Prater criteria, Thiele moduli, and effectiveness factors are given in Appendix B Table B2). Reactions were assumed as first order kinetic with respect to CH_4 and C_7H_8.[133, 134, 141] Effective diffusivities for CH_4 and C_7H_8 in the zeolite were taken from the literature [130, 131] and these values were corrected to 800 °C using a 3/2 power temperature dependency as proposed by Hirschfelder et al [132] (Calculation detail is given Appendix C). Diffusional limitations were found on the SR@ Sil51% catalyst for CH_4 and C_7H_8 SR since Weisz−Prater criteria values were bigger than 1. Thiele modulus and effectiveness factors results also indicated that reactions were performed in the diffusion-limited regimes since $\Phi n > 1$ for all reactions. However, the effect is much more severe for C_7H_8 as a result of the lower effective diffusion coefficient resulting from its larger size. Although C_7H_8 SR with the composite catalyst is under severe internal diffusion limitations, the SR@ Sil51% catalyst still has slight conversion because cracks or inherent grain boundaries.

Table 5.5 Internal diffusion limitations on SR@ Sil51% catalyst

Sample	Reaction	Internal diffusion limitation (Weisz-Prater Criteria)	Thiele Modulus (Φ_n)	Effectiveness Factor (η)
SR@ Sil51%	CH_4 SR	342.4>1	18.5	0.153
SR@ Sil51%	C_7H_8 SR	$1.5 * 10^7 \gg 1$	$1.2*10^6$	$2.5*10^{-6}$

CHAPTER 6: COMBINATION OF ZEOLITE MEMBRANE COATED COMPOSITE STEAM REFORMING CATALYST AND FISCHER-TROPSCH (CRAFT) CATALYST FOR A SINGLE-STEP CONVERSION OF BIOMASS TO LIQUID (BTL) FUELS

6.1 Introduction

The necessity for clean, sustainable, environmental friendly and local produced fuel is pushing the word to investigate production synthetic transportation fuel from biomass. While Biomass to Liquid process (BTL) process look attractive, there is an economy of scale issue which is resistance to invest in smaller facilities and causes massive chemical plants which are not feasible for all feedstock – product combinations. Thus, this promising process is still far from commercialization and only pilot plants are available at the time [154]. To produce affordable synthetic fuel and bring it to the market, combination of BTL process steps such as Steam Reforming (SR) and Fischer-Tropsch Synthesis (FTS) processes to convert biomass directly to hydrocarbons can be a solution for the economy of scale issue. This combination is named as "process intensification" in chemical process engineering for the development of smaller, safer, more flexible, more efficient, and less costly processes based on the use of novel equipment and devices by developing of novel technologies and methodologies[155]. The concept of the Combination of Reforming and FT (CRAFT) processes to convert methane directly to hydrocarbons studied first by Hutchings et al [156]. The authors selected Ru and Co catalysts for study. However, the initial results at 573K indicate that very low conversion of methane of (4%) to C_2–C_4 hydrocarbons can be achieved with un-optimized catalysts.

Steam reforming and FTS reactions are given below:

(1) $CH_4 + H_2O \longrightarrow CO + 3H_2$ $\Delta H_{r,o}(g) = 206\ kJ\ mol\ CO^{-1}$

(2) $nCO + (2n+1)H_2 \rightarrow C_nH_{2n+2} + nH_2O$ $\Delta H_{r,o}(g) \approx -165\ kJ\ mol\ CO^{-1}$

Although CRAFT concept can be a solution for economy of scale issue, there are some challenges in this concept such as operating temperature differences in steam reforming and FTS processes and open active site environment for reactants which causes back reactions. While steam reforming process is happening at relatively high temperature (~800°C), selectivity towards liquid fuels are favored by low temperature (340°C for high temperature FT process) in FTS process[157]. However, there are many studies to reduce the reforming temperature using different supports and promoters to reduce the operating cost. For instance Matsumura et al. studied effect of support such as silica, γ-alumina, and zirconia for nickel catalysts in steam reforming of methane at 500 °C[158]. The authors found that nickel supported on zirconia is the most effective in the stream reforming at 500 °C (25.5% with CH_4 conversion). Elsayed et al. studied platinum loading effect onto 1.34 wt% Ni/1.00 wt% Mg loaded $(Ce_{0.6}Zr_{0.4})O_2$ support by loading 0-0.64wt% Pt in Dry Reforming[159]. The authors found that the lowest CH_4 and CO_2 conversion temperatures at 454 °C and 437 °C, respectively, using a 0.16% Pt–Ni–Mg/$(Ce_{0.6}Zr_{0.4})O_2$ catalyst and they claim that the Pt/Ni/Mg/$Ce_{0.6}Zr_{0.4}O_2$ catalyst has among the highest activities in the literature (if Ir and Rh catalysts are not included).

In this study, the proposed CRAFT catalyst is a combination of a zeolite encapsulated low temperature steam reforming catalyst and high temperature FTS catalyst. In this combination, low temperature 0.16% Pt–Ni–Mg/$(Ce_{0.6}Zr_{0.4})O_2$ reforming catalyst was used as SR catalyst. The high temperature Fe based FTS catalyst will be utilized to surpass operating temperature difference issue. 0.16% Pt–Ni–Mg/$(Ce_{0.6}Zr_{0.4})O_2$ reforming catalyst was coated with H-β zeolite membrane

to hinder back reactions by separating two active sites. The usage of zeolite membrane (to control molecular traffic) allows entering and exiting the small molecules from SR catalyst such as CH_4 and H_2O as reactant and CO and H_2 as product of SR reaction, rejecting others with large molecular size such as FT reaction products and tar molecules (Figure 6.1). Thus, not only achieve local separation of reactants to lower thermodynamic barriers but also protect the steam reforming catalyst from tar species.

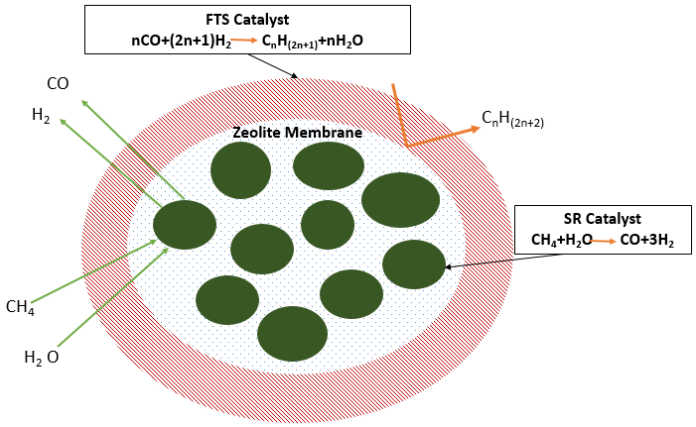

Figure 6.1 Proposed CRAFT (combination of reforming and FT) catalyst

Additionally, steam reforming is endothermic while FTS is exothermic and combining the SR and FTS catalyst, biggest portion of the required heat for SR will be provide from FTS reaction which is demonstrating efficient heat integration. Thus, using CRAFT catalyst, a single-step conversion of methane to liquid fuels will achieves while lowering the cost of heating, cooling, separation and recycle steps (Figure 6.2). In this chapter, the synthesis, characterization and steam reforming (CH_4 and C_7H_8) results of the triple H-β Zeolite encapsulated low temperature steam reforming catalyst, which can be utilized in combination of the triple H-β Zeolite encapsulated low temperature SR catalyst and FTS catalyst, will be explained. Combination of the triple H-β Zeolite

encapsulated low temperature SR catalyst and FTS catalyst will be explained in the next chapter as a future works.

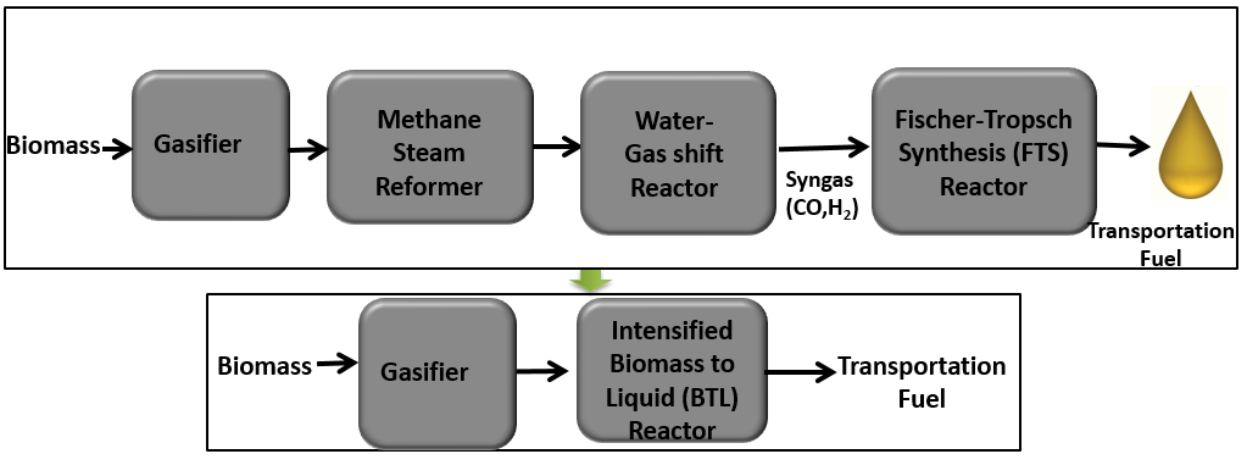

Figure 6.2 Intensified Biomass to Liquid (BTL) process

6.2 Experimental

6.2.1 Synthesis

6.2.1.1 Synthesis of H-β Zeolite

The H-β zeolite was synthesized with the hydrothermal synthesis method described in our previous study.[124] For preparation H-β zeolite precursor solution, 14.4 g of 25 wt% Tetraethylammonium Hydroxide (TEAOH) in water (Acros Organics, Inc.), 4.1 g of SiO_2 (99.98% pure; CAB-O-SIL M-5, scintillation grade, Acros Organics, Inc.), 0.3 g of $((CH_3)_2CHO)_3Al$ (Aluminum iso-propoxide, ≥98% pure; Sigma–Aldrich, Inc.), and 3.6 g of deionized (DI) water was used. All chemicals were mixed under continuous stirring at room temperature for 2 h and then the precursor solution was added into an autoclave and it was kept at 155°C for 3 days for crystallization. After that, the solution was centrifuged to separate liquid and solid phases. The

solid part was washed with distilled water until its pH value was less than 8. Then, it was dried at 120°C for 12 h and was calcined at 550 °C for 8 h.

6.2.1.2 Synthesis of $(Ce_{0.6}Zr_{0.4})O_2$ / 0.16wt%Pt–1.34wt%Ni–1.00wt%Mg Steam Reforming Core Catalyst

The steam reforming $(Ce_{0.6}Zr_{0.4})O_2$/0.16wt%Pt–1.34wt%Ni–1.00wt%Mg catalyst was synthesized by Elsayed et al.[159] The procedure to synthesis the catalyst was given in the literature. According to procedure, Cerium-Zirconium oxide support synthesized first via a co-precipitation The $Ce(NO_3)_3 \times 6H_2O$ (99.5% pure metal basis) and $ZrO(NO_3)_2 \times H_2O$ (99.9% pure metal basis) were dissolved in 150ml DI water and precipitated with NH_4OH (27%, w/w NH3). The solution was filtered and re-dispersed into a 0.25 M NH_4OH solution. The re-filtered solution dried in an oven at 60 °C for 1 h and 120 °C overnight. After drying, calcination was performed at 800 °C for 4 h. Ni, Mg and Pt were loaded by incipient wetness impregnation. All of the precursors (desired amount) were dissolved in an appropriate amount of DI water. The solution was then added to the support until incipient wetness and then dried in an oven for 2 h at 120 °C. The incipient wetness process was repeated until all the solution was added. The powder was calcined at 600 °C for 3 h after the final drying step.

6.2.1.3 Synthesis of Triple H-β Zeolite (60 wt %) Coated Composite Steam Reforming Catalyst

The 60 wt % H-β zeolite coated composite SR catalyst was prepared by triple physical coating method by modifying the single physical coating (physically adhesive) method given in the literature.[18, 103] Silica sol (Ludox: 40 wt%, Sigma–Aldrich, Inc.) was used as binder for H-β zeolite to SR catalyst. Silica sol (3.08 g) was diluted with 1.5 times DI water (4.6 g) by weight. The encapsulation of the H-β zeolite was performed in two steps. First, 0.52 g SR catalyst was wet

impregnated by spraying the prepared silica sol solution and 0.16 g of the H-β zeolite powder was mixed with the moistened SR catalyst in a round bottomed flask, which followed by vigorously shaken until zeolite shell formed. The obtained catalyst was dried at 120°C for 12 h and calcined at 500°C for 3 h. Then, the resulting material was wet impregnated one more time with prepared silica sol solution and 0.38 g of H-β zeolite powder was mixed with the moistened SR catalyst in a combustion boat, vigorously and carefully shaken until the formation of second zeolite shell coating. The obtained catalyst was dried again at 120°C for 12 h and calcined at 500°C for 3 h. After the second calcination, the coating step was repeated third time using 0.24 g of the H-β zeolite powder. The obtained catalyst was dried at 120°C for 12 h and calcined at 500°C for 3 h to increase the mechanical strength of zeolite shell, which resulted in a 60 wt% of H-β zeolite encapsulated composite SR catalyst.

6.2.2 Characterization Methods

X-ray diffraction (XRD) was conducted using a Bruker AXS XRD equipped with a Cu Kα radiation source (0.154 nm) at 40 kV and 40 mA. The machine was operated in a Bragg angle (2θ) range of 20°−90°. The step size was 0.02 for H-β zeolite and 0.004 for the SR catalyst. N_2 physisorption experiments were performed using a Quantachrome Autosorb-iQ to obtain the Brunauer−Emmett−Teller (BET) surface area, pore volumes. The morphology of the samples was determined with Hitachi S-800 scanning electron microscopy (SEM) equipped with an Ametek EDAX, which provides the information on surface elements (using a tilt angle of 30°).

6.2.3 Reaction Studies

The reactions were performed in a fixed-bed quartz U-tube microreactor with internal diameter of 4 mm. The catalyst was loaded between two layers of high-temperature quartz wool in the U-tube, and it was placed into a Thermoscientific Thermolyne furnace. The temperature of

the furnace was controlled using a Eurotherm 3110 proportional −integral − derivative (PID) controller. A manifold that was connected to Alicat Scientific mass flow controllers and two quartz bubblers (toluene and steam) was used to feed the U-tube reactor. The total flow rate was 75 standard cubic centimeters per minute (sccm) (0.64% CH_4, 0.64% H_2O, and 98.7% He) for CH_4 SR, 32.6 sccm (1% C_7H_8, 7% H_2O, and 92% He) for C_7H_8 SR. PerkinElmer gas chromatography (GC) that has a Hayesep-D packed column and thermal conductivity detector (TCD) was used to analyze the effluent gas from the reactor. All of the feed and outlet lines were wrapped with heating tape to prevent condensation prior to entering GC. The mass of catalysts for CH_4 SR was 23.6 mg of H-β Zeolite coated SR catalyst and for C_7H_8 SR was 21 mg of H-β Zeolite coated SR catalyst. Reaction conditions were 450 and 500°C, atmospheric pressure, and stoichiometric feeds (i.e., molar ratios of CH_4/H_2O = 1 and C_7H_8/H_2O = 1:7 for the respective reactions). The reaction procedure was similar for both the CH_4 and C_7H_8 SR reactions. The catalyst was heated (with a ramp rate of 1 °C/min) to 800 °C and then reduced with 5% H_2/He (50 sccm total flow) gas flow for 2 h. After the reduction, the temperature was increased to the highest reaction temperature and the reaction was started. Typical time on stream (TOS) was 1 h at each temperature for both reactions (CH_4 and C_7H_8 reforming experiments). Equilibrium conversion for both CH_4 and C_7H_8 was also calculated using ASPEN PLUS software at the same conditions as the experiments (temperature at between 350- 500 °C, pressure at 1 atm, feed ratios: CH_4:H_2O=1/1 and C_7H_8:H_2O=1/7).

6.3 Results and Discussion

6.3.1 Catalyst Characterization

XRD was carried out to determine whether the zeolite phase was successfully formed in composite catalysts. The results for uncoated low temperature SR catalyst (a), pure H-β zeolite

powder (b), and triple 60 wt% H-β Zeolite coated composite steam reforming catalyst (c), CH_4 SR post-reaction composite catalyst (d), and C_7H_8 SR post-reaction composite catalyst (e) are shown in Figure 6.3, with Miller indices as red and black text indicating the SR and H-β zeolite phases, respectively. The XRD patterns of the SR catalyst (a) and H-β zeolite (b) are compatible with the literature. The 60 wt% H-β Zeolite coated composite steam reforming catalyst profile perfectly matched with the H-β zeolite and SR catalyst showing that the composite catalyst did not change during the preparation process. XRD patterns of the CH_4 and C_7H_8 SR post-reaction samples demonstrated all H-β zeolite and SR catalyst diffraction lines, indicating that the structure of the composite catalysts was maintained during the reactions.

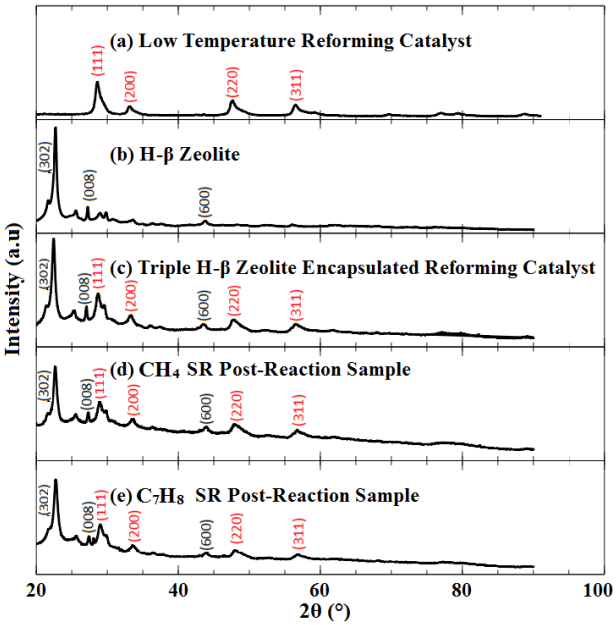

Figure 6.3 XRD patterns. (a) Low temperature reforming catalyst [159], (b) H-β Zeolite, (c) triple 60 wt% H-β Zeolite coated composite steam reforming catalyst

BET surface areas, total pore volumes, mesopore volumes [Barrett−Joyner−Halenda (BJH) method], and micropore volumes (SF method) of the pre- and post-reaction samples are listed in

Table 6.1. The BET surfaces area of the triple 60 wt% H-β Zeolite coated composite steam reforming catalyst was found as 283.7m^2/g which was between the surface areas of the H-β zeolite and SR core catalyst, as expected. The surface area and the pore volume of the composite catalyst did not change after C_7H_8 SR reaction, indicated that the composite catalyst was not altered under reaction conditions.

Table 6.1 BET surface area and pore volume results

Catalyst	BET surface area (m^2/g)	Total Pore Volume (cm^3/g)	Mesopore volume (BJH method) (cm^3/g)	Micropore pore volume (SF method) (cm^3/g)
Reforming[159]	31	0.069	0.008	0.007
H-β Zeolite	723	0.455	0.105	0.356
Fresh Composite	284	0.246	0.123	0.137
C_7H_8 SR Post-Reaction	284	0.246	0.123	0.137

SEM image of the triple 60wt% H-β Zeolite coated composite steam reforming catalyst shown in Figure 6.4. The composite catalyst demonstrated a very uniform and homogeneous shell in Figure 6.4 A, which helps to judge further that the H-β zeolite shell coated successfully. Energy-dispersive spectroscopy (EDS) analysis was also employed to analyze the elemental composition of the SR@ β51% pre-reaction catalyst and cross-section of this sample. The EDS spectra are shown in Figure 6.4 B, with weight and atomic percentages of elements as insets. From the EDS spectrum of the triple 60 wt% H-β Zeolite coated composite steam reforming catalyst, the SR core catalyst elements (Ni, Mg, Ce, and Zr) were not detected on the surface of the composite catalyst. Additionally, Pd and Au elements were detected because Au−Pd was coated to make the composite catalyst conductive. From EDS analysis, SEM images, and XRD patterns showed that the encapsulation of the core SR catalyst by H-β zeolite was successful.

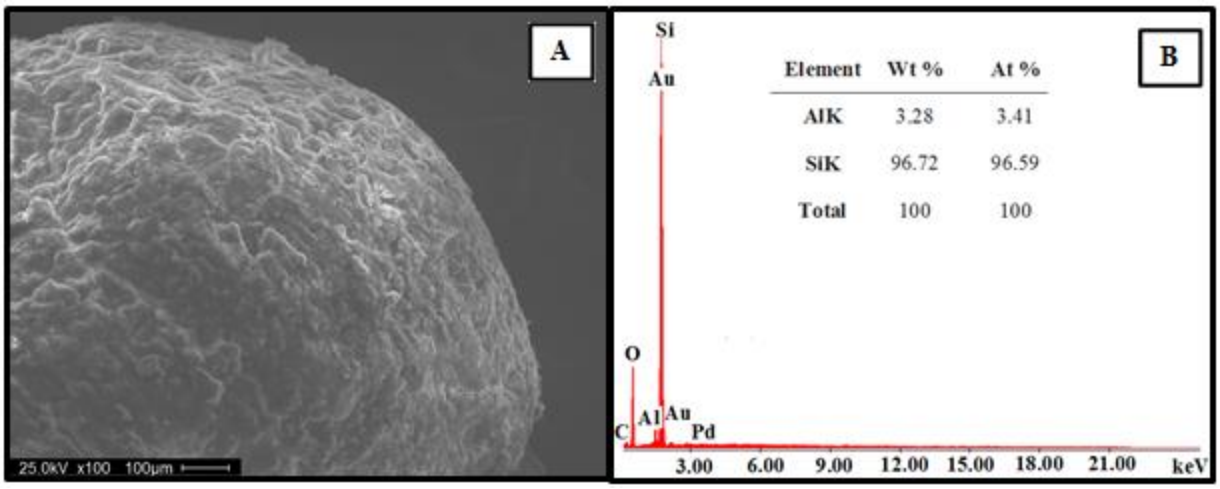

Figure 6.4 SEM images of triple H-β zeolite coated composite steam reforming catalyst (A), EDS analysis result of the triple H-β zeolite coated composite steam reforming catalyst (B)

6.3.2 Reaction and ASPEN Simulation Results

CH_4 and C_7H_8 steam reforming was performed on the triple 60 wt % and double 51 wt % H-β Zeolite coated composite steam reforming catalyst to conversions and the results are presented in Table 6.2. When compare the CH_4 and C_7H_8 conversions results on 60 wt% and 51 wt% composite catalyst, CH_4 conversions was similar on both composite catalysts, however C_7H_8 conversion decreased on the 60 wt% composite catalyst as a result of the increased diffusion limitation with increase zeolite loading.

Table 6.2 CH_4 and C_7H_8 steam reforming results

Temperature (°C)	**60 wt%**	**51 wt%**
	CH_4 Conversion (%)	
450	3.3	3.2
500	5.2	4.9
	C_7H_8 Conversion (%)	

Table 6.2 (Continued)

450	~No Conversion	0.7
500	~No Conversion	1.2

Equilibrium conversion for both CH_4 and C_7H_8 steam reforming was also calculated using ASPEN PLUS software at the same conditions as the experiments (temperature at between 350-500 °C, pressure at 1 atm, feed ratios: CH_4:H_2O=1/1 and C_7H_8:H_2O=1/7) and the result for the CH_4 conversion is given in Figure 6.5 C_7H_8 conversion was found 100 % at the specified temperatures (Details are given in Appendix E).

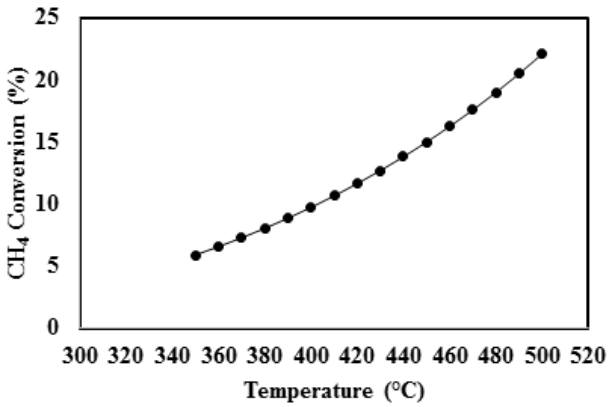

Figure 6.5 CH_4 equilibrium conversion modeling result

From characterization and the reaction results, it can be concluded that the 60 wt% H-β Zeolite coated composite steam reforming catalyst can be utilized to synthesis of combination of zeolite encapsulated low temperature steam reforming catalyst and high temperature FTS catalyst.

CHAPTER 7: CONCLUSIONS AND FUTURE WORKS

Biomass to Liquid (BTL) is one of the promising processes available to produce renewable liquid fuels. However, two major challenges in the BTL process need to be solved to synthesize affordable fuel from biomass. First major challenge is insufficient H_2:CO ratio of biomass gasification product for FTS step due to formation of methane and tars. The steam reforming of hydrocarbons is used to improve the H_2:CO ratio but tars cause the catalysts deactivation rapidly. Second one is economy-of-scale issue. Encapsulated catalysts with inorganic materials have been studied widely in the literature to synthesize active, selective and stable catalysts for XTL process. Thus, to obtain a catalyst which is capable of reforming methane without potential for deactivation by tars, the encapsulation of a core reforming catalyst with porous zeolite shell was examined in this dissertation.

In the 2nd chapter of this study, 34.3 wt% H-β zeolite encapsulated 1.6wt%Ni/1.2wt%Mg/$Ce_{0.6}Zr_{0.4}O_2$ composite SR catalyst was studied to investigate reactant selectivity effect of the H-β zeolite shell on methane and toluene (as a tar model) steam reforming. SEM, XRD and EDS characterization results of the catalysts proved that H-β zeolite shell was coated successfully on the SR catalyst. The pore size of H-β zeolite was found between molecular size of CH_4 and C_7H_8 from the physisorption experiments. CH_4 SR results indicated that coating SR catalyst with the H-β zeolite shell increased the catalyst activity due to either prolonged interactions with the catalyst and/or Al^{+3} promotion to active sites. However, C_7H_8 SR results showed that the H-β zeolite coated composite catalyst had lower C_7H_8 conversions than uncoated

SR catalyst due to reactant selectivity effect of the shell. These results confirmed that H-β zeolite encapsulated composite SR catalyst can be used as a size selective catalyst in reforming.

In the 3rd chapter, the effect of zeolite shell thickness, which is proportional to zeolite amount added, on the reactant selectivity was studied on 51 wt% H-β zeolite encapsulated 1.6wt%Ni-1.2wt%Mg/$Ce_{0.6}Zr_{0.4}O_2$ steam reforming composite catalyst. SEM-EDS and XRD analyses indicated that H-β zeolite shell was coated successfully on the core catalyst. The reaction results indicated that increasing the zeolite shell thickness decreased both the CH_4 and C_7H_8 conversions, due to increased diffusion limitation. Weisz-Prater Criterion and effectiveness factor calculations showed that the reactions were occurring in the diffusion limited regime and diffusion control increased with increasing zeolite loading. Reactant selectivity increased by 1.5 times with increasing zeolite thickness. WHSV comparison of physical mixture samples for C_7H_8 SR confirmed that H-Beta zeolite improved the C_7H_8 conversion by its acidity and/or Al^{3+} promotion. Even though grain boundaries or the polycrystalline nature of the zeolite shell could provide access of C_7H_8 to the SR catalyst core, negligible C_7H_8 conversion was contributed to the core because the zeolite alone control experiment yielded similar conversion to the 51 wt% H-β zeolite encapsulated catalyst. Combined steam reforming was performed on the 51 wt% H-β zeolite encapsulated and uncoated SR catalysts for 10 h TOS indicated that composite catalyst was stable during the reaction but uncoated SR catalyst deactivated.

In the 4th Chapter, zeolite acidity effect was studied on the reactant selectivity using a 51 wt% non-acidic silicalite-1 zeolite encapsulated 1.6wt%Ni-1.2wt%Mg/$Ce_{0.6}Zr_{0.4}O_2$ steam reforming composite catalyst. The catalyst characterization (XRD, SEM, EDS) results demonstrated that the silicalite-1 shell was encapsulated successfully on the SR catalyst. The CH_4 and C_7H_8 SR results indicated that encapsulated non-acidic (Silicalite-1) zeolite on the SR core

catalyst decreased both the CH_4 and C_7H_8 conversions compared to the acidic H-β zeolite because of eliminating contribution to the conversion by zeolite shell acidity. A small conversion of C_7H_8 was observed, possibly due to shell imperfections, such as grain boundaries, the polycrystalline nature of the zeolite shell, or the cracks formed at high temperatures. These imperfections may provide access of C_7H_8 to the SR catalyst core. Weisz-Prater Criterion and effectiveness factor calculations showed that the reactions were occurring in the diffusion limited regime. Simultaneous steam reforming was carried out on the SR@ Sil51% and uncoated SR catalysts for 10 h TOS indicated that composite catalyst was stable during the reaction but uncoated SR catalyst deactivated as expected.

Lastly, in the 5th chapter, 60 wt% H-β zeolite encapsulated low temperature 0.16wt%Pt–1.34wt%Ni–1.00wt%Mg/$(Ce_{0.6}Zr_{0.4})O_2$ steam reforming composite catalyst was synthesized for use in the combination of steam reforming and Fischer-Tropsch synthesis catalyst. SEM and EDS results demonstrated that the H-β zeolite shell was encapsulated successfully on the low temperature SR catalyst. The CH_4 and C_7H_8 steam reforming results showed that this composite catalyst can be used to synthesis of combination steam reforming and Fischer-Tropsch synthesis catalyst since no C_7H_8 conversion was seen at 450°C and 500°C while there is CH_4 activation on it. To sum up, we demonstrated through multiple studies that zeolite coated SR catalyst structures can be used to control reactant selectivity, allowing it to be used in practical industrial reactors to reduce deactivation as well as in process intensification.

Future directions based on the study presented herein include (i) examination of the combination of BTL process steps such as Steam Reforming (SR) and Fischer-Tropsch Synthesis (FTS) processes to convert biomass directly to hydrocarbons for a possible solution for the economy of scale issue (as explained chapter 5). To synthesize combine catalyst, high temperature

Fe based FTS catalyst (Fe/Cu/K) can be coated onto the synthesized H-β Zeolite encapsulated low temperature steam reforming catalyst to overcome temperature differences with the steam reforming and FTS reactions. After synthesizing the combined catalyst, CH_4 steam reforming can be performed on it to analyze the catalyst performance. Thereby, the syngas which produced by steam reforming will be the reactants of the FTS catalyst. (ii) Reaction-diffusion modeling on the zeolite encapsulated composite catalyst to investigate the concentration changes of the reactants (CH_4 and C_7H_8) and products with time and position through the zeolite shell using MATLAB or COMSOL modeling tools. (iii) Investigation of scaled up versions of the encapsulation process onto the reforming catalyst to make the techniques more commercially viable. The zeolite encapsulated steam reforming composite catalyst was synthesized by vigorously shaking of the wet impregnated steam reforming catalyst and zeolite until the zeolite shell formed. This procedure was done by hand and since the synthesis was lab scale it was not a challenge. However, shaking by hand will be a big challenge to scaling up the synthesis of the composite catalyst. Thus, other encapsulating methods (such as hydrothermal synthesis method) which hand-shaking was not being used can be applied to synthesis zeolite shell directly over the steam reforming catalyst.

REFERENCES

[1] Yin Y, Rioux RM, Erdonmez CK, Hughes S, Somorjai GA, Alivisatos AP. Formation of hollow nanocrystals through the nanoscale Kirkendall effect. Science 2004; 304: 711-714.

[2] Kuo C-H, Tang Y, Chou L-Y, Sneed BT, Brodsky CN, Zhao Z, Tsung C-K. Yolk–shell nanocrystal@ ZIF-8 nanostructures for gas-phase heterogeneous catalysis with selectivity control. Journal of the American Chemical Society 2012; 134: 14345-14348.

[3] Trovarelli A. Catalysis by ceria and related materials. World Scientific, 2002.

[4] Gawande MB, Goswami A, Asefa T, Guo H, Biradar AV, Peng D-L, Zboril R, Varma RS. Core–shell nanoparticles: synthesis and applications in catalysis and electrocatalysis. Chemical Society Reviews 2015; 44: 7540-7590.

[5] Fang X, Liu S, Zang J, Xu C, Zheng M-S, Dong Q-F, Sun D, Zheng N. Precisely controlled resorcinol–formaldehyde resin coating for fabricating core–shell, hollow, and yolk–shell carbon nanostructures. Nanoscale 2013; 5: 6908-6916.

[6] Li G, Tang Z. Noble metal nanoparticle@ metal oxide core/yolk–shell nanostructures as catalysts: recent progress and perspective. Nanoscale 2014; 6: 3995-4011.

[7] Wei J. Nonlinear phenomena in zeolite diffusion and reaction. Industrial & engineering chemistry research 1994; 33: 2467-2472.

[8] Plawsky JL. Transport phenomena fundamentals. CRC Press, 2014.

[9] Corma A. Inorganic solid acids and their use in acid-catalyzed hydrocarbon reactions. Chemical Reviews 1995; 95: 559-614.

[10] Flanigen EM, Jansen J, van Bekkum H. Introduction to Zeolite Science and Practice. Elsevier, 1991.

[11] Csicsery SM. Shape-selective catalysis in zeolites. Zeolites 1984; 4: 202-213.

[12] Bao J, He J, Zhang Y, Yoneyama Y, Tsubaki N. A core/shell catalyst produces a spatially confined effect and shape selectivity in a consecutive reaction. Angewandte Chemie 2008; 120: 359-362.

[13] Bao J, Yang G, Okada C, Yoneyama Y, Tsubaki N. H-type zeolite coated iron-based multiple-functional catalyst for direct synthesis of middle isoparaffins from syngas. Applied Catalysis A: General 2011; 394: 195-200.

[14] He J, Liu Z, Yoneyama Y, Nishiyama N, Tsubaki N. Multiple-Functional Capsule Catalysts: A Tailor-Made Confined Reaction Environment for the Direct Synthesis of Middle Isoparaffins from Syngas. Chemistry–A European Journal 2006; 12: 8296-8304.

[15] He J, Yoneyama Y, Xu B, Nishiyama N, Tsubaki N. Designing a capsule catalyst and its application for direct synthesis of middle isoparaffins. Langmuir 2005; 21: 1699-1702.

[16] Li X, He J, Meng M, Yoneyama Y, Tsubaki N. One-step synthesis of H–β zeolite-enwrapped Co/Al 2 O 3 Fischer–Tropsch catalyst with high spatial selectivity. Journal of Catalysis 2009; 265: 26-34.

[17] Yang G, Tsubaki N, Shamoto J, Yoneyama Y, Zhang Y. Confinement effect and synergistic function of H-ZSM-5/Cu-ZnO-Al2O3 capsule catalyst for one-step controlled synthesis. Journal of the American Chemical Society 2010; 132: 8129-8136.

[18] Yang G, Xing C, Hirohama W, Jin Y, Zeng C, Suehiro Y, Wang T, Yoneyama Y, Tsubaki N. Tandem catalytic synthesis of light isoparaffin from syngas via Fischer–Tropsch synthesis by newly developed core–shell-like zeolite capsule catalysts. Catalysis today 2013; 215: 29-35.

[19] Yoneyama Y, San X, Iwai T, Tsubaki N. One-step synthesis of isoparaffin from synthesis gas using hybrid catalyst with supercritical butane. Energy & Fuels 2008; 22: 2873-2876.

[20] Joo SH, Park JY, Tsung C-K, Yamada Y, Yang P, Somorjai GA. Thermally stable Pt/mesoporous silica core–shell nanocatalysts for high-temperature reactions. Nature materials 2009; 8: 126-131.

[21] Galanti M, Fanelli D, Angioletti-Uberti S, Ballauff M, Dzubiella J, Piazza F. Reaction rate of a composite core–shell nanoreactor with multiple nanocatalysts. Physical Chemistry Chemical Physics 2016; 18: 20758-20767.

[22] Lu Y, Mei Y, Drechsler M, Ballauff M. Thermosensitive core–shell particles as carriers for Ag nanoparticles: modulating the catalytic activity by a phase transition in networks. Angewandte Chemie International Edition 2006; 45: 813-816.

[23] Suib SL. New and future developments in catalysis: Catalysis for remediation and environmental concerns. Newnes, 2013.

[24] Li D, Nakagawa Y, Tomishige K. Methane reforming to synthesis gas over Ni catalysts modified with noble metals. Applied Catalysis A: General 2011; 408: 1-24.

[25] Hirai T, Ikenaga N-o, Miyake T, Suzuki T. Production of hydrogen by steam reforming of glycerin on ruthenium catalyst. Energy & Fuels 2005; 19: 1761-1762.

[26] Kikuchi E, Tanaka S, Yamazaki Y, Morita Y. Steam reforming of hydrocarbons on noble metal catalysts (part 1). Bulletin of the Japan Petroleum Institute 1974; 16: 95-98.

[27] Rostrupnielsen J, Hansen JB. CO 2-reforming of methane over transition metals. Journal of Catalysis 1993; 144: 38-49.

[28] Cheekatamarla PK, Finnerty C. Reforming catalysts for hydrogen generation in fuel cell applications. Journal of Power Sources 2006; 160: 490-499.

[29] Mark MF, Maier WF. CO 2-reforming of methane on supported Rh and Ir catalysts. Journal of Catalysis 1996; 164: 122-130.

[30] Guggilla VS, Akyurtlu J, Akyurtlu A, Blankson I. Steam Reforming of n-Dodecane over Ru− Ni-Based Catalysts. Industrial & Engineering Chemistry Research 2010; 49: 8164-8173.

[31] Sutthiumporn K, Kawi S. Promotional effect of alkaline earth over Ni–La 2 O 3 catalyst for CO 2 reforming of CH 4: role of surface oxygen species on H 2 production and carbon suppression. International Journal of Hydrogen Energy 2011; 36: 14435-14446.

[32] Mayne JM, Tadd AR, Dahlberg KA, Schwank JW. Influence of thiophene on the isooctane reforming activity of Ni-based catalysts. Journal of Catalysis 2010; 271: 140-152.

[33] Sehested J. Four challenges for nickel steam-reforming catalysts. Catalysis Today 2006; 111: 103-110.

[34] Christensen KO, Chen D, Lødeng R, Holmen A. Effect of supports and Ni crystal size on carbon formation and sintering during steam methane reforming. Applied Catalysis A: General 2006; 314: 9-22.

[35] Rostrup-Nielsen JR, Sehested J, Nørskov JK. Hydrogen and synthesis gas by steam-and C0 2 reforming. Advances in catalysis 2002; 47: 65-139.

[36] Gould TD, Izar A, Weimer AW, Falconer JL, Medlin JW. Stabilizing Ni catalysts by molecular layer deposition for harsh, dry reforming conditions. Acs Catalysis 2014; 4: 2714-2717.

[37] Li Z, Mo L, Kathiraser Y, Kawi S. Yolk–satellite–shell structured Ni–yolk@ Ni@ SiO2 nanocomposite: superb catalyst toward methane CO2 reforming reaction. ACS Catalysis 2014; 4: 1526-1536.

[38] Li Z, Kathiraser Y, Ashok J, Oemar U, Kawi S. Simultaneous Tuning Porosity and Basicity of Nickel@ Nickel–Magnesium Phyllosilicate Core–Shell Catalysts for CO2 Reforming of CH4. Langmuir 2014; 30: 14694-14705.

[39] Mond L, Langer C. British Patent 12 1888; 608.

[40] Smirniotis P, Gunugunuri K. Water Gas Shift Reaction: Research Developments and Applications. Elsevier, 2015.

[41] Muhler M. JM Thomas and WJ Thomas: Principles and Practice of Heterogeneous Catalysis, VCH, Weinheim, 1997, ISBN 3-527-29239-X, Preis: 88,–DM. Berichte der Bunsengesellschaft für physikalische Chemie 1997; 101: 1560-1560.

[42] Mendes D, Mendes A, Madeira L, Iulianelli A, Sousa J, Basile A. The water-gas shift reaction: from conventional catalytic systems to Pd-based membrane reactors—a review. Asia-Pacific Journal of Chemical Engineering 2010; 5: 111-137.

[43] Qi X, Flytzani-Stephanopoulos M. Activity and stability of Cu-CeO2 catalysts in high-temperature water-gas shift for fuel-cell applications. Industrial & engineering chemistry research 2004; 43: 3055-3062.

[44] Chen C-S, Cheng W-H, Lin S-S. Study of iron-promoted Cu/SiO 2 catalyst on high temperature reverse water gas shift reaction. Applied Catalysis A: General 2004; 257: 97-106.

[45] Yeung CMY, Tsang SC. Some optimization in preparing core-shell Pt–ceria catalysts for water gas shift reaction. Journal of Molecular Catalysis A: Chemical 2010; 322: 17-25.

[46] Li Y, Fu Q, Flytzani-Stephanopoulos M. Low-temperature water-gas shift reaction over Cu- and Ni-loaded cerium oxide catalysts. Applied Catalysis B: Environmental 2000; 27: 179-191.

[47] Ratnasamy C, Wagner JP. Water gas shift catalysis. Catalysis Reviews 2009; 51: 325-440.

[48] Fu Q, Saltsburg H, Flytzani-Stephanopoulos M. Active nonmetallic Au and Pt species on ceria-based water-gas shift catalysts. Science 2003; 301: 935-938.

[49] Andreeva D, Idakiev V, Tabakova T, Ilieva L, Falaras P, Bourlinos A, Travlos A. Low-temperature water-gas shift reaction over Au/CeO 2 catalysts. catalysis Today 2002; 72: 51-57.

[50] Tsipouriari V, Efstathiou A, Zhang Z, Verykios X. Reforming of methane with carbon dioxide to synthesis gas over supported Rh catalysts. Catalysis today 1994; 21: 579-587.

[51] Kim CH, Thompson LT. Deactivation of Au/CeO x water gas shift catalysts. Journal of Catalysis 2005; 230: 66-74.

[52] Saw ET, Oemar U, Ang ML, Hidajat K, Kawi S. Highly Active and Stable Bimetallic Nickel–Copper Core–Ceria Shell Catalyst for High-Temperature Water–Gas Shift Reaction. ChemCatChem 2015; 7: 3358-3367.

[53] Yeung CM, Yu KMK, Fu QJ, Thompsett D, Petch MI, Tsang SC. Engineering Pt in ceria for a maximum metal-support interaction in catalysis. Journal of the American Chemical Society 2005; 127: 18010-18011.

[54] Tian H, Li X, Zeng L, Gong J. Recent Advances on the Design of Group VIII Base-Metal Catalysts with Encapsulated Structures. ACS Catalysis 2015; 5: 4959-4977.

[55] Yeung CM, Meunier F, Burch R, Thompsett D, Tsang SC. Comparison of new microemulsion prepared "Pt-in-Ceria" catalyst with conventional "Pt-on-Ceria" catalyst for water-gas shift reaction. The Journal of Physical Chemistry B 2006; 110: 8540-8543.

[56] Yeung CMY, Tsang SC. Noble Metal Core− Ceria Shell Catalysts For Water− Gas Shift Reaction. The Journal of Physical Chemistry C 2009; 113: 6074-6087.

[57] Wieder NL, Cargnello M, Bakhmutsky K, Montini T, Fornasiero P, Gorte RJ. Study of the Water-Gas-Shift Reaction on Pd@ CeO2/Al2O3 Core− Shell Catalysts†. The Journal of Physical Chemistry C 2010; 115: 915-919.

[58] Cargnello M, Wieder NL, Montini T, Gorte RJ, Fornasiero P. Synthesis of Dispersible Pd@ CeO2 Core− Shell Nanostructures by Self-Assembly. Journal of the American Chemical Society 2009; 132: 1402-1409.

[59] Cargnello M, Montini T, Polizzi S, Wieder NL, Gorte RJ, Graziani M, Fornasiero P. Novel embedded Pd@ CeO 2 catalysts: a way to active and stable catalysts. Dalton Transactions 2010; 39: 2122-2127.

[60] Fischer F, Tropsch H. Uber die Herstellung synthetischer olgemische (Synthol) durch Aufbau aus Kohlenoxyd und Wasserstoff. Brennst. Chem 1923; 4: 276-285.

[61] de Smit E, Weckhuysen BM. The renaissance of iron-based Fischer–Tropsch synthesis: on the multifaceted catalyst deactivation behaviour. Chemical Society Reviews 2008; 37: 2758-2781.

[62] Dry M, Hoogendoorn J. Technology of the Fischer-Tropsch process. Catalysis Reviews—Science and Engineering 1981; 23: 265-278.

[63] Kölbel H, Ralek M. The Fischer-Tropsch synthesis in the liquid phase. Catalysis Reviews Science and Engineering 1980; 21: 225-274.

[64] Rao V, Stiegel G, Cinquegrane G, Srivastava R. Iron-based catalysts for slurry-phase Fischer-Tropsch process: Technology review. Fuel processing technology 1992; 30: 83-107.

[65] Satterfield CN, Hanlon RT, Tung SE, Zou ZM, Papaefthymiou GC. Effect of water on the iron-catalyzed Fischer-Tropsch synthesis. Industrial & engineering chemistry product research and development 1986; 25: 407-414.

[66] Srivastava R, Rao V, Cinquegrane G, Stiegel G. Catalysts for Fischer-Tropsch. Hydrocarbon Processing;(USA) 1990; 69:

[67] Zhang Q, Kang J, Wang Y. Development of novel catalysts for Fischer–Tropsch synthesis: tuning the product selectivity. ChemCatChem 2010; 2: 1030-1058.

[68] Van Der Laan GP, Beenackers A. Kinetics and selectivity of the Fischer–Tropsch synthesis: a literature review. Catalysis Reviews 1999; 41: 255-318.

[69] Dalai A, Davis B. Fischer–Tropsch synthesis: a review of water effects on the performances of unsupported and supported Co catalysts. Applied Catalysis A: General 2008; 348: 1-15.

[70] Schulz H. Short history and present trends of Fischer–Tropsch synthesis. Applied Catalysis A: General 1999; 186: 3-12.

[71] Dry ME. The fischer–tropsch process: 1950–2000. Catalysis today 2002; 71: 227-241.

[72] Jiang N, Yang G, Zhang X, Wang L, Shi C, Tsubaki N. A novel silicalite-1 zeolite shell encapsulated iron-based catalyst for controlling synthesis of light alkenes from syngas. Catalysis Communications 2011; 12: 951-954.

[73] Iglesia E, Soled SL, Baumgartner JE, Reyes SC. Synthesis and catalytic properties of eggshell cobalt catalysts for the Fischer-Tropsch synthesis. Topics in Catalysis 1995; 2: 17-27.

[74] Iglesia E, Vroman H, Soled S, Baumgartner J, Fiato RA, Selective catalysts and their preparation for catalytic hydrocarbon synthesis, Google Patents, 1991.

[75] Magrini-Bair KA, Jablonski WS, Parent YO, Yung MM. Bench-and Pilot-Scale Studies of Reaction and Regeneration of Ni–Mg–K/Al_2O_3 for Catalytic Conditioning of Biomass-Derived Syngas. Topics in Catalysis 2012; 55: 209-217.

[76] Chen Cs, Feng Sj, Ran S, Zhu Dc, Liu W, Bouwmeester HJ. Conversion of Methane to Syngas by a Membrane-Based Oxidation–Reforming Process. Angewandte Chemie International Edition 2003; 42: 5196-5198.

[77] Swierczynski D, Courson C, Kiennemann A. Study of steam reforming of toluene used as model compound of tar produced by biomass gasification. Chem. Eng. Process. 2008; 47: 508-513.

[78] Simell PA, Hepola JO, Krause AOI. Effects of gasification gas components on tar and ammonia decomposition over hot gas cleanup catalysts. Fuel 1997; 76: 1117-1127.

[79] Xu J, Froment GF. Methane steam reforming, methanation and water-gas shift: I. Intrinsic kinetics. AIChE Journal 1989; 35: 88-96.

[80] Kuhn JN, Zhao Z, Felix LG, Slimane RB, Choi CW, Ozkan US. Olivine catalysts for methane- and tar-steam reforming. Applied Catalysis B 2008; 81: 14-26.

[81] Abu El-Rub Z, Bramer E, Brem G. Review of catalysts for tar elimination in biomass gasification processes. Industrial and Engineering Chemistry Research 2004; 43: 6911-6919.

[82] Dayton D, A review of the literature on catalytic biomass tar destruction, US DOE NREL Report Golden, CO, 2002, pp. 510-32815.

[83] Al-Khattaf S, Ali SA, Aitani AM, Žilková N, Kubička D, Čejka J. Recent Advances in Reactions of Alkylbenzenes Over Novel Zeolites: The Effects of Zeolite Structure and Morphology. Catalysis Reviews - Science and Engineering 2014; 56: 333-402.

[84] Jafari M, Mohammadi T, Kazemimoghadam M. Synthesis and characterization of ultrafine sub-micron Na-LTA zeolite particles prepared via hydrothermal template-free method. Ceramics International 2014; 40: 12075-12080.

[85] Walker DM, Pettit SL, Wolan JT, Kuhn JN. Synthesis gas production to desired hydrogen to carbon monoxide ratios by tri-reforming of methane using Ni–MgO–$(Ce,Zr)O_2$ catalysts. Appl. Catal. A: Gen. 2012; 445: 61-68.

[86] Dal Santo V, Gallo A, Naldoni A, Guidotti M, Psaro R. Bimetallic heterogeneous catalysts for hydrogen production. Catalysis Today 2012; 197: 190-205.

[87] Sukonket T, Khan A, Saha B, Ibrahim H, Tantayanon S, Kumar P, Idem R. Influence of the catalyst preparation method, surfactant amount, and steam on CO_2 reforming of CH_4 over $5Ni/Ce_{0.6}Zr_{0.4}O_2$ catalysts. Energy and Fuels 2011; 25: 864-877.

[88] LeValley TL, Richard AR, Fan M. The progress in water gas shift and steam reforming hydrogen production technologies–A review. International Journal of Hydrogen Energy 2014; 39: 16983-17000.

[89] Roberge TM, Blavo SO, Holt C, Matter PH, Kuhn JN. Effect of Molybdenum on the Sulfur-Tolerance of Cerium–Cobalt Mixed Oxide Water–Gas Shift Catalysts. Topics in Catalysis 2013; 56: 1892-1898.

[90] Kuhn JN, Zhao Z, Senefeld-Naber A, Felix LG, Slimane RB, Choi CW, Ozkan US. Ni-olivine catalysts prepared by thermal impregnation: structure, steam reforming activity, and stability. Applied Catalysis A 2008; 341: 43-49.

[91] Takeguchi T, Furukawa S-N, Inoue M, Eguchi K. Autothermal reforming of methane over Ni catalysts supported over $CaO–CeO_2–ZrO_2$ solid solution. Applied Catalysis A 2003; 240: 223-233.

[92] Laosiripojana N, Sutthisripok W, Assabumrungrat S. Synthesis gas production from dry reforming of methane over CeO_2 doped Ni/Al_2O_3: Influence of the doping ceria on the resistance toward carbon formation. Chemical Engineering Journal 2005; 112: 13-22.

[93] Halabi M, De Croon M, Van der Schaaf J, Cobden P, Schouten J. Low temperature catalytic methane steam reforming over ceria–zirconia supported rhodium. Applied Catalysis A 2010; 389: 68-79.

[94] Roh H, Jun K, Dong W, Park S, Baek Y. Highly stable Ni catalyst supported on $Ce–ZrO_2$ for oxy-steam reforming of methane. Catalysis letters 2001; 74: 31-36.

[95] Roh H-S, Platon A, Wang Y, King DL. Catalyst deactivation and regeneration in low temperature ethanol steam reforming with Rh/CeO2–ZrO2 catalysts. Catalysis letters 2006; 110: 1-6.

[96] Andache M, Rezaei M, Kazemi Moghadam M. A nanocrystalline MgO support for Ni catalysts for steam reforming of CH_4. Chinese Journal of Catalysis 2013; 34: 1443-1448.

[97] Hu YH, Ruckenstein E. Binary MgO-based solid solution catalysts for methane conversion to syngas. Catalysis Reviews - Science and Engineering 2002; 44: 423-453.

[98] Bárcia PS, Silva JA, Rodrigues AE. Adsorption equilibrium and kinetics of branched hexane isomers in pellets of BETA zeolite. Microporous and mesoporous materials 2005; 79: 145-163.

[99] Millini R, Perego C, Parker W, Flego C, Girotti G. Stability upon thermal treatment of coked zeolite beta. Studies in Surface Science and Catalysis 2004; 154: 1214-1221.

[100] Corma A, Rey F, Valencia S, Jordá JL, Rius J. A zeolite with interconnected 8-, 10-and 12-ring pores and its unique catalytic selectivity. Nature materials 2003; 2: 493-497.

[101] Li X, He J, Meng M, Yoneyama Y, Tsubaki N. One-step synthesis of H–β zeolite-enwrapped Co/Al_2O_3 Fischer–Tropsch catalyst with high spatial selectivity. J. Catal. 2009; 265: 26-34.

[102] Rossignol S, Gérard F, Duprez D. Effect of the preparation method on the properties of zirconia-ceria materials. Journal of Materials Chemistry 1999; 9: 1615-1620.

[103] Pinkaew K, Yang G, Vitidsant T, Jin Y, Zeng C, Yoneyama Y, Tsubaki N. A new core–shell-like capsule catalyst with SAPO-46 zeolite shell encapsulated Cr/ZnO for the controlled tandem synthesis of dimethyl ether from syngas. Fuel 2013; 111: 727-732.

[104] Robson H. Verified synthesis of zeolitic materials. (second). Elsevier, 2001.

[105] Lee J-K, Rhee H-K. Characteristics of Pt/H-beta and Pt/H-mordenite catalysts for the isomerization of n-hexane. Catalysis Today 1997; 38: 235-242.

[106] Biswas P, Kunzru D. Steam reforming of ethanol for production of hydrogen over Ni/CeO_2–ZrO_2 catalyst: effect of support and metal loading. International Journal of Hydrogen Energy 2007; 32: 969-980.

[107] Wang L, Murata K, Inaba M. Development of novel highly active and sulphur-tolerant catalysts for steam reforming of liquid hydrocarbons to produce hydrogen. Applied Catalysis A 2004; 257: 43-47.

[108] Jacobs P, Flanigen E, Jansen J, van Bekkum H. Introduction to zeolite science and practice. Elsevier, 2001.

[109] Yu M, Noble RD, Falconer JL. Zeolite membranes: microstructure characterization and permeation mechanisms. Accounts of chemical research 2011; 44: 1196-1206.

[110] Freyhardt C, Tsapatsis M, Lobo R, Balkus K, Davis M. A high-silica zeolite with a 14-tetrahedral-atom pore opening. Nature 1996; 381: 295-298.

[111] Lai Z, Bonilla G, Diaz I, Nery JG, Sujaoti K, Amat MA, Kokkoli E, Terasaki O, Thompson RW, Tsapatsis M. Microstructural optimization of a zeolite membrane for organic vapor separation. Science 2003; 300: 456-460.

[112] Willhammar T, Sun J, Wan W, Oleynikov P, Zhang D, Zou X, Moliner M, Gonzalez J, Martínez C, Rey F. Structure and catalytic properties of the most complex intergrown zeolite ITQ-39 determined by electron crystallography. Nature Chemistry 2012; 4: 188-194.

[113] Rocha J, Anderson MW. Microporous Titanosilicates and other Novel Mixed Octahedral-Tetrahedral Framework Oxides. European Journal of Inorganic Chemistry 2000; 2000: 801-818.

[114] Anderson M, Terasaki O, Ohsuna T, Philippou A, MacKay S, Ferreira A, Rocha J, Lidin S. Structure of the microporous titanosilicate ETS-10. Nature 1994; 367: 347-351.

[115] Davis ME. Ordered porous materials for emerging applications. Nature 2002; 417: 813-821.

[116] Christensen CH, Johannsen K, Schmidt I, Christensen CH. Catalytic benzene alkylation over mesoporous zeolite single crystals: improving activity and selectivity with a new family of porous materials. Journal of the american chemical society 2003; 125: 13370-13371.

[117] Hartmann M. Hierarchical zeolites: A proven strategy to combine shape selectivity with efficient mass transport. Angewandte Chemie International Edition 2004; 43: 5880-5882.

[118] Fechete I, Wang Y, Védrine JC. The past, present and future of heterogeneous catalysis. Catalysis Today 2012; 189: 2-27.

[119] Corma A. State of the art and future challenges of zeolites as catalysts. Journal of Catalysis 2003; 216: 298-312.

[120] Weisz P, Frilette V. Intracrystalline and molecular-shape-selective catalysis by zeolite salts. The Journal of Physical Chemistry 1960; 64: 382-382.

[121] Derouane EG. Zeolites as solid solvents. J. Mol. Catal. A: Chem. 1998; 134: 29-45.

[122] Csicsery SM. Catalysis by shape selective zeolites-science and technology. Pure and Applied Chemistry 1986; 58: 841-856.

[123] Cimenler U, Joseph B, Kuhn JN. Molecular-size selective H-β zeolite-encapsulated Ce-Zr/Ni-Mg catalysts for steam reforming. Applied Catalysis A: General 2015; 505: 494-500.

[124] Cimenler U, Joseph B, Kuhn JN. Molecular-Size Selective H–β Zeolite-Encapsulated Ce-Zr/Ni-Mg Catalysts for Steam Reforming. Appl. Catal., A 2015; 505: 494–500.

[125] Xomeritakis G, Nair S, Tsapatsis M. Transport properties of alumina-supported MFI membranes made by secondary (seeded) growth. Microporous and Mesoporous Materials 2000; 38: 61-73.

[126] Walker DM, Pettit SL, Wolan JT, Kuhn JN. Synthesis gas production to desired hydrogen to carbon monoxide ratios by tri-reforming of methane using Ni–MgO–(Ce, Zr) O 2 catalysts. Applied Catalysis A: General 2012; 445: 61-68.

[127] Baertsch CD, Funke HH, Falconer JL, Noble RD. Permeation of aromatic hydrocarbon vapors through silicalite-zeolite membranes. The Journal of Physical Chemistry 1996; 100: 7676-7679.

[128] Feller A, Guzman A, Zuazo I, Lercher JA. On the mechanism of catalyzed isobutane/butene alkylation by zeolites. Journal of Catalysis 2004; 224: 80-93.

[129] Kotrel S, Rosynek M, Lunsford J. Intrinsic catalytic cracking activity of hexane over H-ZSM-5, H-β and HY zeolites. The Journal of Physical Chemistry B 1999; 103: 818-824.

[130] Jobic H, Bée M, Caro J, Bülow M, Kärger J. Molecular self-diffusion of methane in zeolite ZSM-5 by quasi-elastic neutron scattering and nuclear magnetic resonance pulsed field gradient technique. Journal of the Chemical Society, Faraday Transactions 1: Physical Chemistry in Condensed Phases 1989; 85: 4201-4209.

[131] Muller G, Narbeshuber T, Mirth G, Lercher JA. Infrared microscopic study of sorption and diffusion of toluene in ZSM-5. The Journal of Physical Chemistry 1994; 98: 7436-7439.

[132] Hirschfelder JO, Curtiss CF, Bird RB, Mayer MG. Molecular theory of gases and liquids. New York: Wiley 1954.

[133] Jones G, Jakobsen JG, Shim SS, Kleis J, Andersson MP, Rossmeisl J, Abild-Pedersen F, Bligaard T, Helveg S, Hinnemann B. First principles calculations and experimental insight into methane steam reforming over transition metal catalysts. Journal of Catalysis 2008; 259: 147-160.

[134] Swierczynski D, Courson C, Kiennemann A. Study of steam reforming of toluene used as model compound of tar produced by biomass gasification. Chemical Engineering and Processing: Process Intensification 2008; 47: 508-513.

[135] Aoki K, Kusakabe K, Morooka S. Separation of gases with an A-type zeolite membrane. Industrial & engineering chemistry research 2000; 39: 2245-2251.

[136] Morigami Y, Kondo M, Abe J, Kita H, Okamoto K. The first large-scale pervaporation plant using tubular-type module with zeolite NaA membrane. Separation and Purification Technology 2001; 25: 251-260.

[137] Coronas J, Santamaria J. The use of zeolite films in small-scale and micro-scale applications. Chemical Engineering Science 2004; 59: 4879-4885.

[138] Zhang T, Zhang X, Yan X, Lin L, Liu H, Qiu J, Yeung KL. Core–shell Pd/ZSM-5@ ZIF-8 membrane micro-reactors with size selectivity properties for alkene hydrogenation. Catalysis Today 2014; 236: 41-48.

[139] Chen P, Chen X, Chen X, Kita H. Preparation and catalytic activity of titanium silicalite-1 zeolite membrane with TPABr as template. Journal of Membrane Science 2009; 330: 369-378.

[140] de la Iglesia Ó, Mallada R, Menéndez M, Coronas J. Continuous zeolite membrane reactor for esterification of ethanol and acetic acid. Chemical Engineering Journal 2007; 131: 35-39.

[141] Cimenler U, Joseph B, Kuhn JN. Effect oF Zeolite Memebrane Shell Thickness on Reactant Selectivity for Hydrocarbon Steam Reforming Using Layered Catalysts. Energy & Fuels 2016;

[142] Jin F, Li Y. A FTIR and TPD examination of the distributive properties of acid sites on ZSM-5 zeolite with pyridine as a probe molecule. Catalysis Today 2009; 145: 101-107.

[143] Biswas J, Maxwell I. Octane enhancement in fluid catalytic cracking: II. Operation in the overcracking regime. Applied Catalysis 1990; 58: 19-27.

[144] Yan TY. Zeolite-based catalysts for hydrocracking. Industrial & Engineering Chemistry Process Design and Development 1983; 22: 154-160.

[145] Maxwell I. Zeolite catalysis in hydroprocessing technology. Catalysis Today 1987; 1: 385-413.

[146] Bhatia S. Zeolite catalysts: principles and applications. CRC press, 1989.

[147] Tuan VA, Falconer JL, Noble RD. Isomorphous substitution of Al, Fe, B, and Ge into MFI-zeolite membranes. Microporous and Mesoporous Materials 2000; 41: 269-280.

[148] Weitkamp J. Zeolites and catalysis. Solid State Ionics 2000; 131: 175-188.

[149] Li X, Zhang Y, Meng F, San X, Yang G, Meng M, Takahashi M, Tsubaki N. Hydroformylation of 1-hexene on Silicalite-1 zeolite membrane coated Pd–Co/AC catalyst. Topics in Catalysis 2010; 53: 608-614.

[150] Naik S, Chiang A, Thompson R, Huang F. Formation of silicalite-1 hollow spheres by the self-assembly of nanocrystals. Chemistry of materials 2003; 15: 787-792.

[151] Guo H, Zhu G, Li H, Zou X, Yin X, Yang W, Qiu S, Xu R. Hierarchical Growth of Large-Scale Ordered Zeolite Silicalite-1 Membranes with High Permeability and Selectivity for Recycling CO2. Angewandte Chemie 2006; 118: 7211-7214.

[152] Wang X, Yang W, Tang Y, Wang Y, Fu S, Gao Z. Fabrication of hollow zeolite spheres. Chemical communications 2000; 2161-2162.

[153] Liu W, Zhang L, Wang H, Xu N. Preparation of silicalite-1 microtube arrays supported on cordierite honeycomb by using palm fibers as templates. Studies in Surface Science and Catalysis 2007; 170: 408-413.

[154] Damartzis T, Zabaniotou A. Thermochemical conversion of biomass to second generation biofuels through integrated process design—A review. Renewable and Sustainable Energy Reviews 2011; 15: 366-378.

[155] Veser G. Multiscale process intensification for catalytic partial oxidation of methane: From nanostructured catalysts to integrated reactor concepts. Catalysis Today 2010; 157: 24-32.

[156] Johns M, Collier P, Spencer MS, Alderson T, Hutchings GJ. Combined steam reforming of methane and Fischer–Tropsch synthesis for the formation of hydrocarbons: a proof of concept study. Catalysis letters 2003; 90: 187-194.

[157] Hu J, Yu F, Lu Y. Application of Fischer–Tropsch synthesis in biomass to liquid conversion. Catalysts 2012; 2: 303-326.

[158] Matsumura Y, Nakamori T. Steam reforming of methane over nickel catalysts at low reaction temperature. Applied Catalysis A: General 2004; 258: 107-114.

[159] Elsayed NH, Roberts NR, Joseph B, Kuhn JN. Low temperature dry reforming of methane over Pt–Ni–Mg/ceria–zirconia catalysts. Applied Catalysis B: Environmental 2015; 179: 213-219.

APPENDIX A: COPYRIGHT PERMISSIONS

A.1 Permission for Use of Material in Chapter 1

Below is permission for the use of materials in Chapter 1.

License Number	3952770333117
License date	Sep 19, 2016
Licensed Content Publisher	Royal Society of Chemistry
Licensed Content Publication	Chemical Society Reviews
Licensed Content Title	Core–shell nanoparticles: synthesis and applications in catalysis and electrocatalysis
Licensed Content Author	Manoj B. Gawande,Anandarup Goswami,Tewodros Asefa,Huizhang Guo,Ankush V. Biradar,Dong-Liang Peng,Radek Zboril,Rajender S. Varma
Licensed Content Date	Aug 19, 2015
Licensed Content Volume	44
Licensed Content Issue	21
Type of Use	Thesis/Dissertation
Requestor type	academic/educational
Portion	figures/tables/images
Number of figures/tables/images	1
Distribution quantity	100000
Format	print and electronic
Will you be translating?	no
Order reference number	
Title of the thesis/dissertation	Molecular-Size Selective Zeolite Membrane Encapsulated Novel Catalysts for XTL Processes
Expected completion date	Dec 2016
Estimated size	125

License Number	3952790244605
License date	Sep 19, 2016
Licensed Content Publisher	Royal Society of Chemistry
Licensed Content Publication	Nanoscale
Licensed Content Title	Precisely controlled resorcinol–formaldehyde resin coating for fabricating core–shell, hollow, and yolk–shell carbon nanostructures
Licensed Content Author	Xiaoliang Fang,Shengjie Liu,Jun Zang,Chaofa Xu,Ming-Sen Zheng,Quan-Feng Dong,Daohua Sun,Nanfeng Zheng
Licensed Content Date	May 23, 2013
Licensed Content Volume Number	5
Licensed Content Issue Number	15
Type of Use	Thesis/Dissertation
Requestor type	academic/educational
Portion	figures/tables/images
Number of figures/tables/images	1
Format	print and electronic
Distribution quantity	100000
Will you be translating?	no
Order reference number	
Title of the thesis/dissertation	Molecular-Size Selective Zeolite Membrane Encapsulated Novel Catalysts for XTL Processes

Copyright Clearance Center RightsLink®

Home | Create Account | Help

ACS Publications
Most Trusted. Most Cited. Most Read.

Title: Inorganic Solid Acids and Their Use in Acid-Catalyzed Hydrocarbon Reactions
Author: A. Corma
Publication: Chemical Reviews
Publisher: American Chemical Society
Date: May 1, 1995
Copyright © 1995, American Chemical Society

LOGIN
If you're a copyright.com user, you can login to RightsLink using your copyright.com credentials. Already a RightsLink user or want to learn more?

PERMISSION/LICENSE IS GRANTED FOR YOUR ORDER AT NO CHARGE

This type of permission/license, instead of the standard Terms & Conditions, is sent to you because no fee is being charged for your order. Please note the following:

- Permission is granted for your request in both print and electronic formats, and translations.
- If figures and/or tables were requested, they may be adapted or used in part.
- Please print this page for your records and send a copy of it to your publisher/graduate school.
- Appropriate credit for the requested material should be given as follows: "Reprinted (adapted) with permission from (COMPLETE REFERENCE CITATION). Copyright (YEAR) American Chemical Society." Insert appropriate information in place of the capitalized words.
- One-time permission is granted only for the use specified in your request. No additional uses are granted (such as derivative works or other editions). For any other uses, please submit a new request.

If credit is given to another source for the material you requested, permission must be obtained from that source.

License Number	3952791229189
License date	Sep 19, 2016
Licensed Content Publisher	Elsevier
Licensed Content Publication	Zeolites
Licensed Content Title	Shape-selective catalysis in zeolites
Licensed Content Author	Sigmund M. Csicsery
Licensed Content Date	July 1984
Licensed Content Volume	4
Licensed Content Issue	3
Licensed Content Pages	12
Type of Use	reuse in a thesis/dissertation
Portion	figures/tables/illustrations
Number of figures/tables/illustrations	1
Format	both print and electronic
Are you the author of this Elsevier article?	No
Will you be translating?	No
Order reference number	
Original figure numbers	Figure 2
Title of your thesis/dissertation	Molecular-Size Selective Zeolite Membrane Encapsulated Novel Catalysts for XTL Processes
Expected completion date	Dec 2016
Estimated size (number of pages)	125
Elsevier VAT number	GB 494 6272 12

License Number	3952800959330
License date	Sep 19, 2016
Licensed Content Publisher	John Wiley and Sons
Licensed Content Publication	Angewandte Chemie
Licensed Content Title	A Core/Shell Catalyst Produces a Spatially Confined Effect and Shape Selectivity in a Consecutive Reaction
Licensed Content Author	Jun Bao,Jingjiang He,Yi Zhang,Yoshiharu Yoneyama,Noritatsu Tsubaki
Licensed Content Date	Nov 15, 2007
Licensed Content Pages	4
Type of use	Dissertation/Thesis
Requestor type	University/Academic
Format	Print and electronic
Portion	Figure/table
Number of figures/tables	1
Original Wiley figure/table number(s)	Figure 6
Will you be translating?	No
Title of your thesis / dissertation	Molecular-Size Selective Zeolite Membrane Encapsulated Novel Catalysts for XTL Processes
Expected completion date	Dec 2016
Expected size (number of pages)	125

License Number	3953150442744
License date	Sep 20, 2016
Licensed Content Publisher	Royal Society of Chemistry
Licensed Content Publication	Nanoscale
Licensed Content Title	Noble metal nanoparticle@metal oxide core/yolk–shell nanostructures as catalysts: recent progress and perspective
Licensed Content Author	Guodong Li,Zhiyong Tang
Licensed Content Date	Jan 29, 2014
Licensed Content Volume	6
Licensed Content Issue	8
Type of Use	Thesis/Dissertation
Requestor type	academic/educational
Portion	figures/tables/images
Number of figures/tables/images	1
Distribution quantity	100000
Format	print and electronic
Will you be translating?	no
Order reference number	
Title of the thesis/dissertation	Molecular-Size Selective Zeolite Membrane Encapsulated Novel Catalysts for XTL Processes
Expected completion date	Dec 2016
Estimated size	125

License Number	3953151348719
License date	Sep 20, 2016
Licensed Content Publisher	John Wiley and Sons
Licensed Content Publication	Angewandte Chemie International Edition
Licensed Content Title	Thermosensitive Core–Shell Particles as Carriers for Ag Nanoparticles: Modulating the Catalytic Activity by a Phase Transition in Networks
Licensed Content Author	Yan Lu,Yu Mei,Markus Drechsler,Matthias Ballauff
Licensed Content Date	Dec 19, 2005
Licensed Content Pages	4
Type of use	Dissertation/Thesis
Requestor type	University/Academic
Format	Print and electronic
Portion	Figure/table
Number of figures/tables	1
Original Wiley figure/table number(s)	Figure 1
Will you be translating?	No
Title of your thesis / dissertation	Molecular-Size Selective Zeolite Membrane Encapsulated Novel Catalysts for XTL Processes
Expected completion date	Dec 2016
Expected size (number of pages)	125

A.2 Permission for Use of Material in Chapter 2

Below is permission for the use of materials in Chapter 2.

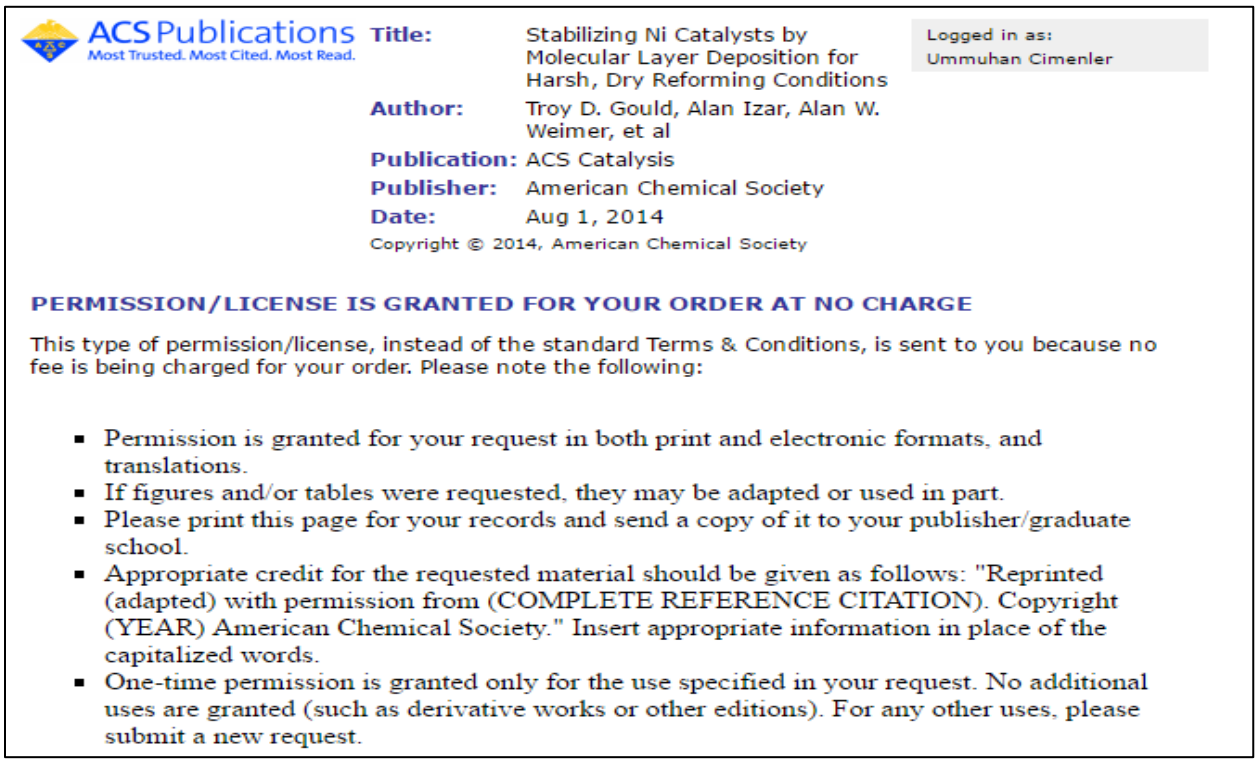

ACS Publications
Most Trusted. Most Cited. Most Read.

Title: Stabilizing Ni Catalysts by Molecular Layer Deposition for Harsh, Dry Reforming Conditions

Author: Troy D. Gould, Alan Izar, Alan W. Weimer, et al

Publication: ACS Catalysis

Publisher: American Chemical Society

Date: Aug 1, 2014

Copyright © 2014, American Chemical Society

Logged in as:
Ummuhan Cimenler

PERMISSION/LICENSE IS GRANTED FOR YOUR ORDER AT NO CHARGE

This type of permission/license, instead of the standard Terms & Conditions, is sent to you because no fee is being charged for your order. Please note the following:

- Permission is granted for your request in both print and electronic formats, and translations.
- If figures and/or tables were requested, they may be adapted or used in part.
- Please print this page for your records and send a copy of it to your publisher/graduate school.
- Appropriate credit for the requested material should be given as follows: "Reprinted (adapted) with permission from (COMPLETE REFERENCE CITATION). Copyright (YEAR) American Chemical Society." Insert appropriate information in place of the capitalized words.
- One-time permission is granted only for the use specified in your request. No additional uses are granted (such as derivative works or other editions). For any other uses, please submit a new request.

Copyright Clearance Center RightsLink®

Home | Account Info | Help

ACS Publications
Most Trusted. Most Cited. Most Read.

Logged in as:
Ummuhan Cimenler

Title: Yolk–Satellite–Shell Structured Ni–Yolk@Ni@SiO2 Nanocomposite: Superb Catalyst toward Methane CO2 Reforming Reaction

Author: Ziwei Li, Liuye Mo, Yasotha Kathiraser, et al

Publication: ACS Catalysis

Publisher: American Chemical Society

Date: May 1, 2014

PERMISSION/LICENSE IS GRANTED FOR YOUR ORDER AT NO CHARGE

This type of permission/license, instead of the standard Terms & Conditions, is sent to you because no fee is being charged for your order. Please note the following:

- Permission is granted for your request in both print and electronic formats, and translations.
- If figures and/or tables were requested, they may be adapted or used in part.
- Please print this page for your records and send a copy of it to your publisher/graduate school.
- Appropriate credit for the requested material should be given as follows: "Reprinted (adapted) with permission from (COMPLETE REFERENCE CITATION). Copyright (YEAR) American Chemical Society." Insert appropriate information in place of the capitalized words.
- One-time permission is granted only for the use specified in your request. No additional uses are granted (such as derivative works or other editions). For any other uses, please submit a new request.

License Number	3953190653760
License date	Sep 20, 2016
Licensed Content Publisher	Royal Society of Chemistry
Licensed Content Publication	Dalton Transactions
Licensed Content Title	Novel embedded Pd@CeO2 catalysts: a way to active and stable catalysts
Licensed Content Author	Matteo Cargnello,Tiziano Montini,Stefano Polizzi,Noah L. Wieder,Raymond J. Gorte,Mauro Graziani,Paolo Fornasiero
Licensed Content Date	Dec 23, 2009
Licensed Content Volume	39
Licensed Content Issue	8
Type of Use	Thesis/Dissertation
Requestor type	academic/educational
Portion	figures/tables/images
Number of figures/tables/images	1
Distribution quantity	10000
Format	print and electronic
Will you be translating?	no
Order reference number	
Title of the thesis/dissertation	Molecular-Size Selective Zeolite Membrane Encapsulated Novel Catalysts for XTL Processes
Expected completion date	Dec 2016
Estimated size	125

Copyright Clearance Center RightsLink®

Home | Account Info | Help

ACS Publications Most Trusted. Most Cited. Most Read.

Logged in as: Ummuhan Cimenler

Title: Designing a Capsule Catalyst and Its Application for Direct Synthesis of Middle Isoparaffins
Author: Jingjiang He, Yoshiharu Yoneyama, Bolian Xu, et al
Publication: Langmuir
Publisher: American Chemical Society
Date: Mar 1, 2005

PERMISSION/LICENSE IS GRANTED FOR YOUR ORDER AT NO CHARGE

This type of permission/license, instead of the standard Terms & Conditions, is sent to you because no fee is being charged for your order. Please note the following:

- Permission is granted for your request in both print and electronic formats, and translations.
- If figures and/or tables were requested, they may be adapted or used in part.
- Please print this page for your records and send a copy of it to your publisher/graduate school.
- Appropriate credit for the requested material should be given as follows: "Reprinted (adapted) with permission from (COMPLETE REFERENCE CITATION). Copyright (YEAR) American Chemical Society." Insert appropriate information in place of the capitalized words.
- One-time permission is granted only for the use specified in your request. No additional uses are granted (such as derivative works or other editions). For any other uses, please submit a new request.

ACS Publications Most Trusted. Most Cited. Most Read.

Logged in as: Ummuhan Cimenler

Title: Confinement Effect and Synergistic Function of H-ZSM-5/Cu-ZnO-Al2O3 Capsule Catalyst for One-Step Controlled Synthesis
Author: Guohui Yang, Noritatsu Tsubaki, Jun Shamoto, et al
Publication: Journal of the American Chemical Society
Publisher: American Chemical Society
Date: Jun 1, 2010

PERMISSION/LICENSE IS GRANTED FOR YOUR ORDER AT NO CHARGE

This type of permission/license, instead of the standard Terms & Conditions, is sent to you because no fee is being charged for your order. Please note the following:

- Permission is granted for your request in both print and electronic formats, and translations.
- If figures and/or tables were requested, they may be adapted or used in part.
- Please print this page for your records and send a copy of it to your publisher/graduate school.
- Appropriate credit for the requested material should be given as follows: "Reprinted (adapted) with permission from (COMPLETE REFERENCE CITATION). Copyright (YEAR) American Chemical Society." Insert appropriate information in place of the capitalized words.
- One-time permission is granted only for the use specified in your request. No additional uses are granted (such as derivative works or other editions). For any other uses, please submit a new request.

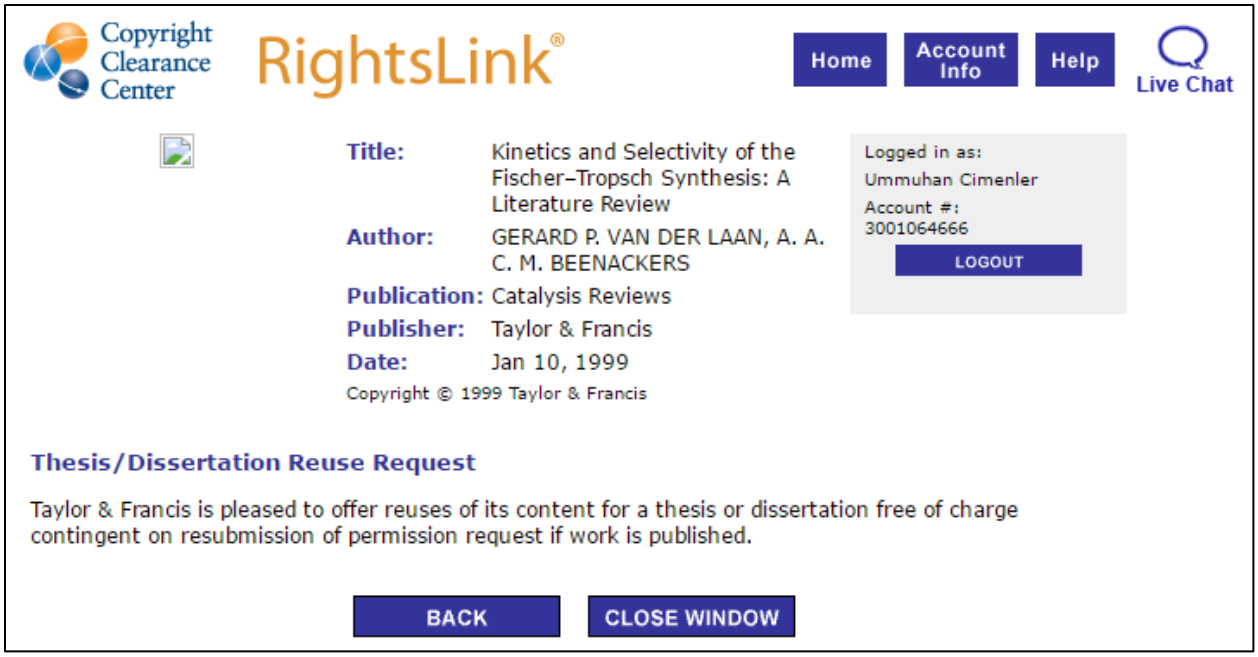
Copyright Clearance Center
RightsLink®
Home
Account Info
Help
Live Chat
Title: Kinetics and Selectivity of the Fischer–Tropsch Synthesis: A Literature Review
Author: GERARD P. VAN DER LAAN, A. A. C. M. BEENACKERS
Publication: Catalysis Reviews
Publisher: Taylor & Francis
Date: Jan 10, 1999
Copyright © 1999 Taylor & Francis
Logged in as:
Ummuhan Cimenler
Account #:
3001064666
LOGOUT
Thesis/Dissertation Reuse Request
Taylor & Francis is pleased to offer reuses of its content for a thesis or dissertation free of charge contingent on resubmission of permission request if work is published.
BACK
CLOSE WINDOW

A.3 Permission for Use of Material in Chapter 3

Below is permission for the use of materials in Chapter 3.

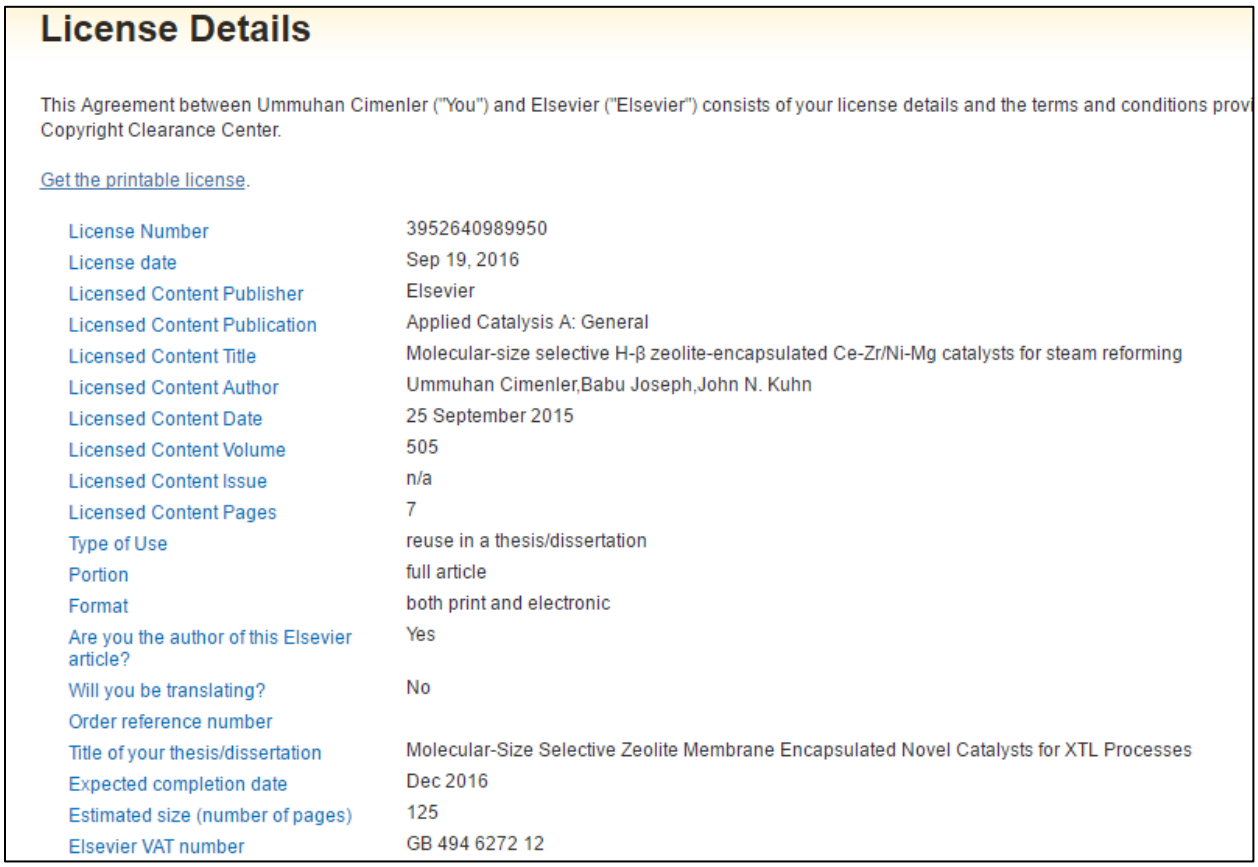

License Details

This Agreement between Ummuhan Cimenler ("You") and Elsevier ("Elsevier") consists of your license details and the terms and conditions provi
Copyright Clearance Center.

Get the printable license.

License Number	3952640989950
License date	Sep 19, 2016
Licensed Content Publisher	Elsevier
Licensed Content Publication	Applied Catalysis A: General
Licensed Content Title	Molecular-size selective H-β zeolite-encapsulated Ce-Zr/Ni-Mg catalysts for steam reforming
Licensed Content Author	Ummuhan Cimenler,Babu Joseph,John N. Kuhn
Licensed Content Date	25 September 2015
Licensed Content Volume	505
Licensed Content Issue	n/a
Licensed Content Pages	7
Type of Use	reuse in a thesis/dissertation
Portion	full article
Format	both print and electronic
Are you the author of this Elsevier article?	Yes
Will you be translating?	No
Order reference number	
Title of your thesis/dissertation	Molecular-Size Selective Zeolite Membrane Encapsulated Novel Catalysts for XTL Processes
Expected completion date	Dec 2016
Estimated size (number of pages)	125
Elsevier VAT number	GB 494 6272 12

A.4 Permission for Use of Material in Chapter 4

Below is permission for the use of materials in Chapter 4.

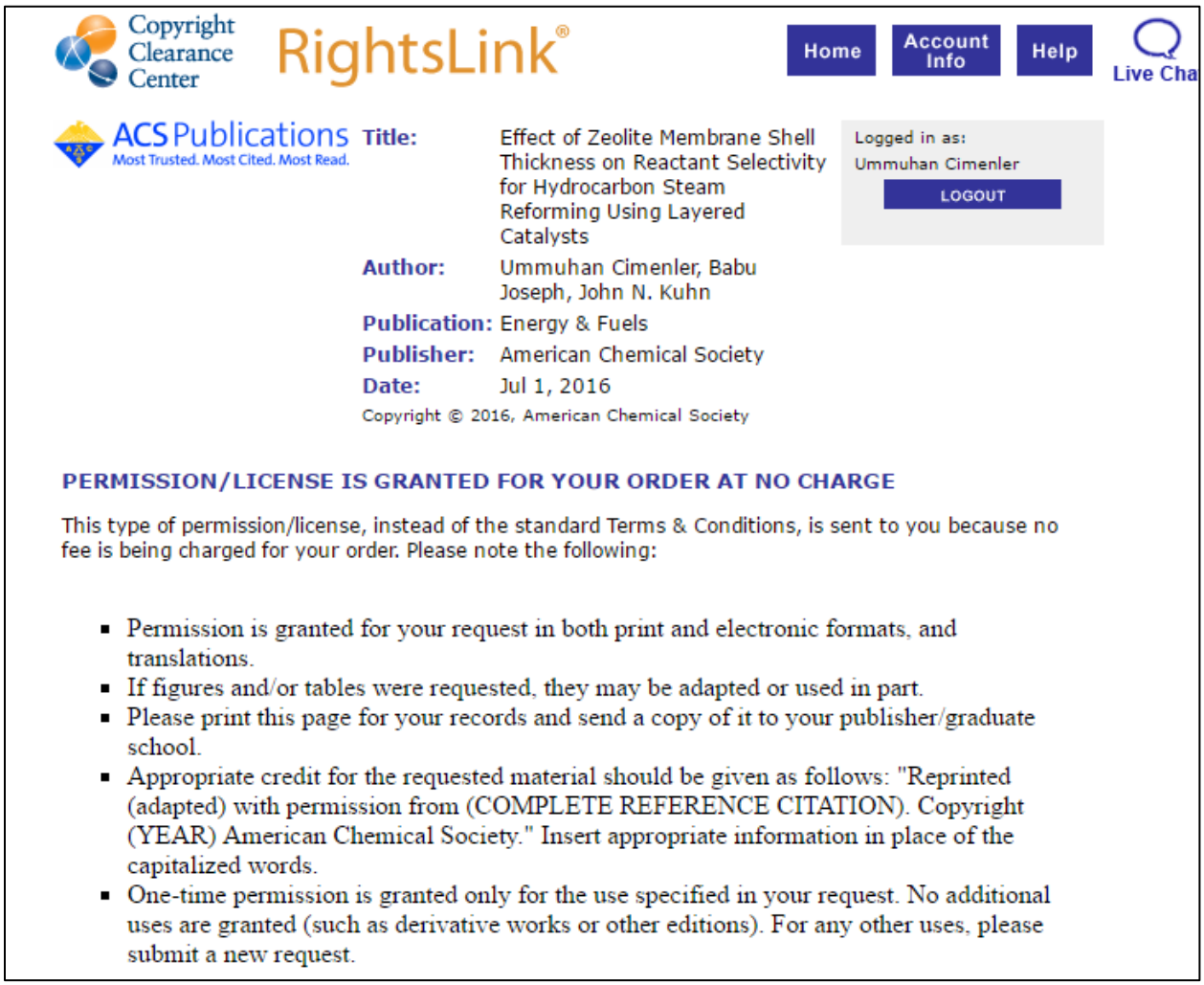

Copyright Clearance Center RightsLink®

Home | Account Info | Help | Live Cha

ACS Publications
Most Trusted. Most Cited. Most Read.

Logged in as:
Ummuhan Cimenler
LOGOUT

Title: Effect of Zeolite Membrane Shell Thickness on Reactant Selectivity for Hydrocarbon Steam Reforming Using Layered Catalysts

Author: Ummuhan Cimenler, Babu Joseph, John N. Kuhn

Publication: Energy & Fuels

Publisher: American Chemical Society

Date: Jul 1, 2016

Copyright © 2016, American Chemical Society

PERMISSION/LICENSE IS GRANTED FOR YOUR ORDER AT NO CHARGE

This type of permission/license, instead of the standard Terms & Conditions, is sent to you because no fee is being charged for your order. Please note the following:

- Permission is granted for your request in both print and electronic formats, and translations.
- If figures and/or tables were requested, they may be adapted or used in part.
- Please print this page for your records and send a copy of it to your publisher/graduate school.
- Appropriate credit for the requested material should be given as follows: "Reprinted (adapted) with permission from (COMPLETE REFERENCE CITATION). Copyright (YEAR) American Chemical Society." Insert appropriate information in place of the capitalized words.
- One-time permission is granted only for the use specified in your request. No additional uses are granted (such as derivative works or other editions). For any other uses, please submit a new request.

A.5 Permission for Use of Material in Chapter 5

Below is permission for the use of materials in Chapter 5.

https://s100.copyright.com/AppDispatchServlet

Copyright Clearance Center RightsLink®

Home | Account Info | Help

Title: Hydrocarbon steam reforming using Silicalite-1 zeolite encapsulated Ni-based catalyst
Author: Ummuhan Cimenler,Babu Joseph,John N. Kuhn
Publication: AIChE Journal
Publisher: John Wiley and Sons
Date: Oct 10, 2016
© 2016 American Institute of Chemical Engineers

Logged in as: Ummuhan Cimenler

Review Order

Please review the order details and the associated terms and conditions.

No royalties will be charged for this reuse request although you are required to obtain a license and comply with the license terms and conditions. To obtain the license, click the Accept button below.

Licensed Content Publisher	John Wiley and Sons
Licensed Content Publication	AIChE Journal
Licensed Content Title	Hydrocarbon steam reforming using Silicalite-1 zeolite encapsulated Ni-based catalyst
Licensed Content Author	Ummuhan Cimenler,Babu Joseph,John N. Kuhn
Licensed Content Date	Oct 10, 2016
Licensed Content Pages	8
Type of use	Dissertation/Thesis
Requestor type	Author of this Wiley article
Format	Print and electronic
Portion	Full article
Will you be translating?	No
Title of your thesis / dissertation	Molecular-Size Selective Zeolite Membrane Encapsulated Novel Catalysts for XTL Processes
Expected completion date	Dec 2016
Expected size (number of pages)	125

APPENDIX B: SUPPORTING INFORMATION FOR CHAPTER 5

Table B.1 Reaction types, catalysts composition and amounts

CH_4 Steam Reforming Total Flow Rate: 75 sccm (0.64%CH_4-0.64%H_2O-98.7%He)		
Catalyst Composition	**Notation**	**Catalyst amount (mg)**
Uncoated steam reforming catalyst:1.6wt%Ni-1.2wt%Mg/$Ce_{0.6}Zr_{0.4}O_2$ [124]	Uncoated SR	11.3
51wt% Silicalite-1 zeolite coated composite steam reforming catalyst	SR@ Sil51%	23.6
51wt% H-β zeolite coated composite steam reforming catalyst [141]	SR@ β51%	23.6
Physical mixture of Silicalite-1 zeolite/SR catalyst	PM-51%Sil/SR	23.6 (11.3 mg SR-12.3mg H-β zeolite)
Silicalite-1 zeolite by itself		12.3
C_7H_8 Steam Reforming Total Flow Rate: 32.6 sccm (1% C_7H_8, 7% H_2O, 92% He)		
Catalyst Composition	**Notation**	**Catalyst amount (mg)**
Uncoated steam reforming catalyst:1.6wt%Ni-1.2wt%Mg/$Ce_{0.6}Zr_{0.4}O_2$[124]	Uncoated SR	10.3
51wt% Silicalite-1 zeolite coated composite steam reforming catalyst	SR@ Sil51%	21
51wt% H-β zeolite coated composite steam reforming catalyst [141]	SR@ β51%	21
Physical mixture of Silicalite-1 /SR catalyst	PM-51%Sil/SR	21 (10.3 mg SR-10.7mg H-β zeolite)
H-β zeolite by itself (powder)		10.7
CH_4-C_7H_8 Steam Reforming A 10-hour time on stream experiment Total Flow Rate: 32.6 sccm (1% C_7H_8, 1.5% CH_4, 7% H_2O, 90.5% He)		
Catalyst Composition	**Notation**	**Catalyst amount (mg)**
51wt% Silicalite-1 zeolite coated composite steam reforming catalyst	SR@ Sil51%	23.6
Uncoated steam reforming catalyst:1.6wt%Ni-1.2wt%Mg/$Ce_{0.6}Zr_{0.4}O_2$[141]	Uncoated SR	11.3

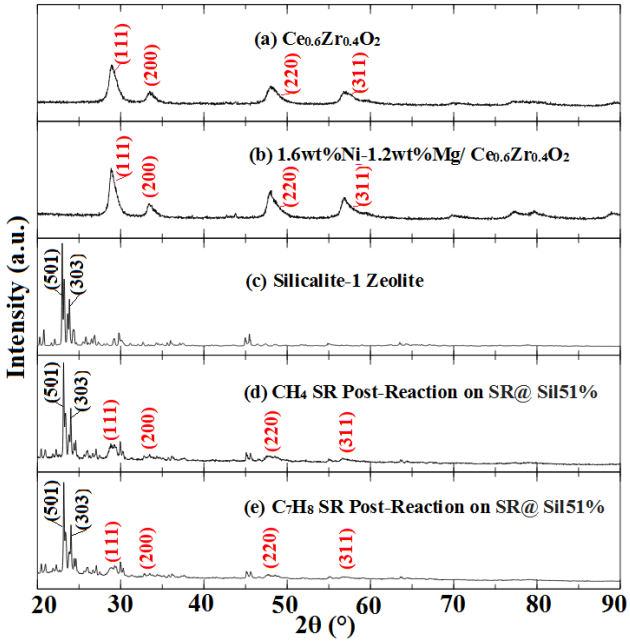

Figure B.1 XRD Patterns of the catalysts. Red and black Miller indices indicate SR catalyst and Silicalite-1 zeolite phases, respectively.

Table B.2 Values that were used in the calculations of Weisz−Prater criteria, Thiele moduli, and effectiveness factors

	$(rA)_{obs}$, observed reaction rate, (kmol/kg cat.s^{-1})	**Effective Diffusivity (cm^2/s at 800°C)**	**q_c, density of solid catalyst, (kg/m^3)**	**R, radius of the catalyst particle, (m)**	**C_{As}, reactant concentration, ($kmol/m^3$)**
CH_4 SR	$1.84*10^{-6}$	$5.6*10^{-4}$	626	$1.1*10^{-3}$	$7.27*10^{-5}$
C_7H_8 SR	$7.44*10^{-7}$	$3.9*10^{-9}$	760	$1.1*10^{-3}$	$1.16*10^{-4}$

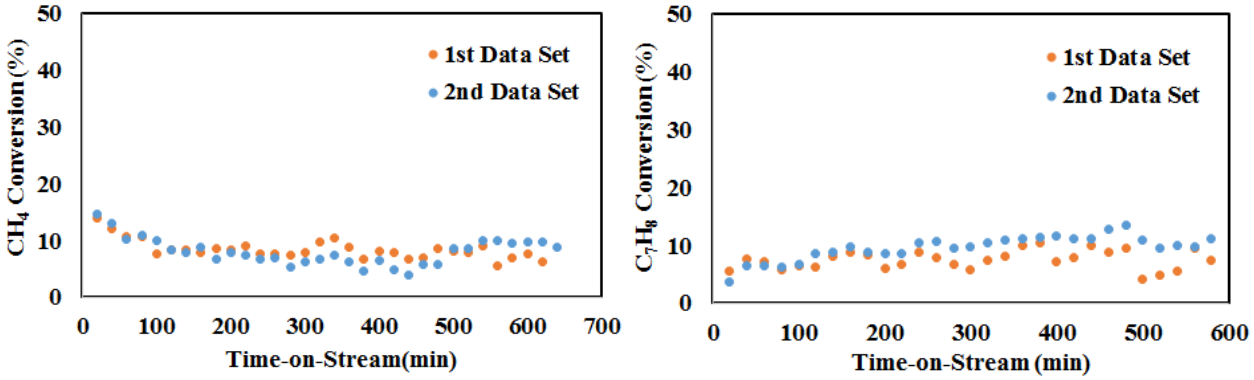

Figure B.2 Repeated experiment for simultaneous CH_4 and C_7H_8 steam reforming on SR@ Sil51% under the same condition with another batch of catalyst that synthesized same way. (left) CH_4 steam conversion with TOS and (right) C_7H_8 conversion with TOS.

APPENDIX C: INTERNAL DIFFUSION LIMITATIONS CALCULATIONS FOR CHAPTER 5

Weisz-Prater Criterion equation is given below.

$$C_{wp}=\frac{-rA(obs)*qc*R^2}{De*C_{As}}$$

where $-rA_{(obs)}$ is the observed reaction rate, q_c is density of solid catalyst, R is radius of a catalyst particle, D_e is effective diffusion coefficient and C_{AS} is reactant concentration at the surface.

Table C.1 Values that were used in the calculations of Weisz−Prater criteria, Thiele moduli, and effectiveness factors

Sample	Reaction	Effective Diffusivity (cm^2/s at 800°C)	-rA (kmol/kgcat.s)	Diameter (D) of the samples (m)	Radius (R) of the samples (m)
51wt%	CH_4 SR	$5.6*10^{-4}$	$1.83819*10^{-6}$	$2.2*10^{-3}$	$1.1*10^{-3}$
51 wt %	C_7H_8 SR	$3.9*10^{-9}$	$7.44478*10^{-7}$	$2.2*10^{-3}$	$1.1*10^{-3}$

$$-rA_{(obs)} = 1.83819*10^{-6}\ \text{kmol/(kg cat.s)}$$

$$qc= \frac{m_{catalyst}}{\frac{\pi D^2}{4}*h}=\frac{23.6*10^{-6}\ kg}{\frac{\pi(0.004m)^2}{4}*0.003m} = 626.32\ \frac{kg}{m^3}$$

$$De=5.6*10^{-4}\ cm^2/s=5.6*10^{-8}\ m^2/s$$

$$n_{CH4}=1.962*10^{-5}\ \text{mol/min} V_{total}=75\ \text{sccm at 298K (25°C)}$$

$$V_{total}=270\ \text{sccm at 1073K (800°C)}$$

$$C_{AS}=C_{A(CH4)}=\frac{1.962*10-5}{270}=7.265*10^{-8}\ mol/cm^3=7.265*10^{-5}\ kmol/m^3$$

$$R_{51wt\%}= 1.1*10^{-3}\ m$$

So,

$$C_{wp}=\frac{(1.83819*10^{-6})*(626.32)*(1.1*10^{-3})^2}{(5.6*10^{-8})*(7.265*10^{-5})} = 342.4 > 1$$

There is internal diffusion limitation for 51 wt% CH_4 SRR.

$$-rA_{(obs)} = 7.44478*10^{-7}\ \text{kmol/(kg cat.s)}$$

$$qc= \frac{m_{catalyst}}{\frac{\pi D^2}{4}*h}=\frac{21*10^{-6}\ kg}{\frac{\pi(0.004m)^2}{4}*0.0022m} = 760\ \frac{kg}{m^3}$$

$$De=3.9*10^{-9}cm^2/s=3.9*10^{-13}\ m^2/s$$

$$n_{C7H8}=1.36*10^{-5}\ \text{mol/min}$$

$$V_{total}=32.6\text{sccm at 298K (25°C)}$$

$$V_{total}=117.32\text{sccm at 1073K (800°C)}$$

$$C_{C7H8}=\frac{1.36*10-5}{117.32}=1.16*10^{-7}\ mol/cm^3=1.16*10^{-4}\ kmol/m^3$$

$$R_{51wt\%}= 1.1*10^{-3}\ m$$

So,

$$C_{wp}=\frac{(7.44478*10^{-7})*(760)*(1.1*10^{-3})^2}{(3.9*10^{-13})*(1.16*10^{-4})} = 1.5 * 10^7 \gg 1$$

There is internal diffusion limitation for 51 wt% C_7H_8 SRR.

Thiele Modulus (Φ_n) and Effectiveness Factor (η) calculation is given below for CH_4 SRR 51 wt%.

$$\Phi n = R * \sqrt{\frac{(-r_A) * (q_c)}{(D_e) * (C_{AS})}}$$

$$\Phi n = 1.1 * 10^{-3} * \sqrt{\frac{(1.83819*10^{-6})*(626.32)}{(5.6*10^{-8})*(7.265*10^{-5})}} = 18.5$$

$$\eta = \frac{\mathbf{3}}{\Phi n^{\mathbf{2}}}(\Phi n coth \Phi n - 1)$$

$$\eta = 0.153$$

Thiele Modulus (Φ_n) and Effectiveness Factor (η) calculation is given below for C_7H_8 SRR 51 wt%.

$$\Phi n = 1.1 * 10^{-3} * \sqrt{\frac{(7.44478*10^{-7})*(760)}{(3.9*10^{-13})*(1.16*10^{-4})}} = 1.2*10^{6}$$

$$\eta = \frac{\mathbf{3}}{\Phi n^{\mathbf{2}}}(\Phi n coth \Phi n - 1)$$

$$\eta = 0.0000025$$

Table C.2 Results of Weisz−Prater criteria, Thiele moduli, and effectiveness factors for Silicalite-1 zeolite composite catalyst

Sample	**Reaction**	**Effective Diffusivity (cm^2/s at 800°C)**	**Internal diffusion limitation (Weisz-Prater Criteria)**	**Thiele Modulus (Φ_n)**	**Effectiveness Factor (η)**
51 wt %	CH_4 SR	$5.6*10^{-4}$	342.4>1	18.5	0.153
51 wt %	C_7H_8 SR	$3.9*10^{-9}$	$1.5 * 10^7 \gg 1$	$1.2*10^6$	0.0000025

APPENDIX D: PROPAGATION OF ERROR FOR CH_4 CONVERSION

To calculate the propagation of error in CH_4 conversion, uncertainties must be known tahat effect the conversion calculation. The uncertainty for the flowmeter is ±.04 sccm. The uncertainty for the area was ± 26 μV*s (for 51wt% composite catalyst sample at 780°C). The linear relationship below was obtained to calibrate CH_4 concentration from GC area under the peak.

$$A=10362*f$$

where A is GC area under peak in μV*s, and f is flow of CH_4 in sccm.

The calibration constant (C_{CH4}) is given below.

$$C_{CH4} = \frac{A}{f}$$

Error in the CH_4 calibration constant can be calculated with the formula below.

$$\sigma=\sqrt{(\frac{\partial C_{CH4}}{\partial A})^2{\sigma_A}^2 + (\frac{\partial C_{CH4}}{\partial f})^2{\sigma_f}^2}$$

$$\frac{\partial C_{CH4}}{\partial A} = \frac{1}{f} \text{ and } \frac{\partial C_{CH4}}{\partial f} = \frac{-A}{f^2}$$

Choosing f to be ±.48 sccm and A to be the average 4597 the uncertainty in the constant can be calculated below.

$$\sigma c_{CH4}=\sqrt{(\frac{1}{0.48})^2 26^2 + (\frac{-4597}{0.48^2})^2 0.04^2}=54.5\frac{\mu V*s}{sccm}$$

The uncertainty in the flow of CH_4 given below.

$$\sigma f_{calc}=\sqrt{(\frac{\sigma f_{calc}}{\partial A})^2{\sigma_A}^2 + (\frac{\sigma f_{calc}}{\partial C_{CH4}})^2{\sigma_{C_{CH4}}}^2}$$

$$\frac{\sigma f_{calc}}{\partial A} = \frac{1}{C_{CH4}}$$

$$\frac{\sigma f_{calc}}{\partial C_{CH4}} = \frac{-A}{{C_{CH4}}^2}$$

The average inlet area was 4597, and calculated constant was 10362. Thus,

$$\sigma f_{calc} = \sqrt{(\frac{1}{10362})^2 26^2 + (\frac{4597}{10362^2})^2 54.5^2} = 3.42 * 10^{-3} \text{ sccm}$$

$$\sigma_n = \sqrt{(\frac{\partial_n}{\partial_T})^2 {\sigma_T}^2 + (\frac{\partial_n}{\partial f_{calc}}) {\sigma_{f_{calc}}}^2}$$

$$n = \frac{P f_{calc}}{RT}$$

$$\frac{\partial n}{\partial T} = \frac{-P f_{calc}}{RT^2}$$

$$\frac{\partial n}{\partial f} = \frac{P}{RT}$$

where P is 1, f_{calc} is 0.44364 sccm and T is 323 K (the GC detector column temperature).

$$\sigma_n = \sqrt{(\frac{-1 * 0.44364}{82.0575 * 323^2})^2 5^2 + (\frac{1}{82.0575 * 323})^2 (3.42 * 10^{-3})^2} = 2.89 * 10^{-7} \frac{mol}{min}$$

$$X = \frac{F_{CH4,0} - F_{CH4}}{F_{CH4,0}}$$

The error in the conversion can be calculated using σ_n:

$$\sigma_X = \sqrt{(\frac{\partial X}{\partial F_{CH4,0}})^2 {\sigma_n}^2 + (\frac{\partial X}{\partial F_{CH4}}) {\sigma_n}^2} \quad \frac{\partial X}{\partial F_{CH4,0}} = -\frac{F_{CH4}}{{F_{CH4,0}}^2}$$

$$\frac{\partial X}{\partial F_{CH4}} = -\frac{1}{F_{CH4,0}}$$

For $F_{CH4,0} = 1.5323*10\text{-}^{5}$ mol/min (using same experimental conditions) and $F_{CH4} = 1.17 * 10^{-5}$ mol/min (the average for all experimental runs), the error in conversion can be calculated:

$$\sigma_X = \sqrt{(-\frac{1.17* 10^{-5}}{1.5323*10^{-5^2}})^2(2.89 * 10^{-7})^2 + (\frac{-1}{1.5323*10^{-5}})^2(2.89 * 10^{-7})^2}=0.024$$

$$\sigma_X = \pm 2.4\%$$

The uncertainty associated with the catalyst mass was 1% (from scale that was used to weigh catalyst). Thus, the final uncertainty (σ_{Xf}) in conversion is:

$$\sigma_{Xf} = \pm 3.4\%$$

APPENDIX E: ASPEN SIMULATION DETAILS

The species of the CH_4 and C_7H_8 steam reforming inlet and outlet streams are given Table E1 and Table E2 for temperature 400°C and pressure 1 atm (Using Ideal Thermodynamic Method).

Table E.1 CH_4 steam reforming inlet and outlet streams

Species	Inlet (kmol/sec)	Outlet (kmol/sec)
CH_4	1	0.903
H_2O	1	0.808
CO	0	0.004
H_2	0	0.386
CO_2	0	0.094

Table E.2 C_7H_8 steam reforming inlet and outlet streams

Species	Inlet (kmol/sec)	Outlet (kmol/sec)
C_7H_8	1	1.1e-16
H_2O	7	1.677
CO	0	0.094
H_2	0	0.739
CO_2	0	2.614
CH_4	0	4.292
C_6H_6	0	3.48e-14

The flowsheet for the model is given below:

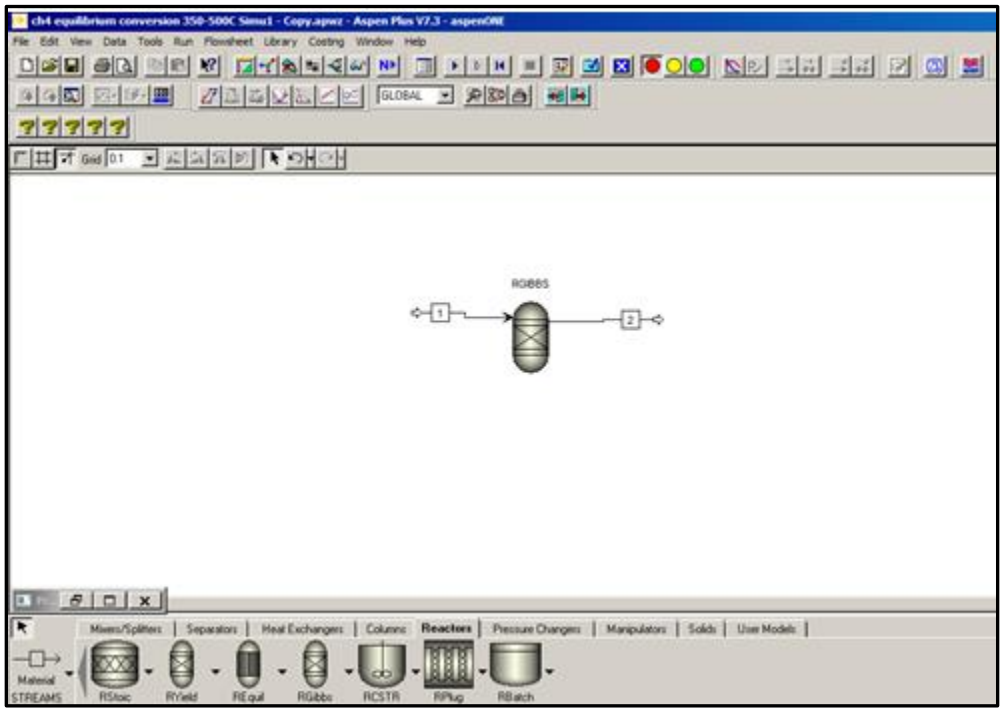

Figure E.1 Flowsheet for the ASPEN model

APPENDIX F: FLOWCHARTS FOR SYNTHESIS PROCEDURES OF THE ENCAPSULATED CATALYSTS

Flowchart is given below for synthesis of H-β Zeolite (Hydrothermal Synthesis Method).

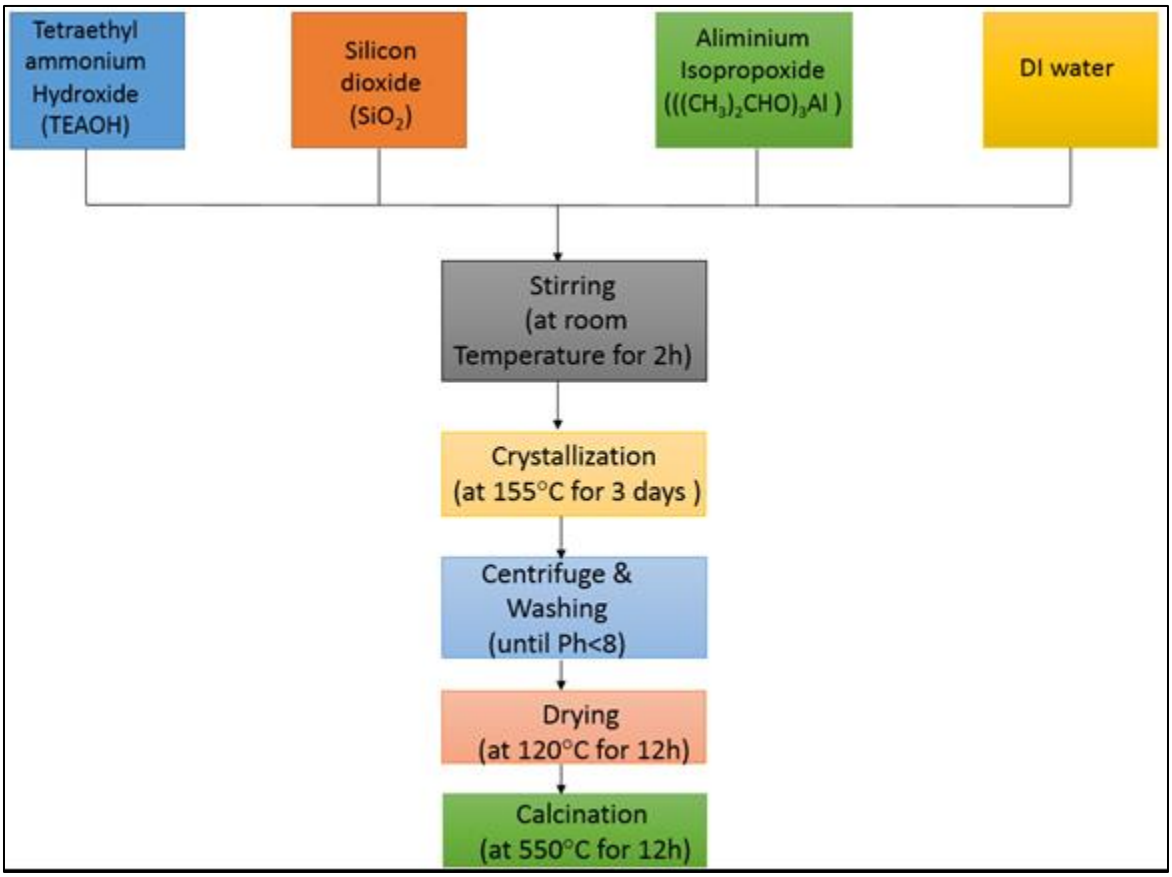

Figure F.1 Flowchart for synthesis of H-β zeolite using Hydrothermal Synthesis Method

Flowchart is given below for synthesis of Silicalite-1 Zeolite (Hydrothermal Synthesis Method).

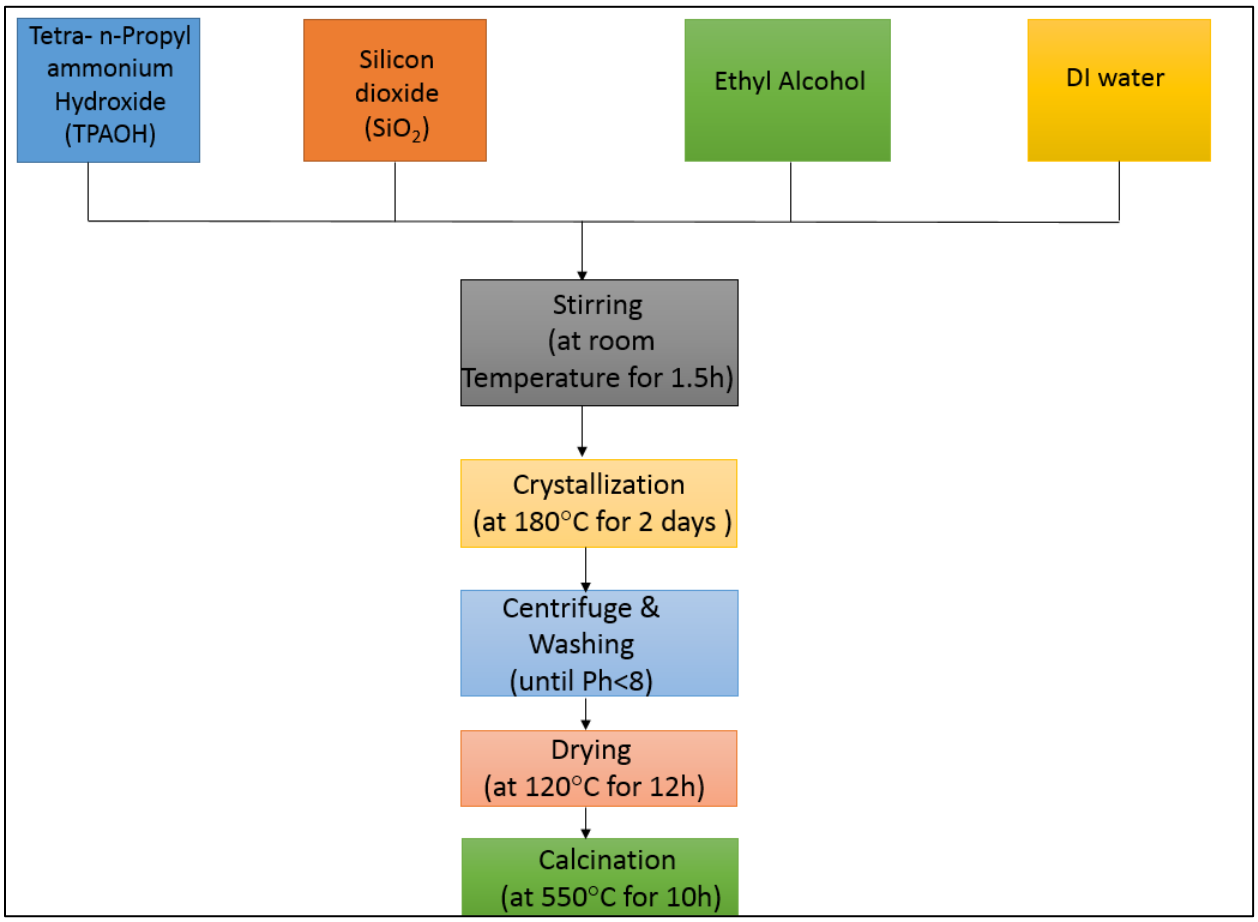

Figure F.2 Flowchart for synthesis of silicalite-1 zeolite using Hydrothermal Synthesis Method

Flowchart is given below for synthesis of 1.6wt%Ni/1.2wt%Mg/$Ce_{0.6}Zr_{0.4}O_2$ steam reforming core catalyst.

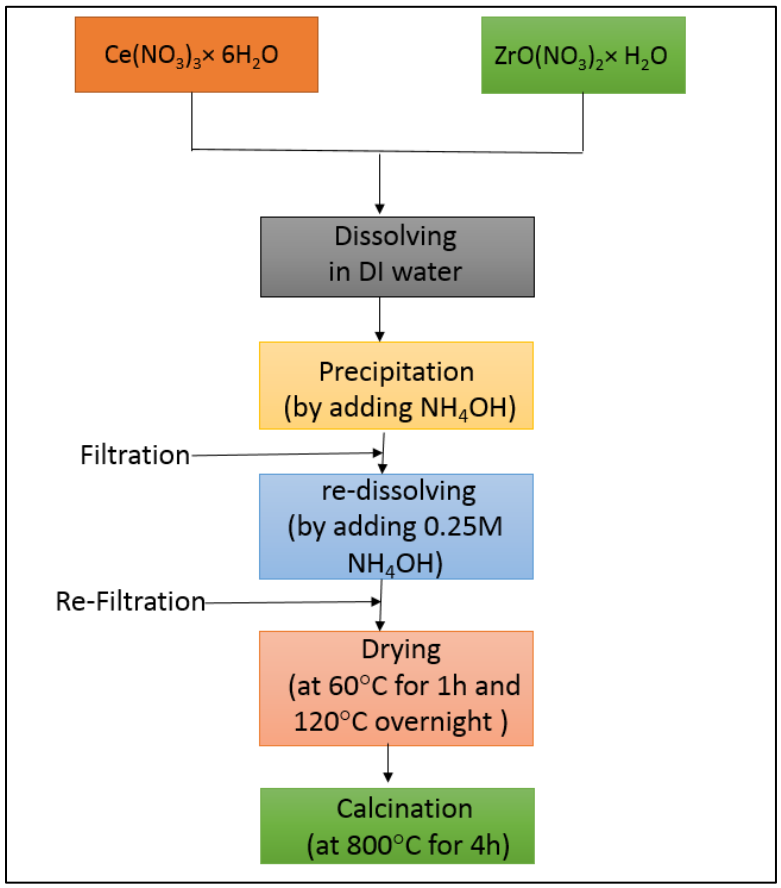

Figure F.3 Flowchart for synthesis of $Ce_{0.6}Zr_{0.4}O_2$ support

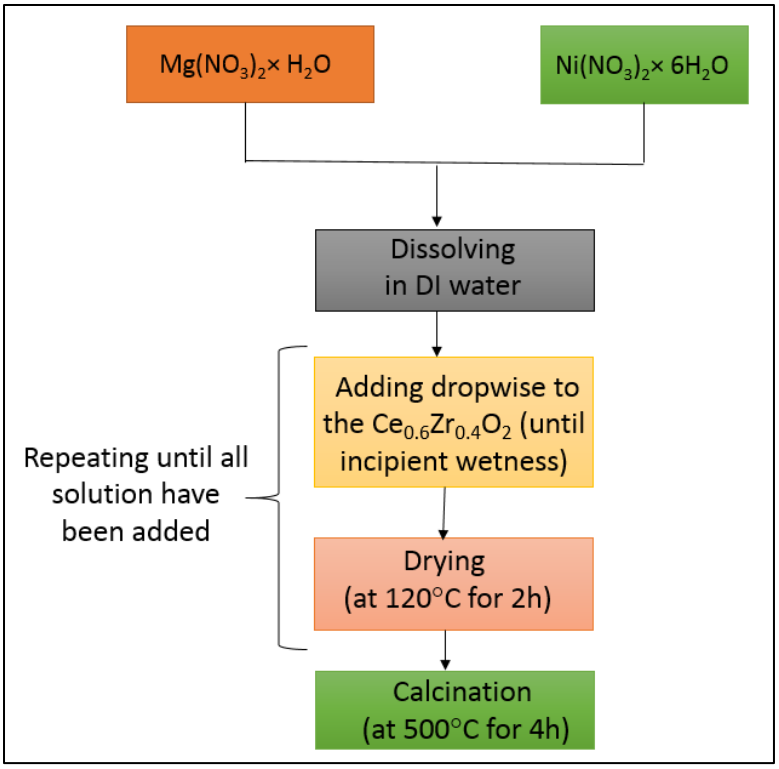

Figure F.4 Flowchart for synthesis of 1.6wt%Ni/1.2wt%Mg/$Ce_{0.6}Zr_{0.4}O_2$ catalyst

Flowchart is given below for synthesis of zeolite encapsulated composite steam reforming catalyst.

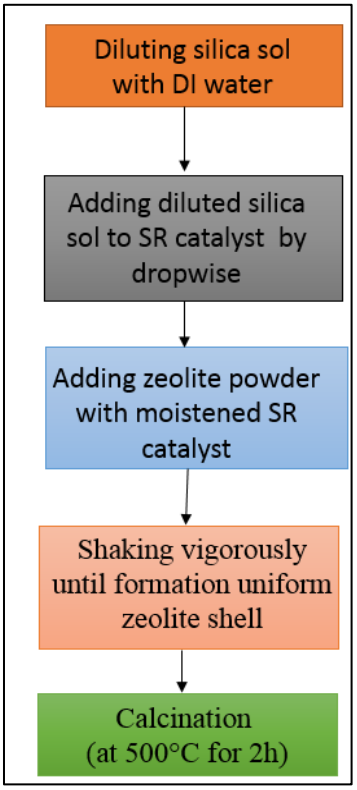

Figure F.5 Flowchart for synthesis of zeolite encapsulated composite steam reforming catalyst.

The pictures of the synthesized catalysts are demonstrated below.

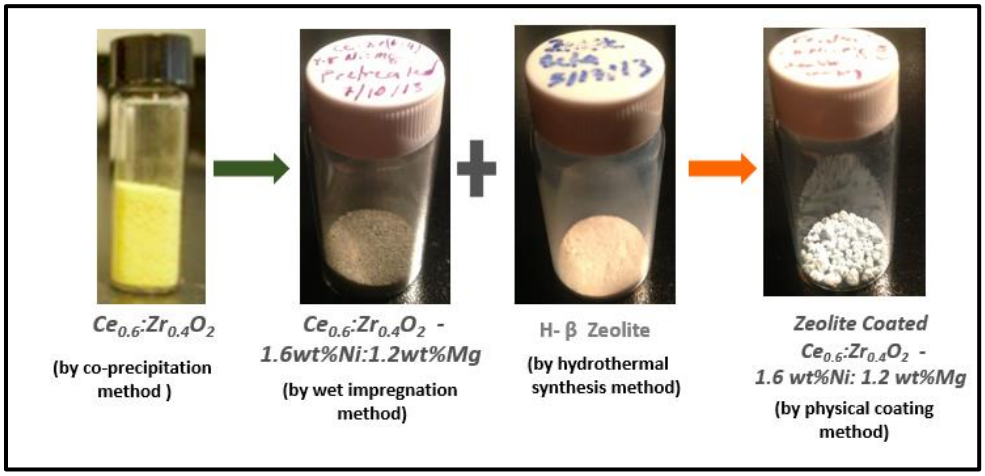

Figure F.6 Pictures of the synthesized catalysts

The electron microscopy image of the cross section of H-β zeolite encapsulated composite catalyst is shown below (sample was placed in epoxy):

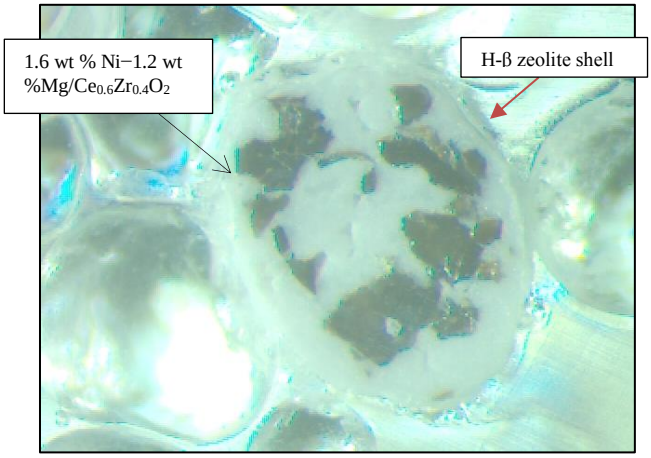

Figure F.7 The electron microscopy image of the cross section of H-β zeolite encapsulated composite catalyst

APPENDIX G: EXAMPLE GC PEAKS AND CONVERSION CALCULATION

Example GC peaks are given below for the sample 34.3 wt% H-β zeolite encapsulated composite catalyst (17.2 mg total catalyst and reaction temperature is for 800 °C). The Figure G.1 and the Figure G.2 demonstrate inlet and outlet species peaks, respectively.

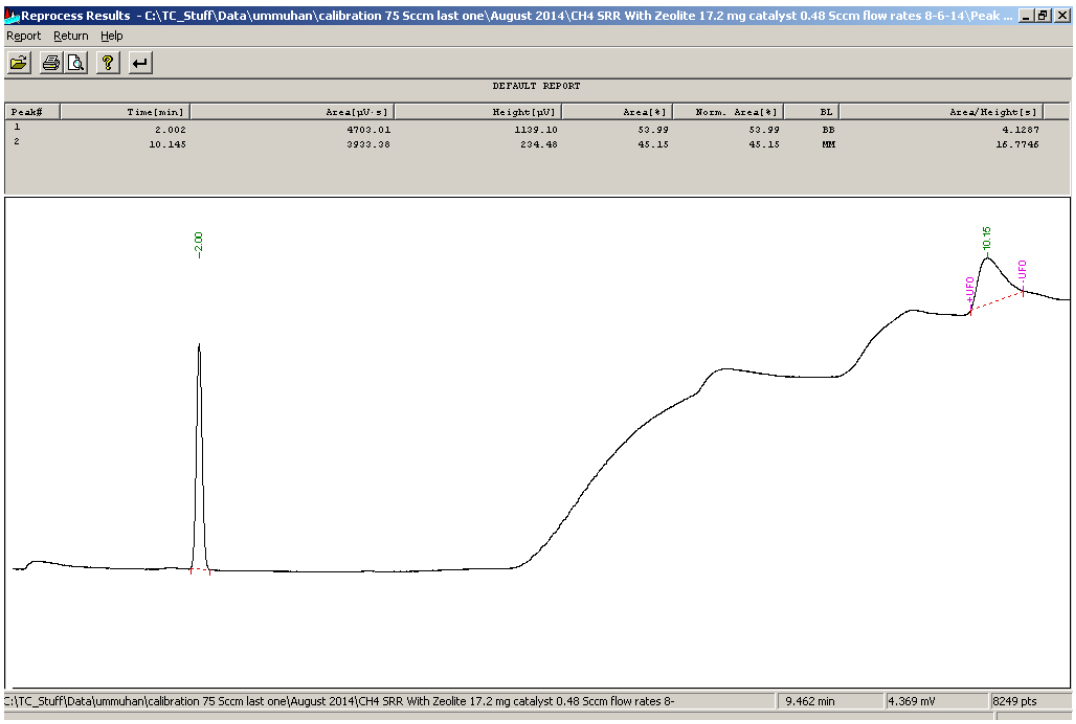

Figure G.1 Inlet stream for the sample 34.3 wt% H-β zeolite encapsulated composite catalyst (17.2 mg total catalyst)

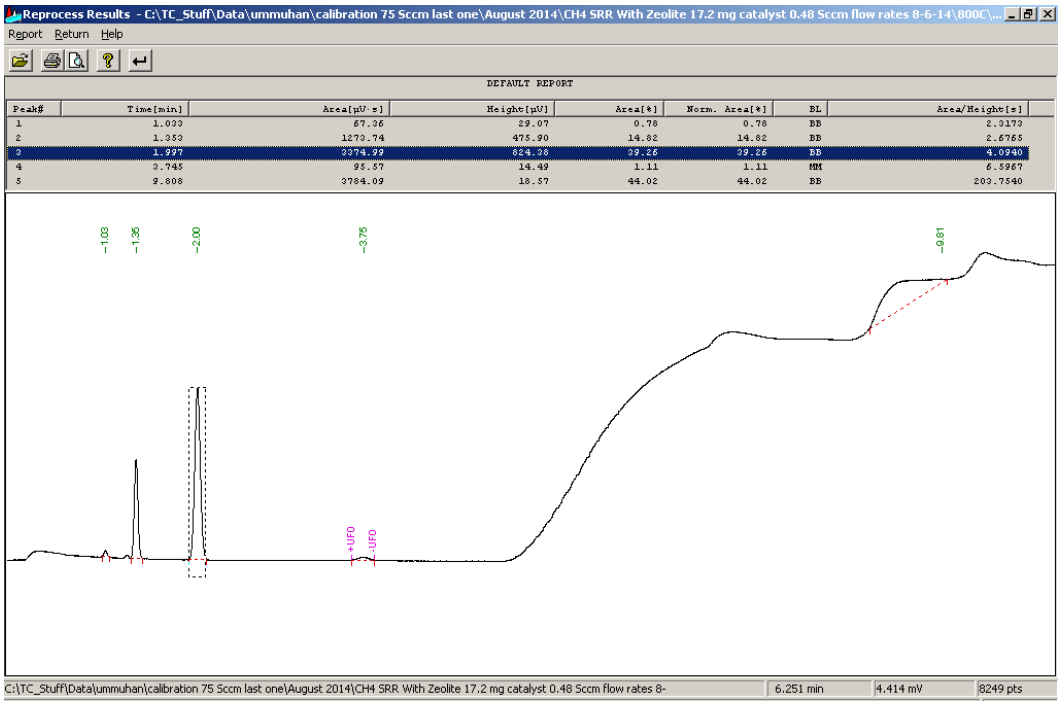

Figure G.2 Outlet stream for the sample 34.3 wt% H-β zeolite encapsulated composite catalyst (17.2 mg total catalyst)

The CH_4 conversion was calculated with the equation below:

$$X_{CH4}=\left(1-\frac{Moles\ of\ CH4\ out}{Moles\ of\ CH4\ in}\right)*100$$

Area under the curve is 4703.01 for CH_4 inlet and 3374.99 for the outlet CH_4 from the GC peaks. Relationship of the area under the curve of the GC peak and the mole of the species can be found from the calibration curve:

$$A=(3*10^{8})*f$$

where A is area and f is flow in mole/min.

Thus, the inlet CH_4 is $1.57*10^{-5}$ mole/min and the outlet CH_4 is $1.12*10^{-5}$ mole/min. So, the CH_4 conversion is:

$$X_{CH4}=\left(1-\frac{1.12*10-5}{1.57*10-5}\right)*100=29$$

ABOUT THE AUTHOR

Ummuhan Cimenler is currently a graduate student in the Heterogeneous Catalysis and Materials Chemistry Group at the University of South Florida. She joined the department of Chemical & Biomedical Engineering at the University of South Florida as a PhD student in 2012. After receiving her B.S degree in Chemical Engineering at Gazi University in Ankara, Turkey in 2009, she obtained her M.S. degree in Chemical Engineering at Yildiz Technical University in Istanbul, Turkey in 2011 and in Materials Science and Engineering at USF in 2015. Her research focuses on size-selective zeolite membrane encapsulated catalysts and process intensification of biomass to liquid fuels.